# OPTICAL AND NEAR–INFRARED SURVEYS IN STAR FORMING REGIONS

Ana Cristina Moreira Machado
Zadra Armond

2005

ANA CRISTINA MOREIRA MACHADO
ZADRA ARMOND

# OPTICAL AND NEAR–INFRARED SURVEYS IN STAR FORMING REGIONS

Tese submetida à UNIVERSIDADE FEDERAL DE MINAS GERAIS como requerimento parcial para a obtenção do grau de Doutora em Física.

Área de concentração : ASTROFÍSICA
Orientador: Prof. Dr. Luiz Paulo Ribeiro Vaz (ICEx–UFMG)
Co-orientador: Prof. Dr. Bo Reipurth (IfA–Univ. of Hawaii)

Departamento de Física - ICEx - UFMG

2005

# Agradecimentos

Agradeço a meus dois orientadores que me ajudaram de maneira indescritível durante essa longa caminhada, cada um a seu modo. Luiz Paulo e Bo, além da orientação científica, serei sempre muito agradecida pela amizade, pela paciência e por tudo o que investiram e confiaram em mim. Luiz Paulo, com seu conhecimento inigualável em todos os assuntos e seu modo prático de ver as coisas, sempre fez tudo ficar mais fácil e tranquilo. Bo, um dos maiores cientistas que conheci, me ensinou muito mais do que ele imagina. Ele é um exemplo para mim.

Bo e Mércia, obrigada por nos fazer sentir em família, quando estávamos longe da nossa.

Agradeço a John Bally pelas oportunidades de observar no Arizona e trabalhar com imagens belíssimas.

Agradeço a George Herbig por compartilhar gentilmente seus dados e programas.

Mãe e Pai, obrigada por tudo. Vocês sempre me apoiaram em todas as minhas escolhas e, mais do que isso, sempre souberam me mostrar o quanto me amam e se orgulham de mim.

Bruno, você me ajudou de todas as maneiras possíveis durante este tempo todo. Obrigada por sua dedicação e seu amor.

A todos os amigos que ajudaram de uma forma ou de outra, na Astrofísica em Belo Horizonte, em Boulder e no Havaí.

Este trabalho não seria realizado sem a ajuda financeira do CNPq, a quem eu agradeço muito.

Agradeço a Bo Reipurth por sua ajuda financeira, também fundamental, enquanto eu estive nos Estados Unidos.

# Acknowledgments

I would like to thank my two advisors, who helped me in indescribable ways during this long journey, each one with his own manners. Luiz Paulo and Bo, besides the scientific orientations, I will always be very thankful for your friendship, for your patience and for everything you invested and trusted in me. Luiz Paulo, with his huge knowledge in all subjects and his practical view of things, made everything look easier and cool. Bo, one of the greatest scientist I know, have taught me much more that he imagines. He is an example for me.

Bo and Mércia, thank you for making us feel among family when we were away from our own.

Thanks to John Bally for the opportunities to observe in Arizona and to work with beautiful images.

Thanks to George Herbig for kindly sharing his data and codes.

Mom and Dad, thanks for everything. You have always supported me in all my choices and, more than that, always showed me how you loved me and how proud you were.

Bruno, you always helped me in all possible manners during all this time. Thanks for your dedication and your love.

Thanks to all the friends who helped me one way or another, in the Astrophysics group in Belo Horizonte, in Boulder and in Hawaii.

This work would not be possible without the financial support of CNPq, whom I would like to express many thanks.

Thanks to Bo Reipurth for his also fundamental financial support while I was abroad.

Para Nuno

# Contents

# List of Figures

# List of Tables

# Resumo

Algumas regiões de formação estelar com características bem diferentes foram medidas em observatórios localizados em alguns dos melhores sítios do mundo: duas missões no *Kitt Peak National Observatory* no Arizona, Estados Unidos, usando os telescópios de 4m e de 0,9m, e outras duas missões no observatório de Mauna Kea no Havaí, com o telescópio óptico de 2.2m e o telescópio infravermelho de 4m (UKIRT). Obtivemos dados de ótima qualidade, imagens com alta resolução, longo tempo de exposição, com *seeing* da ordem de $1''$ ou menos, aliados a grandes campos de visão, com objetivo de obter o maior número possível de informações para cada região.

Para procurar por estrelas jovens, porém já mais evoluídas (opticamente visíveis), analisamos buscas feitas por estrelas com emissão em H$\alpha$ em duas regiões de formação estelar bem conhecidas: NGC 2264 e M 42. As buscas foram feitas usando-se um telescópio Schmidt, com grande campo de visão, associado a filmes fotográficos da melhor qualidade, fornecendo uma pesquisa que cobre uma área de $5^\circ \times 5^\circ$ no céu e sensibilidade suficiente para alcançar limites de magnitudes no vermelho de até 19 mag, resultando na detecção de um número superior de estrelas do que previamente conhecido. Apresentamos tabelas, cartas de identificação, correlação com levantamentos prévios e magnitudes obtidas em catálogos públicos.

Apresentamos também buscas por objetos Herbig-Haro usando imagens ópticas de banda estreita, nas regiões de S140 e L1551. Nesta última, imagens obtidas anteriormente permitiram a determinação de movimentos próprios usando uma técnica de correlação cruzada. Um moderno CCD MOSAIC forneceu uma visão em grande escala de toda a região, bem como resolução ($0''.26$/pix) para se detectar detalhes na estrutura dos nós dentro das regiões de choque. Novos objetos Herbig-Haro foram detectados. Discutimos um possível alinhamento do eixo principal dos jatos com o campo magnético da nuvem. A mesma técnica de correlação foi usada para se medir movimentos próprios no bastante conhecido HH 47, com imagens de resolução ainda maior ($0''.1$/pix) obtidas pelo *Hubble Space Telescope* em duas épocas distintas.

Algumas outras regiões de formação estelar foram pesquisadas em comprimentos de onda no visível e no infravermelho próximo, para um estudo tanto das fontes

jovens quanto dos objetos Herbig-Haro, numa tentativa de relacioná-los e melhorar o entendimento dos processos de formação estelar nessas áreas. Duas das regiões observadas são apresentadas neste trabalho: a nuvem globular IC 1396N e uma região chamada por nós de "Golfo do México", por sua localização na nuvem escura a sudoeste da Nebulosa América do Norte. As imagens ópticas foram obtidas em condições perfeitas em um dos melhores sítios de observação no mundo (o observatório de Mauna Kea, no Havaí). A região pesquisada tinha tamanho de apenas alguns minutos de arco, mas a resolução foi ótima e as áreas cobrem a região principal onde os processos de formação estão acontecendo. Muitos objetos Herbig-Haro novos foram descobertos, bem como novas estrelas com linhas de emissão em H$\alpha$. As observações no infravermelho permitem uma visão do interior da nuvem molecular, detectando estrelas jovens embebidas, bem como ejeções de matéria. Em alguns casos, as observações no infravermelho não possuem a mesma qualidade, necessária para se construir uma visão compreensível das fontes jovens, e não pudemos determinar propriedades físicas para estas estrelas. Mas fomos capazes de detectar estrelas até então desconhecidas, algumas delas criando jatos de vários tipos.

Até agora sete regiões diferentes foram estudadas com uso de técnicas variadas, para as quais discutimos as diferenças e similaridades. Algumas outras regiões também foram observadas e seu estudo está planejado para breve.

Concluimos, através de nosso estudo, que o processo de formação estelar é bem mais complexo do que se acreditava há poucos anos, e que somente o uso de várias técnicas aplicadas a diversas regiões de formação estelar poderá responder às inúmeras questões ainda sem resposta sobre este processo (e provavelmente colocar muitas outras questões ...).

# Abstract

We have observed several different star formation regions, in top quality observatories: two missions at the Kitt Peak National Observatory, in Arizona, using the 4m and the 0.9m telescopes and two other missions at the Mauna Kea observatory in Hawaii, using the 2.2m optical telescope and the 4m infrared telescope (UKIRT). We have obtained very good quality data, high resolution deep images with seeing of the order of $1''$ or less, combined with large field of view, with the objective to obtain as much information on each region as possible.

In order to probe the more evolved optically visible young stars, we have analyzed surveys to detect H$\alpha$ emission stars in two very well known star forming regions: NGC 2264 and M 42. They where obtained with a wide field Schmidt telescope associated with the best quality photographic films, providing a survey of an area of $5^\circ \times 5^\circ$ in the sky and enough sensitivity to reach red photographic magnitudes up to 19 mag, yielding a detection of a much larger number of young stars than previously known. We provide tables with coordinates, finding charts, cross identification with other surveys and magnitudes in public catalogs.

Optical narrow-band surveys to detect Herbig-Haro objects are presented as well, for the star forming regions S140 and L1551. In the latter, previous images allowed the determination of proper motion using a cross correlation technique. A modern wide field MOSAIC CCD was used, providing a large scale view of the entire region, as well as high enough resolution ($0\farcs26$/pix) to detect structure details of the knots inside the shock regions. New Herbig-Haro objects were detected. A possible alignment of the main flow axis with the magnetic field in the cloud is discussed. The same correlation technique was used to measure proper motions in the well known HH 47 jet, using even higher resolution Hubble Space Telescope images ($0\farcs1$/pix) taken in two epochs.

Some other known star forming regions were surveyed at optical and near-infrared wavelengths for a study of both the young sources and the Herbig-Haro objects, in an attempt to relate them and to shed more light into the understanding of the star formation processes in those areas. Two of those regions are presented in this work:

the IC 1396N globule and a region called by us the "Gulf of Mexico", because of its location in the dark cloud southwest of the North America Nebula. The optical images were obtained in perfect conditions in one of the best observing sites in the world (the Mauna Kea observatory in Hawaii). The surveyed regions were only a few arcminutes wide, but the resolution was good and the areas cover the main region where the star formation processes are occurring. Several new Herbig-Haro objects were found, as well as new H$\alpha$ emission line stars. The near-infrared observations allowed a view of the interior of the molecular clouds, probing embedded young stars and outflows. In some cases the near-infrared observations lacked the quality necessary for building a comprehensive view of the young sources, and we could not infer physical properties for those stars. But we were able to detect some previously unknown young stars, some of them powering outflows of various types.

So far we have seven different star forming regions studied using various techniques, for which we discuss differences and similarities. A few other regions were also observed and their study is planned in the near future.

We conclude that the star formation process is much more complex than it was thought a few years ago, and only with the simultaneous use of different techniques applied to several star forming regions will we be able to answer the numerous questions about this process (and probably create many more questions ...).

# Chapter 1

# Introduction

The issue of the origins of stars is one of the most fundamentals in astronomy. Yet, many questions about this process have not been entirely answered till today. But, thanks to the new technological advances of recent years, we are witnessing the development of a coherent theory on stellar formation. The agreement between observations and theory is slowly becoming quite good, especially for low-mass stars.

All the star formation processes known today take place in molecular clouds, the most massive objects in the galaxies, where the raw material to make new stars is found in abundance. The largest complexes are called Giant Molecular Clouds. With masses that can be greater than $10^6$ solar masses ($M_\odot$), they are found in the spiral arms of the Galaxy and are where the more massive stars form (e.g. Orion complex). The smaller complexes, like Taurus, are not necessarily confined to the arms. They form low mass stars and are called Dark Clouds.

All the types of molecular clouds have irregular shapes, with blobs, filaments and clumps, with different densities. Denser structures or cores, gravitationally bound and with masses ranging from fractions of 1 $M_\odot$ to $\sim$ 100 $M_\odot$, may form stars or multiple systems.

At a certain moment, those dense cores may collapse gravitationally and form embedded proto-stars, that will accumulate material of the surrounding cloud. Due to existence of a net angular momentum in the collapsing region, that must be transferred to the forming star, the collapse of a cloud naturally leads to the formation of a flattened disk around the proto-star. The material from the collapsing cloud

falls into the disk that transfers it to the proto-star.

Besides matter accretion, there are energetic ejection of material along the rotation axis. These ejection and strong stellar winds cause the proto-star to lose some mass, and eventually disperse the mass reservoir of the cloud envelope, hindering further accretion. The star, now called a Pre-Main Sequence star, starts to contract, increasing its temperature until the ignition of hydrogen is allowed, becoming then a stable Main Sequence star.

## 1.1 Young stellar objects

When the Pre-Main Sequence star becomes visible, it can be classified according to its mass. It is called a T Tauri star if it is a low mass star ($M < 2\ M_{\odot}$). Those stars show late type absorption lines and strong hydrogen, calcium and iron emission lines in their spectra (an indication of mass loss), and are usually associated with nebulosities and with brightness variations. Their absorption lines are superimposed on a blue continuum emission, known as veiling, coming from an accretion circumstellar disk. They also show infrared excess, due to dust emission, and ultraviolet excess, possibly due to the interaction between disk and star. Those stars still show lithium absorption lines (6707 Å), a characteristics of youth, since this element is destroyed early in the star history. T Tauri stars are also strong X-Ray emitters, due to the magnetic activity at the stellar surface.

Another class of stars, the Weak-line T Tauri stars, have comparable levels of X-Ray emission to the Classical T Tauri stars, but with no ultraviolet excess, little or no infrared excess and very weak emission lines (the equivalent widths of the H$\alpha$ emission lines are by definition smaller than 10 Å). They are probably Classical T Tauri stars that already wiped away most (or all) circumstellar material.

If the Pre-Main Sequence star has an intermediate mass ($2\ M_{\odot} < M < 8\ M_{\odot}$), it is called a Herbig AeBe star. They are also associated with nebulosities, similar to T Tauri stars, but with spectral type A or B with emission lines, infrared excess due to circumstellar dust, and luminosity class III to V. They are the intermediate mass counterparts of T Tauri stars.

For relatively massive stars, the situation is different. They begin to burn hydrogen before the contraction ends, reaching the Main Sequence before accretion stops. These stars, with masses above approximately $8\ M_{\odot}$, are therefore not observed in the Pre-Main Sequence phase.

In some cases the proto-star does not achieve the critical mass necessary to start the hydrogen burning. That could happen if, for some reason, there is no more material

available in the surroundings to continue the accretion process. These extreme low mass objects (with masses smaller than $\sim$0.08 $M_\odot$) are called Brown Dwarfs and, in the last years, have been found in increasing numbers.

*Young Stellar Evolution: Spectral Classification*

The evolutionary stage of a normal star is determined by its position in the Hertzsprung–Russel (HR) diagram, which requires the knowledge of its luminosity and effective temperature (spectral type). The luminosity is determined from the observed flux and the distance to the star, while the temperature is determined from its colors and its spectrum, as long as the star produces a spectrum characterized by a single effective temperature (Lada, 1998).

However, young stars do not behave normally, because they are intimately connected with the material they are being formed with. The circumstellar gas and dust absorb and re-process the emitted radiation, altering its spectrum. Indeed, the youngest objects are completely invisible at optical wavelengths, due to the obscuration of light by the dust, and by the re-emission in the infrared of the radiation of the star. We expect, then, that the shape of the observed spectrum is a function of the type and the distribution of the circumstellar material, and, so, a function of the evolutionary stage of the young star.

An evolutionary scheme for low mass stars from the proto-stellar cores with basis in the shape of the spectral energy distribution (SED) was first proposed by Lada & Wilking (1984). Adams, Lada & Shu (1987) connected the types of SED with an evolutionary sequence that they called Classes I, II and III. André et al. (1993) proposed the existence of a less evolved class, the Class 0.

An illustration of the SED of the different classes is shown in Fig. 1.1. The main characteristics of those classes are:

- Class 0: Visible only at sub-millimetric wavelengths; the SED is as broad as a black body, but with temperatures of 20-30 K. They are the most deeply embedded objects, considered to be small stable hydrostatic cores with massive infalling envelopes of gas and are heated by gravitational contraction. Their nature is proto-stellar. They are associated with highly energetic and collimated bipolar molecular outflows.
- Class I: Strong infrared excess; SED much broader than a black body, peaking at far infrared wavelengths. Usually not visible in the optical, exhibit the silicate characteristic absorption at 10$\mu$m. They are frequently associated with bipolar molecular outflows. They were successfully modeled as systems composed of a proto-stellar core surrounded by a disk and a massive envelope of dust and gas.

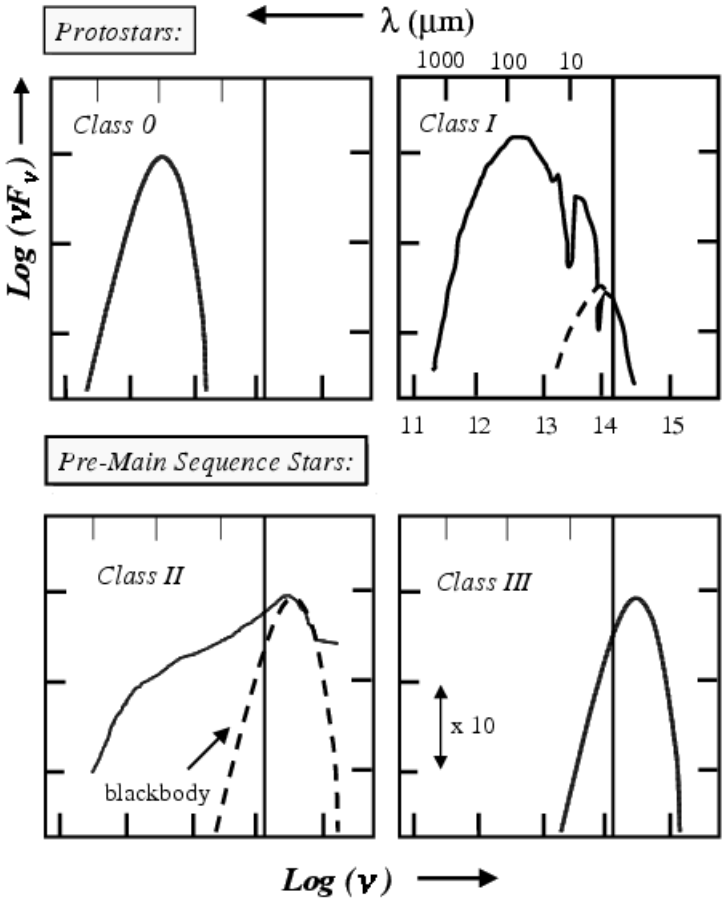


**Figure 1.1**: Empirical classification for the energy distribution of the evolutionary classes of young stars. The vertical line corresponds to $2\mu$m. Adapted from Lada (1998).

- Class II: Infrared excess, but less than in Class I; SED broader than a black body, peaking in the visible or near infrared; above $2\mu$m the flux decreases. Generally they are optically visible and many show emission lines, and because of that their characteristics are more familiar to us than less evolved classes. The spectral characteristics show strong evidence that the system consists of a Pre-Main Sequence star surrounded by a optically thick flattened disk. In this stage they do not show the spherical envelope of gas and dust like in Class I. Many of these stars show characteristics similar to Classical T Tauri stars, also exhibiting ultraviolet excess, possibly due to the accretion of material from the disk onto the star.

- Class III: SED similar to a black body, but reddened. The material of the disk was already incorporated by the star, disrupted by a companion or agglomerated into clusters of particles that may form planetary systems around the

star. Those stars are basically free of the circumstellar material, but still show traces of youth, like X-Ray emission (though variable) and in some cases weak H$\alpha$ emission lines. Class III stars are then Weak-line T Tauri stars

The variation in the SED shape represents an evolutionary sequence, corresponding to a gradual dissipation of the gas and dust envelope around the newly formed star. Possibly the great majority of low mass stars go through all of those phases during their formation, although the duration of the phases are not the same for all the stars, even with similar masses.

An interesting fact to be noticed is that a big part of the young objects observed today belong to binary or multiple systems. Indeed, the fraction of young binaries sometimes is larger than the fraction of field binary stars. There are strong indicators that multiple systems are formed still in the proto-stellar phase, with the possibility of disruption due to the gravitational forces of the formation environment, or by ejection processes (Reipurth 2000).

## 1.2 Outflows

Mass loss is a common phenomenon in Pre-Main Sequence stars. The current models of a young accreting system propose that outflows are launched by magneto-hydrodynamic processes near the star, in the inner accretion disk, and are collimated further away, probably by magnetic field interactions. The outflows are always perpendicular to the rotation axis of the accreting source and usually have bipolar morphology.

When the outflow impacts the dense surrounding material in the molecular cloud, the shocks generated ionize the gas and can be traced at many wavelengths. The structures seen in emission lines at optical wavelengths are called Herbig-Haro (HH) objects. The optical emission occurs mainly in Hydrogen lines, but also in [SII] and [OII] lines, among others. Flux ratios, for example [SII]/H$\alpha$, are used to distinguish an HH flow from a photo-ionized region, and also to define the level of excitation of the HH object. HII regions and "elephant trunks" have [SII]/H$\alpha \sim 0.1$, while HH objects have [SII]/H$\alpha > 0.1$. High excitation HH objects have small line ratios, while low excitation HH objects have larger line ratios ($>\sim 2$).

The most common way of detecting an HH object is to observe it using narrow band filters centered in one or more emission lines and also through broad band filters that avoid the emission lines. If an object appears in the emission image and not in the continuum image, and if it is located in or near a star forming region, it is most

certainly an HH object. But to unequivocally identify an HH object is necessary to take its spectrum.

The Herbig-Haro objects are nebulous structures, showing knots and filaments or having a bow-shock shape. One outflow sometimes consists of many HH objects aligned bilaterally around a young star or proto-star. They can reach many parsecs away from the source. Some HH objects have a curved shape. An S-shape may indicate a change in the flow axis with time; a C-shape may be caused my motion of the source through the cloud; abrupt direction changes may be caused by strong interactions between the proto-stars in a close group. There are more than 800 HH objects identified up to now and they are cataloged and given HH numbers (Reipurth 1999).

The outflows can also emit in the near infrared (for example $H_2$ and [FeII]) when they are more embedded in their parent cloud. Low excitation shocks frequently show strong $H_2$ emission lines, while regions of higher excitation are stronger in [FeII] (the apex of bow shocks, for example).

The high velocity molecular gas can frequently be traced at millimeter wavelengths, especially in CO lines. So, infrared and millimeter observations reach the more embedded parts of the flow, while optical observations trace the flows that have already erupted from the cloud. Images taken at different wavelengths can therefore reveal the full structure and morphology of the outflow, and provide important constraints on the nature of the flow collimation and variability.

The velocities of the outflows are relatively high (typical values are 100 to 200 km/s) and sometimes one can actually "see" the Herbig-Haro objects moving in the sky if the time interval is long enough (usually some years) and if their distance to us is not too large. It is possible, then, to measure their proper motions and to know their projected (tangential) velocities. Knowing the distance of the cloud and the projected distance from the HH to its source, it is possible to estimate a dynamical age and thus precious information about the structure of the HH and even of the source.

The source of the HH flow is not always obvious and it can be difficult to determine. It can be too embedded for direct observation or it can be among several other potential sources. The direction of the proper motion, if detected, usually points back to the source of the HH, and sometimes is the essential information for its determination.

When an outflow occurs in an HII region near early type stars, the intense UV radiation can ionize the jet and make it visible, even if no shocks were present. Those are classified as "irradiated" jets and can be seen as a whole in regions far from dense molecular clouds. Parts of the outflows can also be seen bursting out of the

cloud, into the lower density medium. The outflows "illuminated" this way provide an easier way of determining the physical properties than their more embedded counterparts.

The large fields of view of the recently developed large mosaic CCD detectors have provided images of the HH objects in their full extent with a reasonable resolution, allowing a detailed study and the construction of theories to explain their nature. See Reipurth & Bally (2001) for a review on the recent studies of HH objects.

## 1.3 Modes of star formation

The molecular clouds where stars are formed have properties reasonably well determined and there has been a long effort in order to understand if and how different clouds form different types of stars. The cloud structure is very irregular and have turbulent motions, leading to the assumption that star formation processes could be very chaotic.

As the evolution of the star is mostly determined by its mass, the knowledge of the original distribution of stellar masses right after the formation process, or the stellar initial mass function (IMF), is required to build a coherent theory of stellar formation. The properties of the clouds could then be associated to the properties of the stars formed in there, so we would be able to predict the way the stars will form in a given cloud. Unfortunately that goal has not been achieved yet.

The IMF is defined as the relative number of stars formed per unit volume per unit logarithmic mass interval and its original shape was originally found to be a simple power law by Salpeter (1955), between masses of approximately 0.4 and 10 $M_{\odot}$. Much evidence now suggests a general form of the IMF that is similar to the original Salpeter power law at masses above one solar mass, but flattens below one solar mass and declines below 0.1 solar masses (the brown dwarf regime). The peak of the function at a few tenths of a solar mass shows that most stars formed in the Galaxy are low mass objects.

It is often assumed that the IMF is universal in time and space. But that cannot be derived from theory, it has to be measured directly from observations. In principle, the measurement of a large number of clusters of newly formed stars may provide such information. But to determine star masses is not an easy task, especially for stars that are deeply embedded in their parent cloud, and we also depend on Pre-Main Sequence evolution theories to have their masses derived. Recent developments, both in infrared observing techniques and in modeling the IMF, begin to address those issues, especially for low mass stars.

There are numerous studies in the literature about the IMF nature (e.g. Miller & Scalo 1979; Kroupa, 2001, 2002; Larson 2005). Recent studies predict that the stars themselves help determine their own masses through the action of stellar outflows (e.g. Adams & Fatuzzo 1996). Larson (2005) suggests that the low mass IMF is determined largely by the thermal physics of the star forming clouds. The IMF produced by these models is rather consistent with observations being made nowadays.

Some differences in the stellar mass distribution has been noted, however, for different types of clouds. Giant Molecular Clouds like Orion tend to form both massive and low mass stars, following the standard IMF. But smaller dark clouds like Taurus, of simpler structure, have a deficiency in brown dwarfs and in high mass stars. It may happen, then, that the stars in both extremes can be formed only in clouds with a more complex structure (Larson 2001).

Nevertheless, it seems established that the great majority of stars do form in groups, and not isolated. They are formed following the structure of the dense cores in the parent cloud. The processes involved are violent, especially the outflows, which interfere directly in the formation process by dispersing the material and perhaps determining the final masses of the stars.

There is still much to be done till we get to a complete theory of stellar formation. But, during the last few years a coherent picture of stellar evolution is being developed, observationally and theoretically, at least for low mass stars. The modern observational techniques today, mainly at infrared wavelengths and also with the large fields of view of the mosaic CCD detectors, offer an opportunity to clarify some of the questions. It is important then, to observe as many star forming clouds as possible, probing the cloud cores, the proto-stars, the outflows and the Pre-Main Sequence Stars, and relating them in a coherent picture. In small steps the way to a more complete understanding of star formation will be developed.

In order to probe the more evolved optically visible stars, surveys to detect H$\alpha$ emission stars are very useful and have been made since the 50's. In Chapter 2 I describe such a survey in two very well known star forming regions: NGC 2264 and M42. They where performed with Schmidt plates that have large field of view, combined with very sensitive films, providing a detection of a larger number of stars than previously known.

Optical narrow-band surveys to detect Herbig-Haro objects are presented in Chapter 3 for the star forming regions S140 and L1551. In the latter, previous images allowed the determination of proper motion using a cross correlation technique. This same tool was used to measure proper motions in the well known HH 47 jet, with Hubble Space Telescope images taken in two epochs.

Some other known star forming regions were surveyed at optical and near-infrared wavelengths for a study of both the young sources and the Herbig-Haro objects, in an attempt to relate them and to gain a better understanding of the star formation processes in those areas. We were able to detect some previously unknown young stars, some of them powering outflows of various types. Chapter 4 presents the surveys of two regions observed: the IC 1396N globule and a region called by us the "Gulf of Mexico", for its location in the dark cloud southwest of the North America Nebula.

A summary of the results and the conclusions of the present work and the perspectives for the future are in Chapter 5. In the Appendix I reproduce the published papers related to the work presented in this thesis.

# Chapter 2

# Surveys for H$\alpha$ emission stars

Young stars typically show hydrogen, calcium and iron emission lines in their spectra, indicating mass loss. The search for the H$\alpha$ emission line at 6563 Å in the stellar spectra has been extensively used to identify the low mass young stars in star forming regions, as well as to classify them. By definition, classical T Tauri stars have equivalent widths of the H$\alpha$ emission lines larger than 10 Å, while in Weak-line T Tauri stars this equivalent widths are smaller than 10 Å.

Surveys for H$\alpha$ emission line stars using slit-less spectroscopy have been performed for the past 50 years, starting with Joy (1946). Since the large majority of stars are formed in groups, it is of great interest to study the locations of birth and subsequent dispersal of the young stars. Their surface density will decrease with time if the grouping has or will become unbound, giving the average velocity dispersions of a few kilometers per second. The distribution of H$\alpha$ emission line stars thus reflects both the sites of star formation in a cloud as well as the dispersal of the members of the association or cluster.

We present in this chapter surveys for H$\alpha$ emission line stars of two very well known star forming regions: NGC 2264 and M 42. The surveys use objective prism films obtained at the ESO 1m Schmidt telescope, before it ceased its operations in 1998. Several equatorial and southern star forming regions were observed using the most sensitive and fine grained films currently available. Each film is 30 by 30 cm, which at an imaging scale of $67\farcs5$/mm corresponds to a field on the sky of 5° by 5°. Typically, three to four levels of exposures were made, ranging from very short (e.g. 10 min)

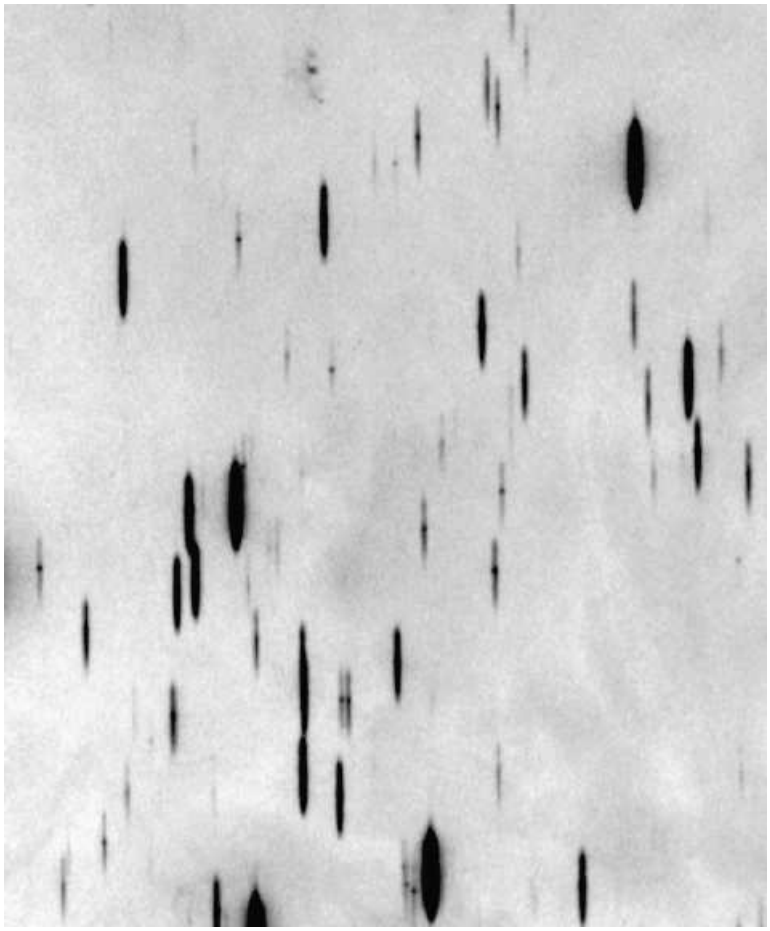

**Figure 2.1**: Representative spectra of H$\alpha$ emission stars, from the region of NGC 2264. The area shown contains 38 H$\alpha$ emission stars. A Herbig-Haro object, HH 284, can also be seen at the top of the image.

to very long (up to 150 min), in order to detect emission from bright as well as faint stars. For details of the observations see Reipurth et al. 2004a (in Appendix A.3).

The type of material obtained is shown in Fig. 2.1, where one can note that H$\alpha$ emission is well centered in the spectral range of the prism spectra, and rather easy to detect if the emission is strong and the continuum not too bright. The films with different exposure times were examined several times using a binocular microscope, by Bertil Pettersson and Bo Reipurth. The detected stars were then marked on finding charts, identified by number and given a classification of the H$\alpha$ emission strength that varied from 1 (weak emission and/or strong continuum) to 5 (strong emission and/or weak continuum). That was the material given to me in order to compile a catalog with cross correlations to other known H$\alpha$ emission surveys and with magnitudes from public optical and near-infrared catalogs.

In Section 2.1 I present the results of the survey for NGC 2264, and in Section 2.2 for M 42.

## 2.1 NGC 2264

The young cluster NGC 2264 is located in the Monoceros OB1 molecular cloud at a distance of less than 1 kpc. There is some uncertainty about the real distance to the cluster, and we adopt here the value of 760 pc (Park et al. 2000). Herbig (1954) derived a census of the young low-mass population of this cluster by using slit-less spectra to identify 84 H$\alpha$ emission stars. This was followed by a photometric study by Walker (1956), who found that stars earlier than A0 are already on the main sequence, while A0-F0 stars are up to 2 magnitudes brighter than the main sequence. Stars have been forming in this region for the last approximately 3 million years. Further photometric determinations of population membership have been done by e.g. Adams et al. (1983) and Sung et al. (1997). The cluster is still associated with abundant molecular material (e.g. Crutcher et al. 1978, Oliver et al. 1996), and star formation is still ongoing as evidenced by the presence of embedded IRAS sources and molecular outflows (e.g. Margulis et al. 1988, 1989). A number of Herbig-Haro objects are also found in this region (e.g. Adams et al. 1979, Walsh et al. 1992, Reipurth et al. 2004). The cluster population has been studied by analysis of near-infrared images (Lada et al. 1993). More recently, Rebull et al. (2002) presented an optical and near-infrared study of NGC 2264, searching for circumstellar disk candidates. They report photometry at optical ($UBVRI$) and near-infrared ($JHK$) wavelengths for $\sim$5600 stars and spectroscopic classifications for a sample of 399 of these stars, for which they measure H$\alpha$ emission-line equivalent widths.

*The survey:*

A total of 357 stars stars were found in our survey. The region surveyed includes the total area studied by Herbig (1954), and out of his 84 stars, 73 were detected now. This is consistent with Herbig's comment that when re-examining a region at a later time, about 10% of the stars have decreased their H$\alpha$ intensity to the point where they are not detected in objective prism surveys, whereas another 10% of new objects have appeared. Our survey is therefore consistent with Herbig's findings.

Ogura (1984) lists 135 H$\alpha$ emission line stars in an area that only partially overlaps with ours. Of his stars, 42 are outside our area (37 to the west, and 5 to the north). Of the remaining 93 stars which coincide with our survey area, only 34 are also seen by us. Our survey was done blindly without knowledge of the survey results of Herbig and of Ogura. After realizing the serious inconsistency with Ogura's

results, his stars were specifically examined, and no emission was found in any of the remaining 59 stars. Given that our film material is much more sensitive and fine grained than Ogura's plates, we suspect that a large number of Ogura's emission line stars are spurious. Only a high resolution spectroscopic study can resolve this issue.

*The table of H$\alpha$ emission stars:*

The H$\alpha$ emission stars detected in NGC 2264 already had coordinates measured and were cross correlated with LH$\alpha$ stars (from Herbig 1954 and Marcy 1980), with KisoH$\alpha$ stars (defined in Ogura 1984 and Walsh et al. 1992), and with Walker (1956) stars. The H$\alpha$ emission line strengths were also given, in a scale varying from 1 (weak emission and/or strong continuum) to 5 (strong emission and/or weak continuum). Emission line strengths were estimated on each film separately, and differences in estimates were indicated as hyphenated values, e.g. 3-4. Such differences were, with a few exceptions, not major, and may represent either variability and/or uncertainty in the estimate.

Rebull et al. (2002) have also surveyed a $45' \times 45'$ region, within the field of our survey, searching for circumstellar disk candidates. Together with optical ($UBVRI$) and near-infrared ($JHK$) photometry, they obtained spectra for 399 specific stars. This sample was selected primarily from a list of variable stars from an initial $I$-band study. The other part of the sample included objects with previously reported X-Ray or H$\alpha$ emission, likely proper motion membership and bright stars projected onto the NGC 2264 molecular cloud. They present a list of 687 disk candidates with optical/infrared magnitudes and 211 of those with spectra and derived parameters. I have cross correlated our coordinates with those, and included the "R" identification in the table. The search was made within a $2''$ radial distance from each star. Each star found was then checked visually in the finding charts. 157 stars were found in common with our survey, 69 of them have spectra and generally the H$\alpha$ equivalent widths measured agree with the "weak/strong" indicator of our survey. Nearly all the strong H$\alpha$ emitters (H$\alpha$ equivalent widths larger then $\sim$15Å) observed by them were detected by us. About 30 more of their stars had H$\alpha$ equivalent widths smaller than 15Å and were also detected by us, most of them with H$\alpha$ strength 1 or 2 in our table. The few that do not agree (less than 10%) are probably very variable stars.

30 stars from the total of 157 in common with Rebull et al. (2002) have H$\alpha$ emission detected and are not included in the previous surveys of NGC 2264. The remaining stars were already known as H$\alpha$ emitters or are simply classified by Rebull et al. (2002) as disk candidates. Thus our final table has a total of 214 new H$\alpha$ emission stars in the region of NGC 2264.

I have also cross correlated the coordinates with different public catalogs of photom-

etry (the optical USNO-B and GSC2.2 and the near infrared 2MASS), also within $2''$, and always checking each identification in the finding charts.

The majority of the blue $m_J$, red $m_F$ and far-red $m_N$ photographic magnitudes obtained for the stars are from the USNO-B catalog. This catalog is based on Schmidt plates from various sky surveys made over the last 50 years (Monet et al. 2003). It is an all-sky catalog that presents positions, proper motions, magnitudes in various optical pass-bands, and star/galaxy estimators for 1,042,618,261 objects. It is believed to be complete to the limiting magnitude of V = 21, except for stars in difficult areas, such as nebulous regions or close to very bright stars. A few stars were not detected or well separated enough from close stars by the USNO-B scanning methods, but they were in the GSC2.2 (Guide Star Catalog 2.2 – extracted from the Digitized Sky Survey II, STScI 2001). That catalog lists only $m_J$ and $m_F$ magnitudes (up to $m_J = 19.5$ and $m_F = 18.5$, accurate to 0.2 mag), but it resolves better the close stars.

Although all of our 357 stars are visible on the Schmidt plates on which USNO-B and GSC2.2 are based, 30 out of the 357 stars in the table are not listed with a red $m_F$ magnitude. Because many of our stars are likely to be variable, both in the continuum and in H$\alpha$, it is difficult to estimate a precise limiting magnitude for our survey, but examining the magnitudes obtained, which includes several stars fainter than $m_F > 19$, suggests that the survey is likely to be reasonably complete down to $m_F \sim 18$. This is several magnitudes deeper than the various earlier surveys in this region.

All but one of our 357 H$\alpha$ emission stars were detected in the 2MASS infrared sky survey, and we list the near-infrared magnitudes in the table. The 2MASS (Two Micron All Sky Survey) provides $J$, $H$ and $K_s$ magnitudes for nearly half a billion stars all over the sky (Cutri et al. 2003). The catalog is complete down to limiting magnitudes of $J < 15.8$, $H < 15.1$ and $K_s < 14.3$, and typical uncertainties in the photometry are 1-2% for bright, non-saturated sources. That can rise up to 20% for stars that saturate the shortest 2MASS exposures (50 ms). The completeness decreases beyond the limiting magnitudes, but sources 0.5-1.0 mag fainter than these limits are included in the catalog. The position uncertainties of 2MASS are expected to be about $0''.1$, which is better than the coordinates previously obtained for the stars, and also than the two optical catalogs. Thus, the coordinates used in the final table are the ones given by the 2MASS catalog.

The table resulting from this survey is fully presented in the Appendix A.3, as Table 2 inside the paper originated by this work (Reipurth et al. 2004a). An example of the data is shown here in Table 2.1, where we selected some representative lines of the full table.

**Table 2.1**: Part of the final table of H$\alpha$ emission line stars in NGC 2264

| ESOH$\alpha$ | LH$\alpha$ | KH$\alpha$ | W | R | $\alpha$(2000) | $\delta$(2000) | H$\alpha$ | $m_J$ | $m_F$ | $m_N$ | $J$ | $H$ | $K_s$ |
|---|---|---|---|---|---|---|---|---|---|---|---|---|---|
| 308 | ... | ... | ... | .... | 06 36 19.3 | +10 54 26 | 2 | 17.41 | 15.46 | 14.37 | 12.53 | 11.63 | 11.18 |
| | ... | 39 | ... | .... | 06 36 22.3 | +10 54 44 | 3 | 15.61 | 11.21 | 12.75 | 11.70 | 10.31 | 8.96 |
| 309 | ... | ... | ... | .... | 06 36 29.3 | +10 50 01 | 2-3 | 18.38 | 16.34 | 15.42 | 13.83 | 13.30 | 12.94 |
| | 4 | ... | ... | .... | 06 39 51.9 | +10 12 39 | 3 | 15.36 | 13.26 | 13.70 | 12.88 | 12.59 | 12.43 |
| 341 | ... | ... | ... | 1588 | 06 40 01.2 | +09 42 36 | 2 | 19.23 | 17.16 | 16.00 | 14.45 | 13.72 | 13.44 |
| 342 | ... | ... | ... | .... | 06 40 01.3 | +09 43 00 | 4-5 | 20.99 | 18.94 | 16.86 | 15.00 | 13.17 | 11.94 |
| | ... | 62 | ... | 1621 | 06 40 02.7 | +09 35 24 | 3-4 | 18.20 | 17.03 | 15.30 | 13.70 | 12.99 | 12.71 |
| | 12 | ... | 55 | 2456 | 06 40 30.9 | +09 34 40 | 3 | 17.27 | 14.59 | 14.74 | 12.69 | 11.51 | 10.67 |
| | 32 | 9 | ... | .... | 06 40 51.3 | +10 28 05 | 3 | 16.60 | 14.37 | 13.43 | 11.40 | 10.73 | 10.12 |
| 446 | ... | ... | ... | .... | 06 40 59.0 | +09 33 22 | 4 | ..... | ..... | ..... | 13.94 | 13.09 | 12.60 |
| 452 | ... | ... | ... | .... | 06 40 59.6 | +10 28 50 | 5 | 20.66 | 19.53 | ..... | $17.68^u$ | 15.78 | 14.45 |
| 549 | ... | ... | ... | .... | 06 42 45.1 | +10 53 50 | 4 | ..... | 18.35 | 16.13 | 14.40 | 13.75 | 13.18 |

Note.– The full table with all the 387 H$\alpha$ emission stars is presented as Table 2 in Appendix A.3. This portion is shown here only for guidance regarding form and content.

The first column of the table gives the identification of all the newly discovered stars for which we gave ESOH$\alpha$ numbers. Previous numbers in this series were published in Pettersson & Reipurth (1994), Reipurth & Eiroa (1992), Reipurth & Zinnecker (1993), and Reipurth et al. (1997). Objects already known from previous H$\alpha$ surveys are not given an ESOH$\alpha$ number, instead the LH$\alpha$ numbers of Herbig (1954) and Marcy (1980) or the KH$\alpha$ numbers of Ogura (1984) are provided in columns two and three. The columns marked W and R refer to the photometric studies of Walker (1956) and of Rebull et al. (2002). The following two columns give the coordinates of the stars derived from the 2MASS catalog, and have expected uncertainties of about $0\farcs1$. The next column gives the H$\alpha$ emission line strength, as described earlier. The next three columns provide blue, red, and far-red photographic magnitudes, $m_J$, $m_F$, and $m_N$, as given in the USNO-B Catalog. Finally, the last three columns give near-infrared $JHK_s$ photometry from the 2MASS survey.

The total spatial distribution of the stars detected is shown in Fig. 2.2, overlaid on a map of the distribution of $^{13}$CO (J = 1$\rightarrow$0) gas. This map was obtained in 1991 with the AT&T Bell Laboratories 7 m offset Cassegrain antenna. The main concentration of H$\alpha$ emitters is clearly located towards the strongest CO emission peak, and has a halo of stars with a radius of less than $20'$ surrounding it. These outlying stars are not closely associated with major CO concentrations, and they may have drifted away from the central molecular cloud core. The velocity dispersion of young stars is of the order of 1-2 km s$^{-1}$ (Dubath, Reipurth, & Mayor 1996), which corresponds to 1-2 pc in a million years. If this is really the case for NGC 2264, it suggests that the CO core has produced stars over a period of several million years. The strong concentration of stars towards the most massive molecular core suggests that star formation has been ongoing in the recent history of the region. Indeed, the massive core contains IRS 1 and other sub-millimeter sources (Ward-Thompson et al. 2000).

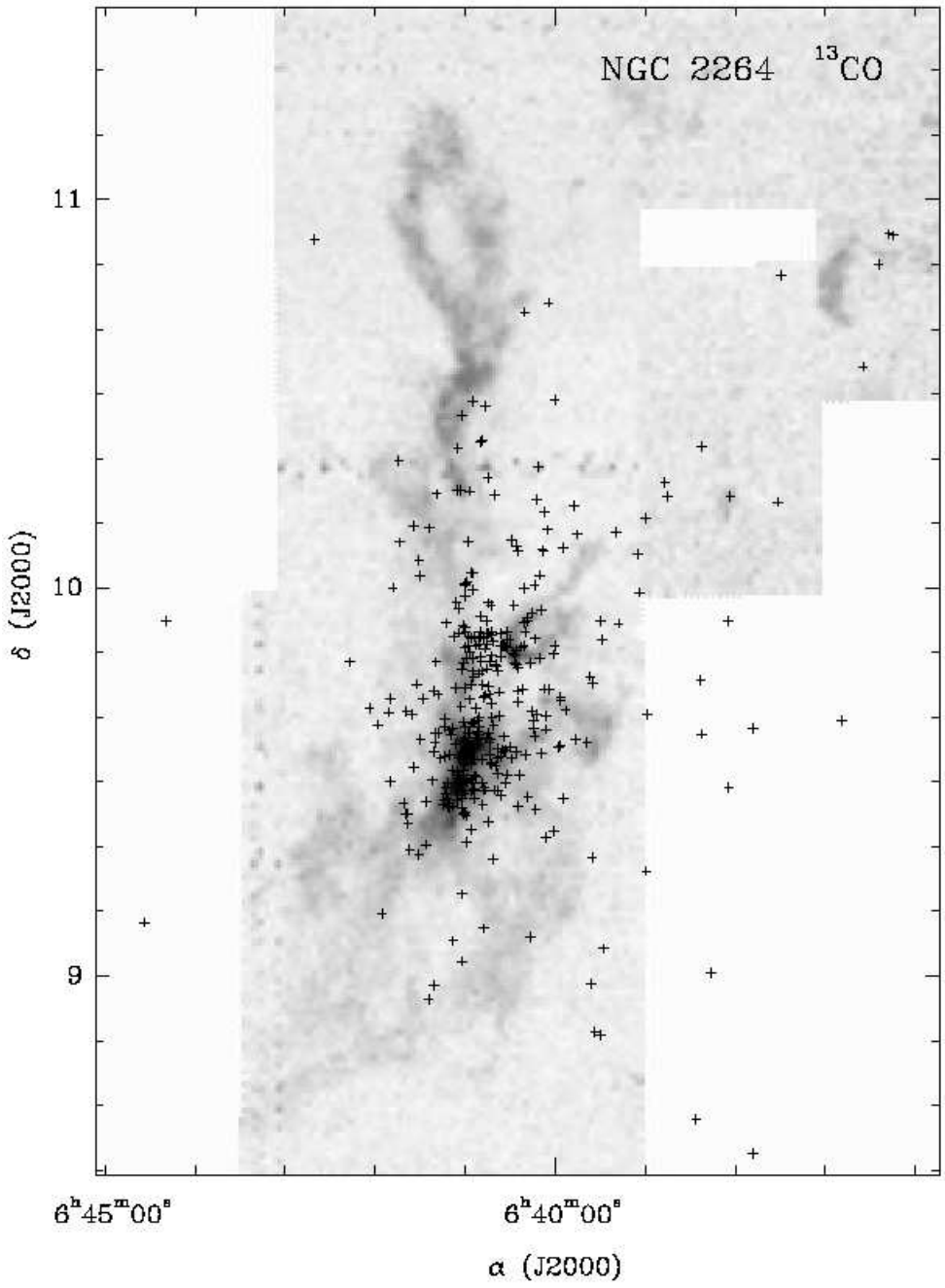


**Figure 2.2**: The spatial distribution of all the H$\alpha$ emission stars in the 3°×3° field surveyed, overlaid on a map of the distribution of $^{13}$CO (J = 1→0) gas. Here and in all the subsequent figures shown in this work, the images are oriented so that North is up and East is left, unless explicitly said otherwise.

It is noteworthy that there are very few H$\alpha$ emitters in the northern part of the cloud complex. Several IRAS sources producing giant HH flows are located in the dense northern cloud cores, indicating that star formation is now starting here, but that the region has not been nearly as active in the past as the southern cloud cores.

A wide field H$\alpha$ CCD MOSAIC image (obtained in 2000 at the 0.9 m reflector on Kitt Peak, through an H$\alpha$ narrow-band filter, with total exposure time of $\sim$30 minutes) is shown in Fig. 2.3 with the largest concentration of H$\alpha$ emission stars located above the Cone Nebula.

I have also produced small finding charts for each one of the 357 stars. Each chart is $60''$ on the side centered on the referred star. For that I have extracted Digitized Sky Survey (DSS) images centered on each star coordinate and made tasks using `IDL` (Interactive Data Language) that automatically inserted the identification for the star and the marking cross in each figure. The tasks produced a final image in the `postscript` format with all the finding charts aligned on the page. Another output of the tasks is an electronic version of the full table in `HTML` format to be displayed on the web, where it is possible to see the individual finding charts by clicking in the identification number of each star. A sample of the finding charts is shown in Fig. 2.4 and the full set of charts is available in the electronic edition of the *Astronomical Journal* or at `www.fisica.ufmg.br/~tina/ngc2264`, where the electronic version of the full table is also available.

Among the 356 stars detected by 2MASS, 346 are above the completeness magnitude limits and are plotted in a $J-H \times H-K_s$ diagram in Fig. 2.5. Taking into account the 2MASS errors (around 0.05 mag), 80 $\pm$ 30 stars ($\sim$ 23%) are located to the right of the two dotted lines representing reddening vectors, demonstrating that they have infrared excess, an indication of the presence of circumstellar material. The fraction of infrared excess stars seems to be related to the evolutionary state of a young stellar group. According to Lada et al. (1996), we can have an age estimate of $\sim 5-7 \times 10^6$ years for a cluster of around 20% of infrared excess stars. Although our sample does not include all members of the NGC 2264 cluster, we can take this number as a rough approximation to the cluster age.

Even taking the 2MASS uncertainties into account, there are still 7 stars located to the left of the main sequence and giant loci and the reddening vector, where there should be no stars. Checking those stars individually in the finding charts, they all seem faint to normal stars. That could indicate that the real 2MASS errors are larger than the ones listed.

The spatial distribution of the infrared excess stars is plotted in Fig. 2.6, overlaid in the distribution of all the stars detected in the three 2MASS bands.

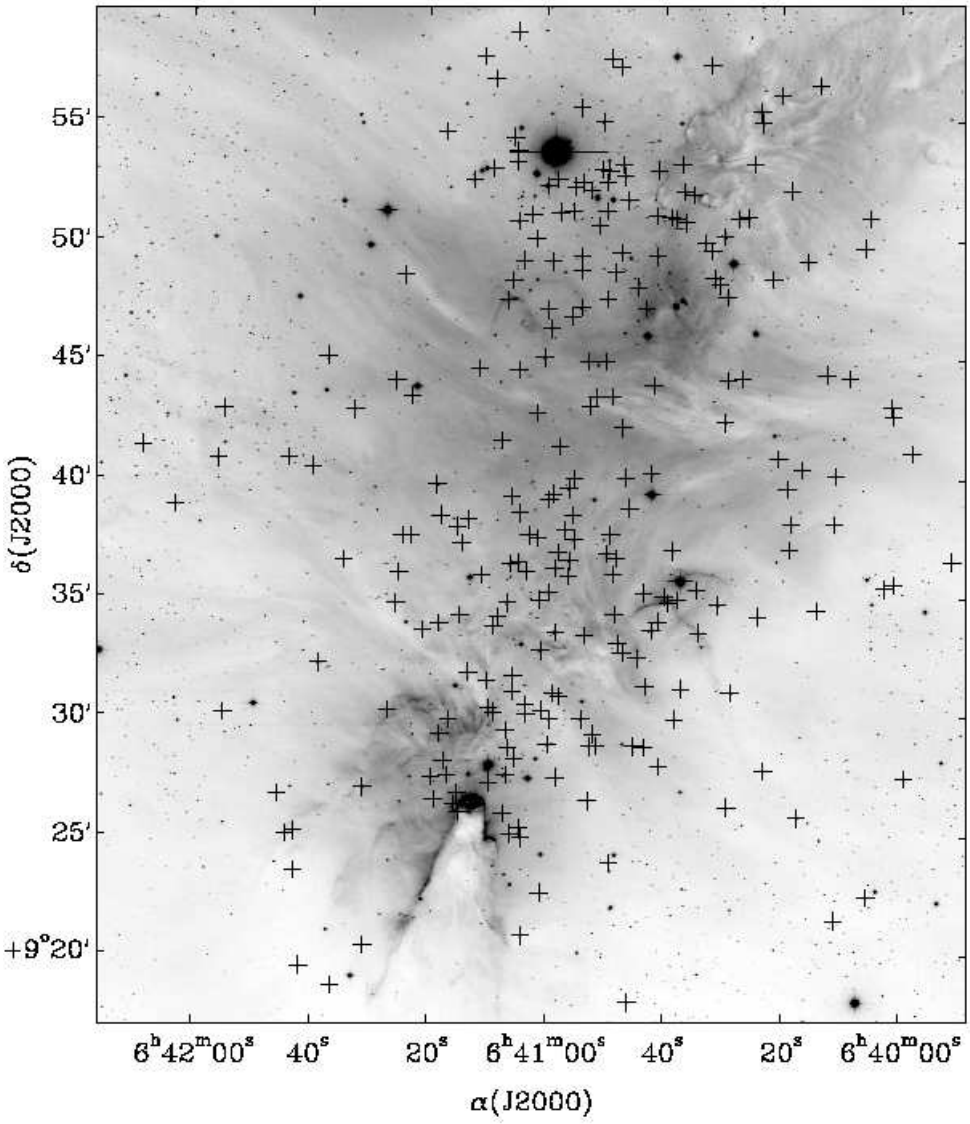


**Figure 2.3**: A wide field H$\alpha$ CCD MOSAIC image with the largest concentration of H$\alpha$ emission stars overlaid. This region shows 261 of the total of 387 stars found in the region. The Cone Nebula appears at the bottom of the image

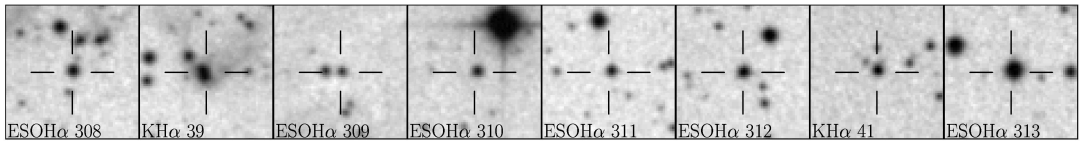


**Figure 2.4**: Examples of the finding charts produced for the H$\alpha$ emission line stars in NGC 2264, made with red images from the Digitized Sky Survey. Each chart is 60″ on the side.

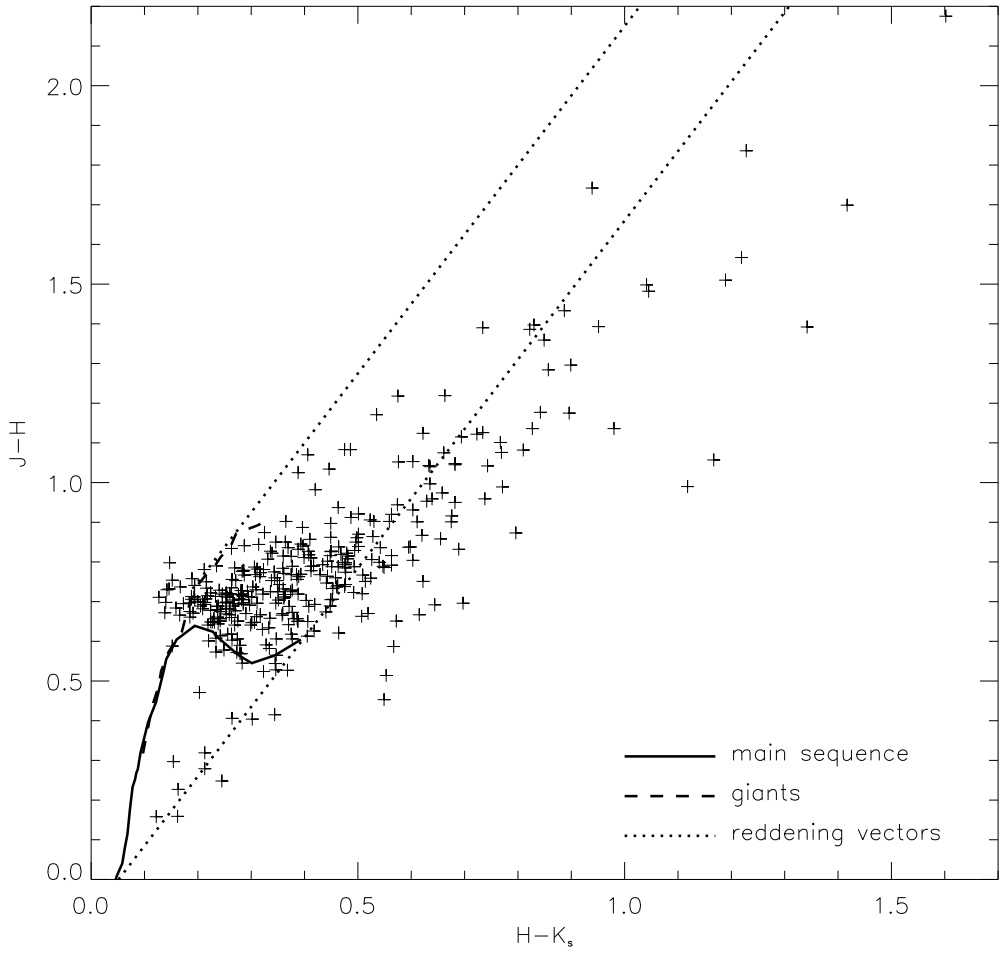


**Figure 2.5**: Near-infrared color-color diagram based on 2MASS data showing all the H$\alpha$ emitters with 2MASS detections in all the three bands ($JHK_s$). Main sequence and giant loci from Bessel & Brett (1988) corrected to the 2MASS photometric system (Carpenter 2001), and extinction law from Rieke & Lebofsky (1985). All the stars located right of the two reddening vectors, represented as the dotted lines, have infrared excess ($\sim 23\%$).

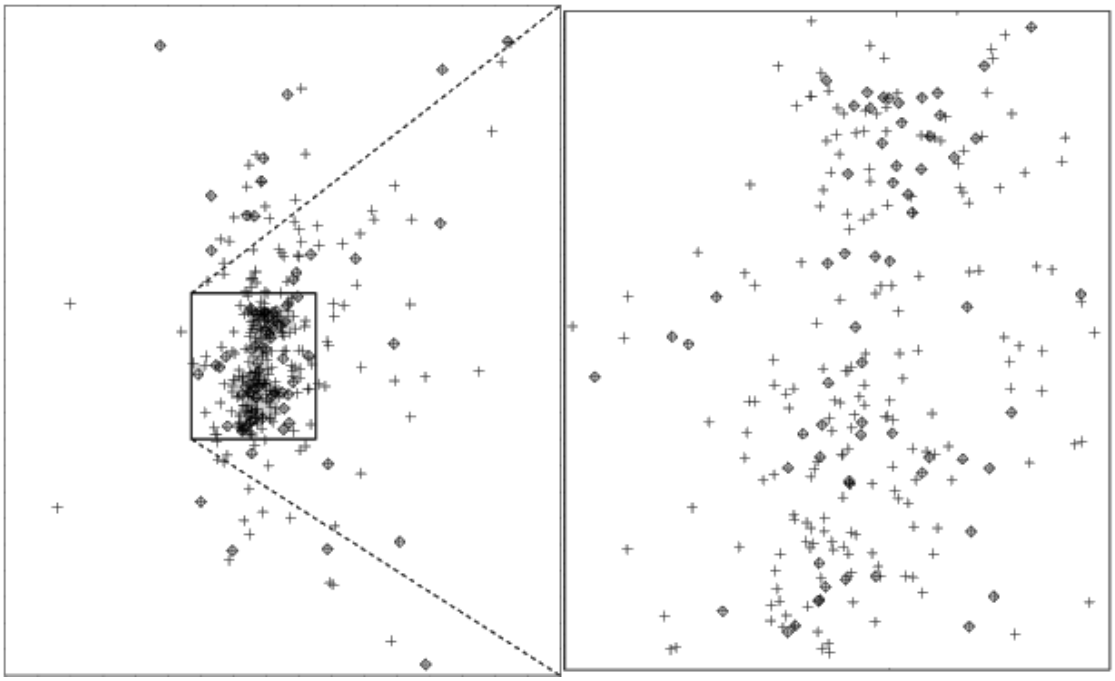

**Figure 2.6**: Spatial distribution of all the H$\alpha$ emission stars in NGC 2264 (+) with the infrared excess stars marked as diamonds. Left: the entire field; Right: a zoom of the highest concentration of H$\alpha$ emission stars.

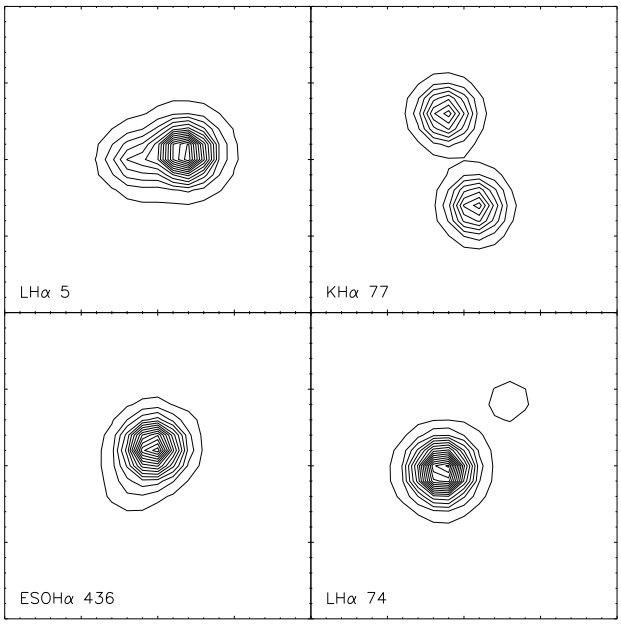


**Figure 2.7**: Examples of four doubles among the population of H$\alpha$ emission stars in NGC 2264. Each field is $8\farcs5 \times 8\farcs5$ and is extracted from an H$\alpha$ CCD image.

*A search for Pre-Main Sequence binaries:*

We have examined those of the H$\alpha$ emission stars which fall within the field of our deep wide-field CCD image obtained with the MOSAIC Camera at the KPNO 0.9m telescope (part of it shown in Fig. 2.3). The image is centered at 06:41:08.4 +09:29:43 (2000) with a field of $61' \times 61'$, a scale of $0\farcs45$/pixel, and contains 282 of the 387 H$\alpha$ emission stars detected. We have inspected each of these stars for the presence of close doubles (see examples in Fig. 2.7).

As discussed by Reipurth & Zinnecker (1993) in their optical CCD survey for companions to T Tauri stars, pollution by background stars is considerably diminished towards star forming clouds, which block much of the light from more distant stars. However, given the distance of about 800 pc to NGC 2264, pollution by foreground stars becomes an issue, and we have therefore restricted ourselves to components which are closer than $4''$ to the survey stars. 23 close binaries were found and are listed in Table 2.2., where we list the identification number, the separation of the stars in arcseconds and the position angle of the fainter component relative to the brighter one. Stars which are not cleanly separated on the images are listed as blends, and their measured separations are merely best estimates.

**Table 2.2**: H$\alpha$ emission stars with close components

| Identification | Separation($''$)[a] | P.A.($^\circ$) | Comment |
|---|---|---|---|
| ESOH$\alpha$ 345 | 2.8 | 205 | |
| LH$\alpha$ 5 | (1.9) | 99 | blend |
| KH$\alpha$ 77 | 2.8 | 18 | |
| ESOH$\alpha$ 377 | (1.2) | 20 | blend |
| LH$\alpha$ 27 | 3.0 | 172 | |
| ESOH$\alpha$ 419 | 3.6 | 180 | |
| ESOH$\alpha$ 427 | 2.7 | 273 | |
| ESOH$\alpha$ 436 | (1.3) | 150 | blend |
| KH$\alpha$ 102 | (1.4) | 153 | blend |
| LH$\alpha$ 43 | (1.2) | 241 | blend |
| ESOH$\alpha$ 450 | (1.3) | 324 | blend |
| KH$\alpha$ 107 | 3.3 | 81 | |
| ESOH$\alpha$ 471 | 3.7 | 165 | blend |
| ESOH$\alpha$ 473 | 3.8 | 95 | |
| ESOH$\alpha$ 474 | (1.4) | 141 | blend |
| ESOH$\alpha$ 476 | 3.2 | 245 | |
| ESOH$\alpha$ 484 | 1.4 | 180 | |
| KH$\alpha$ 115 | 3.1 | 263 | |
| ESOH$\alpha$ 512 | 1.8 | 236 | |
| ESOH$\alpha$ 518 | (1.1) | 32 | blend |
| LH$\alpha$ 368 | (1.3) | 336 | blend |
| LH$\alpha$ 74 | 2.5 | 317 | |
| LH$\alpha$ 79 | 3.3 | 38 | |
| ESOH$\alpha$ 400[b] | 2.3 | 69 | |

Notes:
[a] –For doubles which are not fully separated on the CCD images, the separation listed is only a best estimate.
[b] –This object is outside our wide-field CCD image, but was found to be a binary in the 2MASS survey.

At a distance of $\sim$ 800 pc, the peak of the binary separation distribution function is at less than $0''.1$, so we should expect a gradual increase in number of components towards smaller separations. Our detection limit is around $1''$ or a little higher. If we divide the doubles in Table 2.2 in three bins, with 1-2$''$, 2-3$''$, and 3-4$''$ separations we find 12, 4, and 7 pairs. While keeping in mind that we are certainly affected by small number statistics, this suggests that some of the wider pairs may not be physical binaries. Out of 282 H$\alpha$ emission stars we are thus finding less than 23 binaries with projected separations in the approximate range from 1000 AU to 3200 AU. The study of Reipurth & Zinnecker (1993) used the same detection technique, but they set an upper limit of $12''$ for their statistical analysis, which for objects in nearby clouds like Taurus and Chamaeleon implies an upper limit of about 1700 AU. We

can instead compare our detection of 12 binaries in the 1-2″ bin (800-1600 AU) with the detection of 8 binaries in the 800-1600 AU range by Reipurth & Zinnecker (1993) out of a sample of 238 stars. Within the uncertainties of the numbers, the two estimates of binary frequency are consistent.

A study of the spatial distribution of the H$\alpha$ emission stars and also their correlation with the molecular cloud in the region were performed using the final positions of the stars found. The complete study is presented in Appendix A.3 in the published paper: *H$\alpha$ emission-line stars in molecular clouds. I. The NGC 2264 region* (Reipurth et al. 2004).

*Results of the survey:*

1. A total of 357 H$\alpha$ emission stars were found, of which 113 were known from previous surveys and another 30 were simultaneously detected by another study (Rebull et al. 2002). The survey reaches stars with red photographic magnitudes between 18 and 19. A table with cross correlations were produced (including an electronic version), as well as individual finding charts for the stars.

2. The stars are strongly concentrated towards a region north of the Cone Nebula, coinciding with a major gas cloud core, but with an extended halo of stars that appears uncorrelated with the gas, suggesting that star formation has taken place in the area for several million years, giving time for the young stars to spread out from their birth place. A major cloud in the region north of NGC 2264 is associated with a few H$\alpha$ emiters, and star formation is likely to be in its initial phases there.

3. We have determined the fraction of H$\alpha$ emission line stars with infrared excess using 2MASS $JHK_s$ magnitudes. The fraction of $\sim 23\%$ is consistent with an age of 5 to 7 Myr for the cluster.

4. The fraction of binary stars within the separation range of 1000 AU to 3200 AU was estimated and it is consistent with similar studies in other regions.

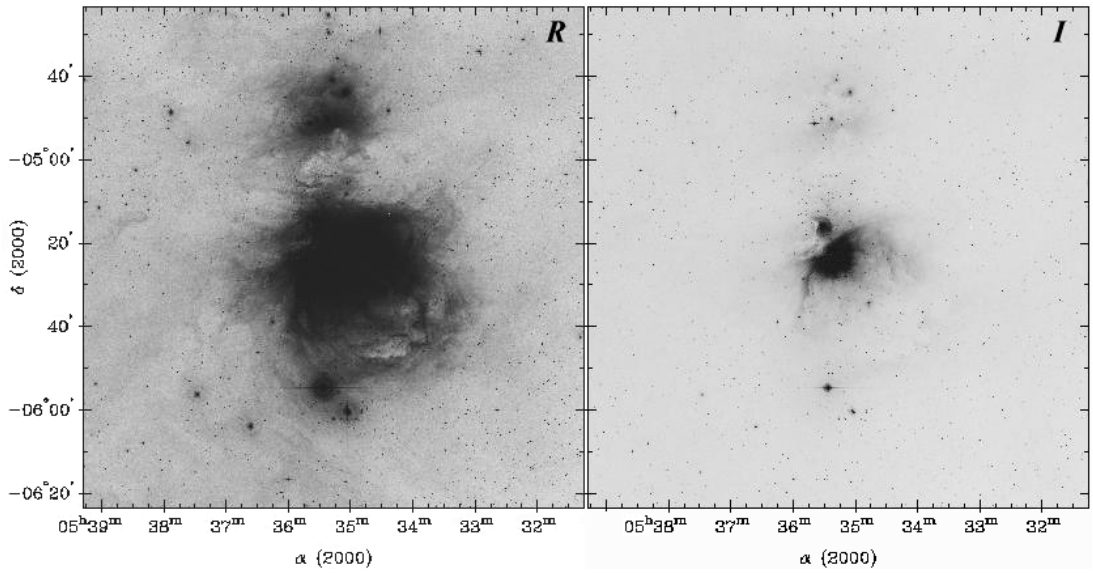


Figure 2.8: DSS images of the central 2°×2° of the field surveyed in the red and far-red filters.

## 2.2 M 42

The Orion Molecular Cloud (OMC) is located at a distance of ∼480 pc (Genzel et al. 1981). This is the nearest Giant Molecular Cloud, extending for many degrees in the sky, site of intense star formation and one of the most intensely studied regions of the sky. The visible part of the OMC, the M42 HII region, is excited by the Trapezium, a cluster of four massive young stars. M42 contains also a rich cluster of intermediate and low-mass young stars.

Of course many optical and near-infrared surveys to detect the cluster components have been performed, including surveys for H$\alpha$ emission stars. Some of the most relevant works include the catalogs of H$\alpha$ emission stars from Parsamian & Chavira (1982), with 537 stars, from Herbig & Bell (1988), with 735 stars, and from Wirami-hardja et al. (1989, 1991, 1993), with more than 1200 stars spanning an area almost 20° sided. Rebull et al. (2000) report the same type of search for circumstellar disk candidates in Orion as they did for NGC 2264 (Rebull et al. 2002, Section 2.1), in a region of ∼1°×1° in the central M 42 cloud. They report ∼230 active accretion disk candidates.

*The survey:*

About 2300 H$\alpha$ emission stars were initially identified by Bertil Pettersson in the Schmidt plates that covered a field of $5^\circ \times 5^\circ$ centered at the position $\alpha$: $05^h37^m00^s$

$\delta$: $-05^d28^m00^s$ (J2000). The finding charts were then given to me with the objective of getting coordinates, cross correlation with other surveys and magnitudes in public catalogs.

In order to get coordinates for the stars, I have extracted $35' \times 35'$ images from the Digitized Sky Survey, creating a mosaic that covered the whole region. The Digitized Sky Survey (DSS) comprises a set of all-sky photographic surveys in several colors performed with the Palomar and UK Schmidt telescopes. The Catalogs and Surveys Branch (CASB) of STScI is digitizing the photographic plates to support Hubble Space Telescope observing programs but also as a service to the astronomical community. The POSS-II surveys (from 1987/1988), that provide $B_jRI$ images with a plate scale of $1''$/pix, were used here. The images were retrieved in `FITS` format and had astrometric information in their headers. The task `MAKEWCS` from the `IRAF` image reducer package was used on each image to add a coordinate system that can be understood by `IRAF`. The task `IMEXAMINE` was then used to determine the coordinates of each star visually identified in the finding charts.

Figure 2.8 shows the central part of the region surveyed, a field of $2^\circ \times 2^\circ$ extracted from $R$ and $I$ plates of the Digitized Sky Survey. $R$ images were used to measure the coordinates for most of the stars, and $I$ images were used in regions where the nebulae are too bright at optical wavelengths.

Bertil Pettersson assigned an H$\alpha$ strength to each star, following the same procedure used for NGC 2264, and then selected only the stars identified as certainly possessing emission, which reduced the number of stars in our survey to 1932. The spatial distribution of those stars is shown in Fig. 2.9.

The Herbig & Bell (1988) catalog (HBC) have 125 stars inside our field, of which we detected 51. The HBC was compiled of stars observed with many different techniques, and many of them have very weak emission. Most of the stars in common with the HBC are listed there with H$\alpha$ equivalent widths larger than 15Å. So, as already suggested by the survey in NGC 2264 (previous section), our surveys does not detect many weak-line emission stars.

Among the 519 stars from the catalog of Wiramihardja et al. (1993) that lie inside our field, only 203 were detected by us, 29 of them overlap with HBC stars. The fraction of stars in common is only about 39%. That small fraction is puzzling and should be checked more carefully. Our survey is much deeper than Wiramihardja's (our long exposures reach 150 minutes while Wiramihardja's maximum exposures are 90 minutes), thus maybe the 316 stars not detected in our survey are spurious detections. It is necessary an individual inspection of those 316 stars in our plates. Only after that checking we will give final ESOH$\alpha$ numbers to the stars in our survey that do not have counterparts in the other surveys.

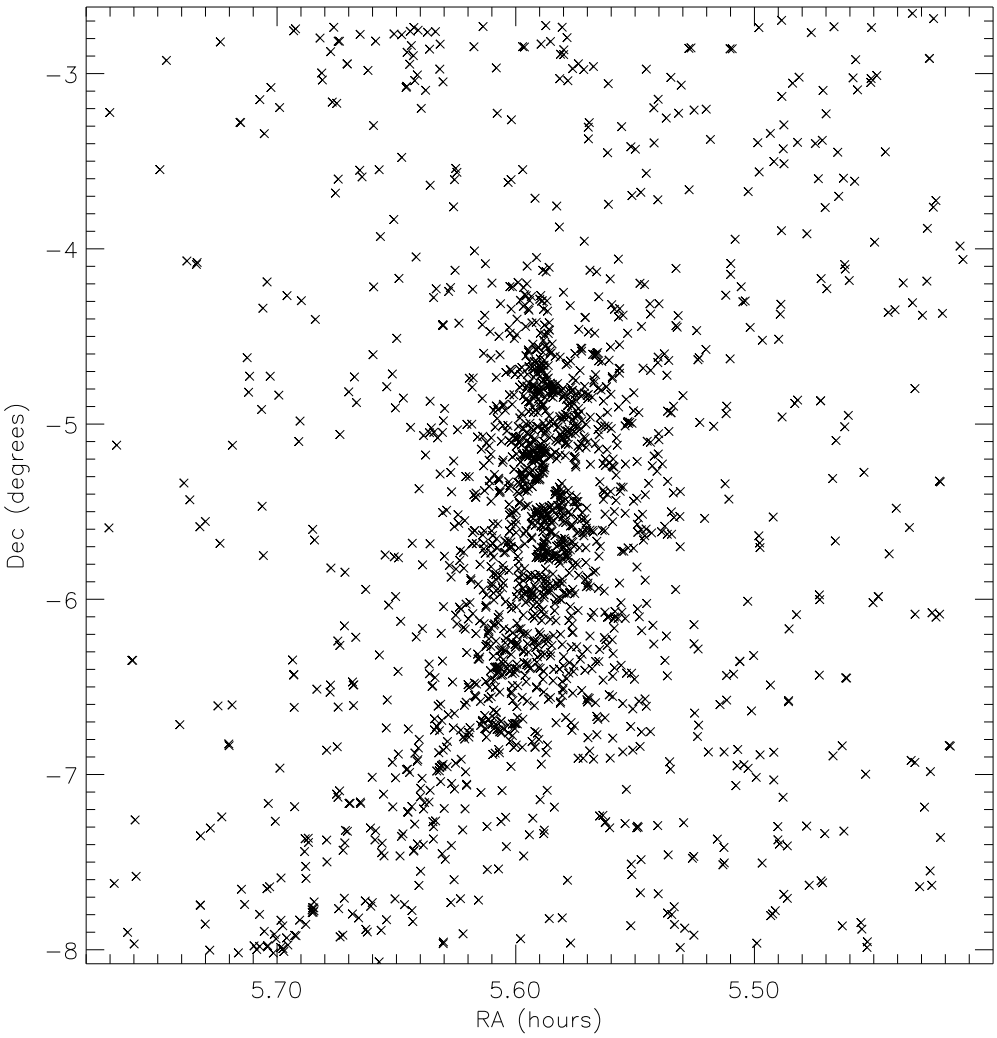


**Figure 2.9**: The spatial distribution of the 1932 H$\alpha$ emission stars in our M42 survey. The patches empty of stars in the central region are located where the reflection is too intense, even in the shortest exposures.

The variability of the young stars may account for some of this difference. The plates used for the Wiramihardja catalog were obtained between 1985 and 1987, a decade before ours. The fraction of stars in common is only about 39%. If we go back to the NGC 2264 survey, in comparison to the Ogura (1984) survey, we have a time interval of more than a decade, and a fraction of common stars of $\sim$ 37%. Thus, the time difference can be the source of the some of the difference between the surveys. That is supported by spectroscopic studies of young stars that reveal that the H$\alpha$ emission stars are very active and that the emission line profiles differ from a large amount even in a small time scale (Alencar & Batalha 2002).

The H$\alpha$ emission stars of our survey detected in all the three bands of the 2MASS near-infrared catalog are plotted in a color-color diagram in Fig. 2.10. Of the 1894 stars with $JHK_s$ magnitudes, 1879 have magnitudes above the completeness limits. $274 \pm 100$ have infrared excess, one indication of the presence of circumstellar material. Fig. 2.11 shows the spatial distribution of those stars, and it is seen that it follows the pattern of density of the H$\alpha$ emission stars. The fraction of about 15% ($\pm$ 5%) of stars with infrared excess is a bit smaller than the fraction of 23% ($\pm$ 8%) obtained for the NGC 2264 region, although within the uncertainties those fractions can be similar. That could indicate that on average the H$\alpha$ emission stars in M 42 have less circumstellar material than the stars in NGC 2264. It may be that the stars in M 42 are more evolved than in NGC 2264, but it is believed that NGC 2264 is slightly older than M 42 (Rebull et al. 2000). Alternatively, it may be that the M42 stars had their surrounding material more rapidly wiped away for the action of the more complex processes in M 42. Many processes can shave off the outer parts of the disks, like close encounters of stars caused by their motion through the potential well of the cluster, the radiation of the brighter energy sources, and the action of numerous and powerful outflows.

Even within the errors, 16 stars (less than 1%) are located in the "forbidden" region to the left of the main sequence loci and the reddening vectors, all of them faint and/or located in nebulous regions, again implying that the 2MASS uncertainties can be greater than thought.

A table with the H$\alpha$ emission stars in M 42 was built similarly to the NGC 2264 survey. Some representative lines are listed in Table 2.3. The full table is available at `http://fisica.ufmg.br/~tina/m42`. The first columns are: the preliminary identification number of our survey, the HBC number and the Wiramihardja et al. (1993) identification number. The fourth column gives the identification number assigned in a study of variability of the stars in M 42, made by Gustavo Lima (Lima 2003). He used digitized versions of direct Schmidt plates scanned by SUPERCOSMOS and developed a software that searches for variability between the different plates (his work is going to be submitted to A&A still in 2005 and a future conjunct

**Table 2.3**: Part of the final table of H$\alpha$ emission line stars in M 42

| Id | HBC | W+ | Var. | $\alpha$(2000) | $\delta$(2000) | H$\alpha$ | $m_J$ | $m_F$ | $m_N$ | $J$ | $H$ | $K_s$ |
|---|---|---|---|---|---|---|---|---|---|---|---|---|
| 80 | ... | 630 | 2210325207:16 | 05 30 38.4 | -05 25 43 | 3 | 15.57 | 14.40 | 13.57 | 12.09 | 11.40 | 11.10 |
| 1 | ... | ... | 2220284008:03 | 05 31 12.8 | -03 12 11 | 1 | 18.83 | 17.44 | 15.99 | 14.23 | 13.60 | 13.34 |
| 559 | 110 | ... | 2200373812:12 | 05 33 55.8 | -04 47 50 | 3 | 17.30 | 15.28 | 14.44 | 13.12 | 11.99 | 11.10 |
| 248 | 488 | 998 | 2210753619:09 | 05 38 03.9 | -04 16 43 | 3 | 14.75 | 15.84 | 13.96 | 12.63 | 11.96 | 11.58 |

Note.– The full table with all the 1932 H$\alpha$ emission stars is presented electronically at `http://fisica.ufmg.br/~tina/m42`. The portion presented here is intended only to show form and content.

analysis of variability $\times$ emission is planned). The coordinates are given in the next columns, followed by the magnitudes obtained in the USNO-B catalog ($m_J$, $m_F$, and $m_N$) and in 2MASS ($JHK_s$).

*Result of the survey:*

We have compiled a catalog of 1932 H$\alpha$ emission stars in M 42, probably $\sim$1680 are newly detected. The fraction of infrared excess stars was estimated. The same study of spatial distribution will be performed, similarly to the NGC 2264 study.

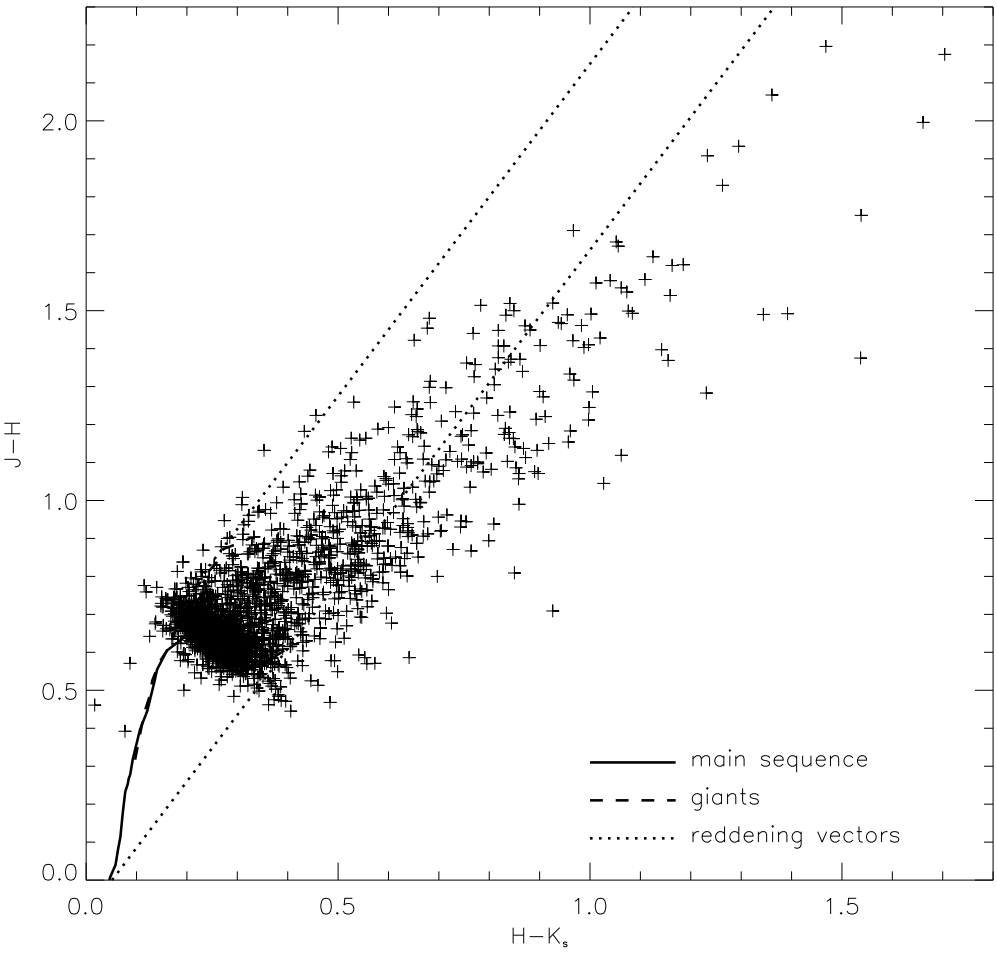


**Figure 2.10**: Near-infrared color-color diagram based on 2MASS data showing all the H$\alpha$ emitters in M42 with 2MASS detections in all the three bands ($JHK_s$). Main sequence and giant loci from Bessel & Brett (1998), corrected to the 2MASS photometric system (Carpenter 2001), and extinction law from Rieke & Lebofsky (1985). All the stars located right of the two reddening vectors, represented as the dotted lines, have infrared excess. There are 281 of them.

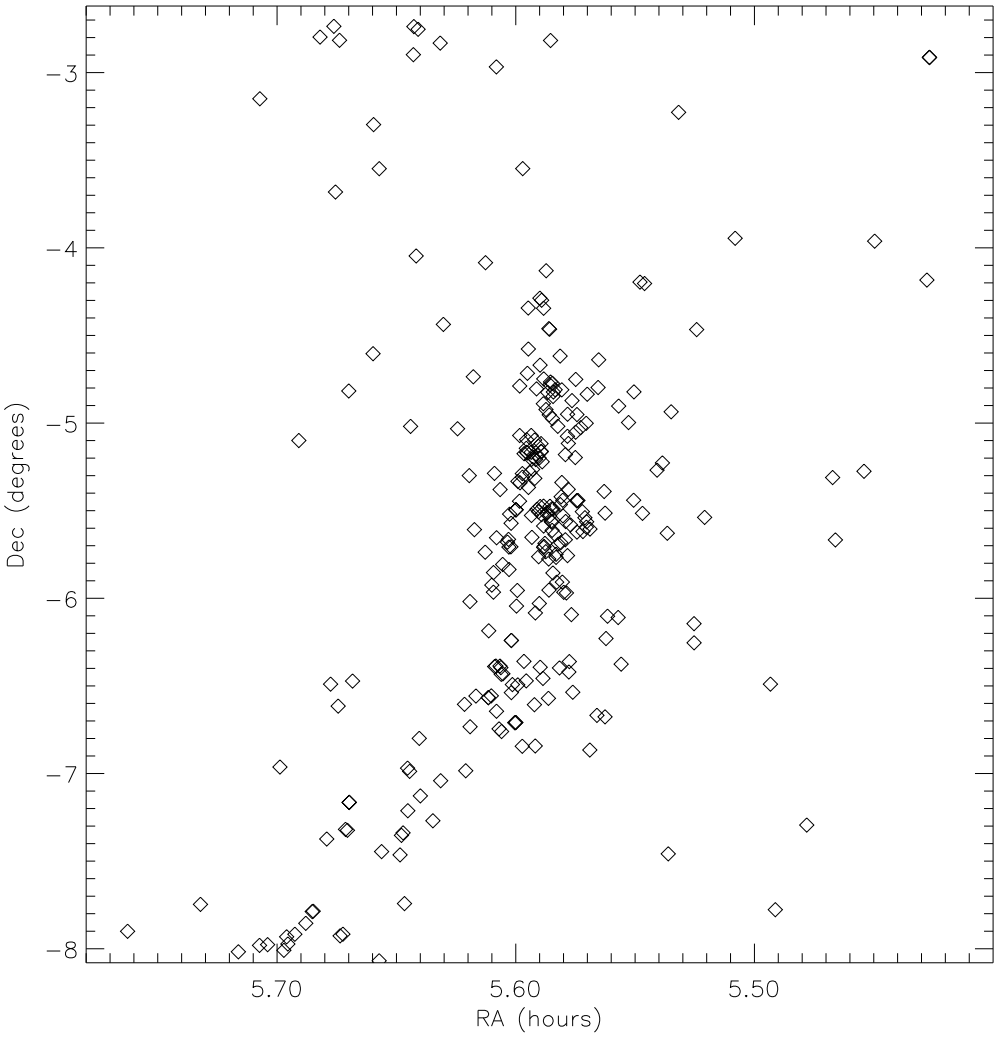


Figure 2.11: The spatial distribution of the 281 H$\alpha$ emission stars with infrared excess in M 42.

# Chapter 3

# Surveys for Herbig-Haro Objects

In this chapter we present observations of Herbig-Haro objects in optical narrow band images, with filters centered on the H$\alpha$ 6563Å and [SII] 6717/6731Å emission lines, tracers of the shocks of the outflows.

In the attempt to detect previously unknown outflows, broad band images are used for comparison. The spectrum of a Herbig-Haro (HH) object shows emission lines, but very weak continuum, thus they are not detected in broad band images that avoid the wavelengths of the characteristic emission lines (images using I-band filters, for example). A reflection nebulae, on the other hand, can also be located near star forming regions and have the same diffuse structure, but it emits in all wavelengths, being visible in broad band images.

When previous images of the same field were available, the proper motion of the outflows were determined, by measuring the difference in position of the HH knots relative to the stars.

Section 3.1 presents a wide field survey of the HII region S140 for Herbig-Haro objects. Section 3.2 describes how we have used previous ground based wide field images of the star forming cloud Lynds 1551 in addition to new observations (after a time interval of 4 years) in order to measure the proper motions of the numerous HH objects in that region. We have also detected new outflows. Section 3.3 describes the use of the same technique for proper motion measurement, this time with Hubble Space Telescope images of the jet HH 47 (with a time separation of 5 years), for future dynamical studies.

## 3.1 S140

S140 is an HII region located at the southeast edge of the Lynds 1204 dark cloud. The ionizing stars are probably the massive stars of the open cluster NGC 7160. (Crampton & Fisher 1974). The cloud core adjacent to S140 contains a compact embedded infrared cluster of about 50 proto-stars, among which are IRS 1, IRS 2 and IRS 3, with luminosities of 5, 3 and 2 $\times$ $10^3$ $L_\odot$, respectively, implying intermediate to high mass proto-stars. Ogura et al. (2002) found 8 H$\alpha$ emission stars just outside the bright rim of the cloud. This suggests that the S140 region may represent an example of propagating star formation induced by the external UV radiation.

The bright infrared sources have been the subject of several studies, and molecular outflows were identified inside the cloud by many authors. Most of them are associated with the IRS 1, 2 and 3. Preibisch & Smith (2002) present high-resolution infrared imaging of the infrared sources and outflows and give an overview of the star formation process in the region. Preibisch et al. (2001) demonstrate that IRS 3 drives outflows in several directions and Preibisch et al. (2003) report the confirmation that two distinct bipolar outflow systems are driven by IRS 1. The outflows are always perpendicular to the rotation axis of the source so, if there are two outflows apparently originated at the same spot, it is most likely a binary source.

In order to search for optical signs of shocks, we have surveyed the region using H$\alpha$ and [SII] filters in wide field images, and we have found a number of Herbig-Haro objects, including two bow shocks bursting out of the molecular cloud into the HII region.

### 3.1.1 Observations

The images presented here were obtained on October 12, 2001, at the f/3.1 prime focus of the 4m Mayall reflector located on the Kitt Peak National Obsevatory (KPNO) near Tucson, Arizona, using the MOSAIC imager. MOSAIC consists of eight 2048 $\times$ 4096 pixel CCDs arranged as an 8192 $\times$ 8192 pixel detector. On the 4m telescope, pixels are $0''.26$ on the sky, providing a field of view of approximately $36' \times 36'$. We used the H$\alpha$ and [SII] narrow-band (FWHM = 80Å) filters, centered at 6569Å and 6730Å respectively. The CCDs are separated by 50 pixel gaps. Sets of 5 dithered exposures were taken, in a way that the combination of frames would remove the gaps from the final images, as well as minimize the effects of bad columns and pixels. We also used the KPNO i' broad band filter, centered on 7732Å with FWHM of 1548Å , to obtain one image of the continuum emission, used for com-

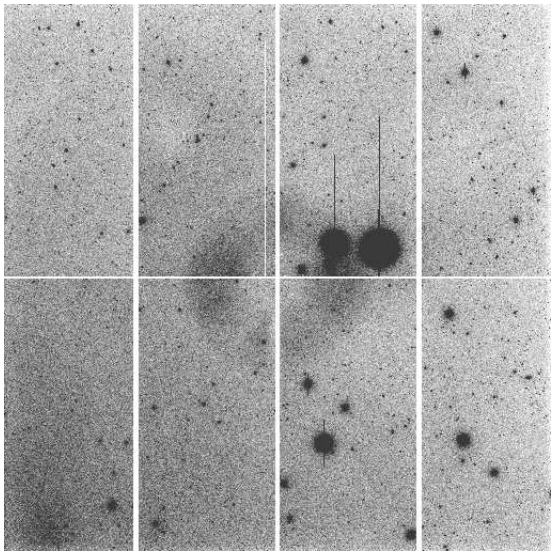

**Figure 3.1**: Exammple of a raw image obtained with the KPNO MOSAIC imager, where the gaps and a bad column can be seen, as well as the central reflection ring (*pupil*).

parison in the search for Herbig-Haro objects. The time exposures were 400 s for each image taken through the narrow band filters and 30 s for the continuum filter.

The images were reduced using the `IRAF` package `MSCRED`, which is designed especially for the reduction of images from mosaic CCD detectors (Valdes 2001). Mosaic images are composed of multiple images, one for each CCD. The reduction process corrects each raw CCD image from instrumental artifacts and photometric variations. This includes the removal of crosstalk artifacts, electronic bias subtraction using over-scan data, exposure bias patterns subtraction using a zero calibration mosaic and dark pattern subtraction. Flat fielding is done using the mean of all the images in the flat field calibration mosaic, ensuring that the relative gains between the images are also removed.

Despite anti-reflection coatings in the corrector there is a faint *pupil image* caused by reflections in the KPNO Mayall telescope. This appears as a large ring pattern in the center of the field of view (see Fig. 3.1). The task `MSCPUPIL` is used to model such a pupil pattern and the task `RMPUPIL` is used to scale and remove the pupil from the mosaic exposures.

It is fundamental to perform astrometric calibration for a mosaic in order to create single images where the pixels from the different pieces of the CCD are in the proper relation to each other. The pixel positions and sizes have to be geometrically corrected to make it possible to register and stack the multiple exposures. The packages `MSCSETWCS, MSCZERO` and `MSCCMATCH` are used in this procedure. A *world*

*coordinate system* (WCS) is derived for each mosaic image by associating object coordinates from a reference catalog with the pixel positions of the objects in the image. The task `MSCIMAGE` re-samples the mosaic images into a single image. The next step is to combine dithered exposures which have been re-sampled into a single image with a uniform and registered pixel sampling, with the task `MSCSTACK`. That will fill in the mosaic gaps, eliminate bad pixels and create deeper final images.

In order to search for Herbig-Haro objects, each section of the final images were examined very carefully, comparing each filter. Any nebulous structure identified in the H$\alpha$ or [SII] images were searched for in the i' band image. If there was no counterpart, the object was identified as a probable Herbig-Haro object. Its structure and location was then analyzed to certify the identification. The location nearby young sources and/or along the axis of other shock structures makes the identification almost certain, while further spectral analysis can confirm it.

### 3.1.2 New Outflows

Two bow shocks, named HH 616 and HH 617, were identified bursting out of the cloud into the HII region. They trace the lobes of protostellar outflows as they break out of their parent molecular cloud into the low-density interior of the S140 HII region. The northern bow shock, HH 617, is likely the counterflow of the P.A. = 65° / 245° molecular hydrogen outflow from S140 IRS 3 (Preibisch et al. 2001). The larger and higher velocity southern bow shock, HH 616, has an axis of symmetry that extends toward the southwest at P.A. = 60°. It consists of a series of smaller bow shocks, indicated in Fig. 3.2 as A to F. Since this shock is located about 1.′5 south of the northern object, the axis passes about 1′ south of the infrared cluster, so this flow is probably energized by an unknown source south of the cluster. A spectral analysis of the velocities and the large [SII]/H$\alpha$ line ratio indicate that those are indeed Herbig-Haro objects, and not just elephant trunks (commonly seen projected into HII regions). A faint [SII] jet, consisting of a 40″ long chain of knots, can be traced from the tip of HH 616 back into the molecular cloud. It was named HH 615 and traces the jet that powers the bow shock HH 616. $H_2$ images by Preibisch & Smith (2002) show knots that probably trace embedded components of this flow.

The bright inner shocks of HH 616 are surrounded by a much fainter and much larger shell of H$\alpha$ streamers that is concentric with the bow (labeled *arch* in Fig. 3.2 and best seen in Fig. 3.3). This feature is about 3 times as large as the [SII] bright bow and may indicate the extent of the region that has been influenced by the outflow bursting out of the cloud.

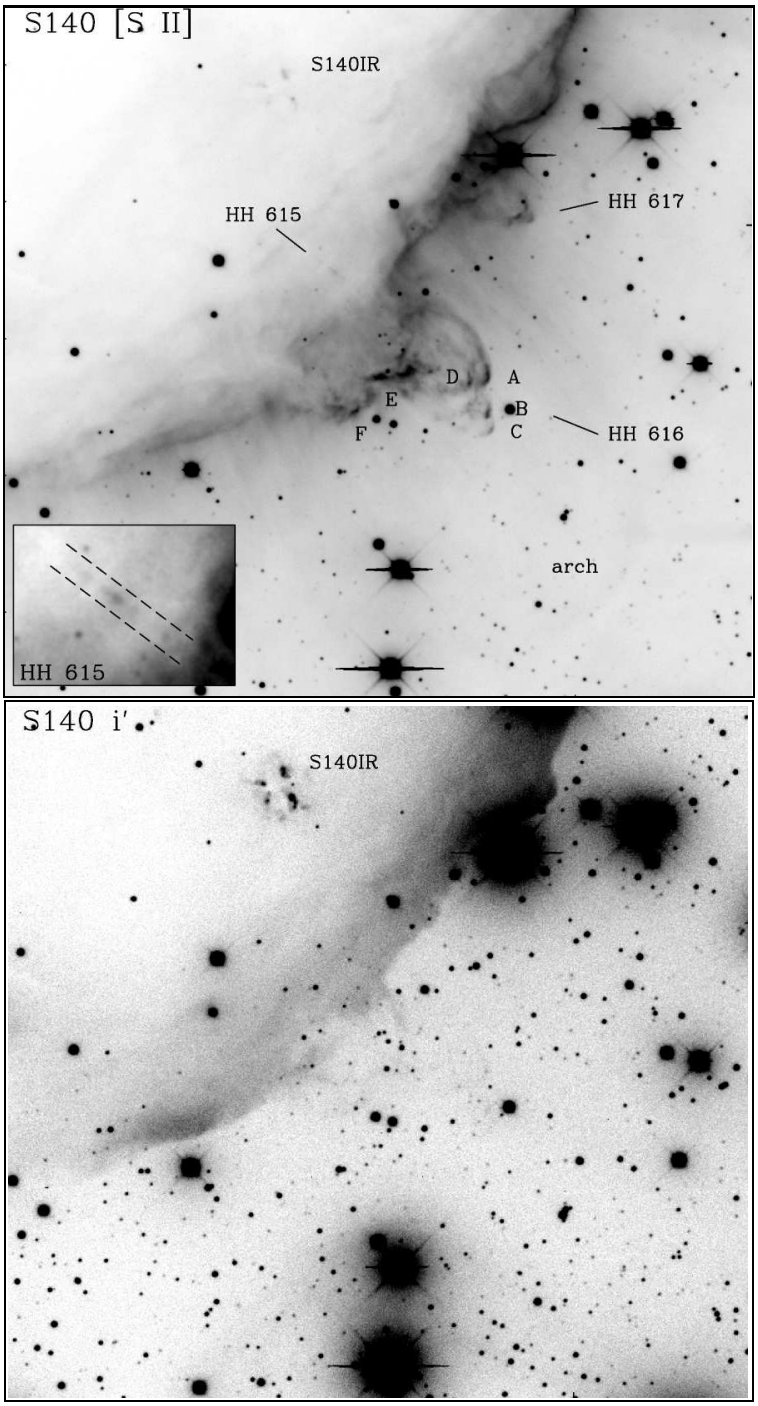


**Figure 3.2**: The S140 ionization front in a $5' \times 5'$ field. The upper figure is an [SII] image showing the Herbig-Haro objects identified. The inset at lower left shows HH 615 in more detail ($46'' \times 33''$). The lower figure is the continuum i' image of the same region, where the Herbig-Haro objects are not seen. S140IR indicates the position of the infrared cluster.

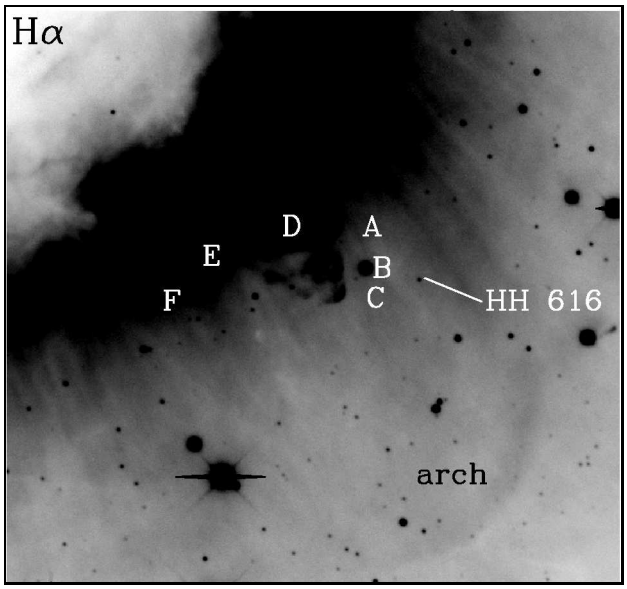


**Figure 3.3**: A deep cut of the Hα image with indication of the positions of the HH 616 knots and the arch feature. The field is 3′×3′.

Other faint Herbig-Haro objects, HH 618 and HH 623, were found in the L1204 cloud about 3′ east of the infrared cluster complex (Fig. 3.4). These HH knots are so faint that it is very hard to conclude anything about their morphology or point of origin.

Another center of star formation, S140 North, is located 11′ north of the S140 infrared cluster, where an IRAS source (22178+6317) is known to drive two molecular outflows. One of them (Fukui et al. 1986) is associated with a line of four Herbig-Haro objects, HH 251 to 254 (Eiroa et al. 1993) and with $H_2$ flows found by Davis et al. (1998), that also report the existence of the second CO flow, with an east-west orientation. Four new Herbig-Haro objects were found in this region (Fig. 3.5). One of the new shocks, HH 621, likely represents the counterflow to the previously known HH 251–254. It is indicated in Fig. 3.5. Another pair of new Herbig-Haro objects, HH 619 and HH 620, is located due west of IRAS 22178+6317 and appear to be associated with the east-west CO outflow. Finally, there is a prominent arc-shaped reflection nebula facing southwest located about 3′ northeast of IRAS 22178+6317 that appears to be associated with a star located on the northeast rim of the arc. A compact and [SII] bright HH object, HH 622, is located along the western rim of the reflection nebula. It seems, then, that S140N has at least three active outflows.

Additional new HH objects, HH 609 to 614, and faint reflection nebulae were identified in a previously unknown region of star formation, here dubbed S140NE, in the L1204 dark cloud about 15′ northeast of the infrared cluster (see Fig. 3.6). Table 3.1

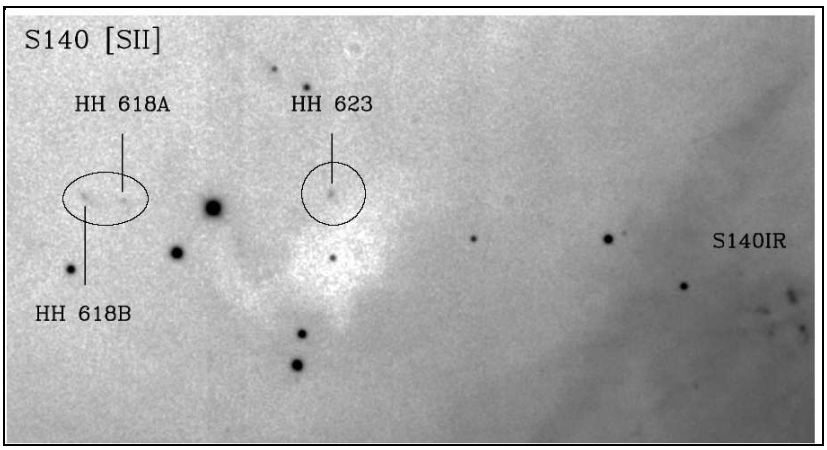


**Figure 3.4**: [SII] image of the region east to the infrared cluster showing HH 618 and HH 623. The field is $2\farcm5 \times 5'$.

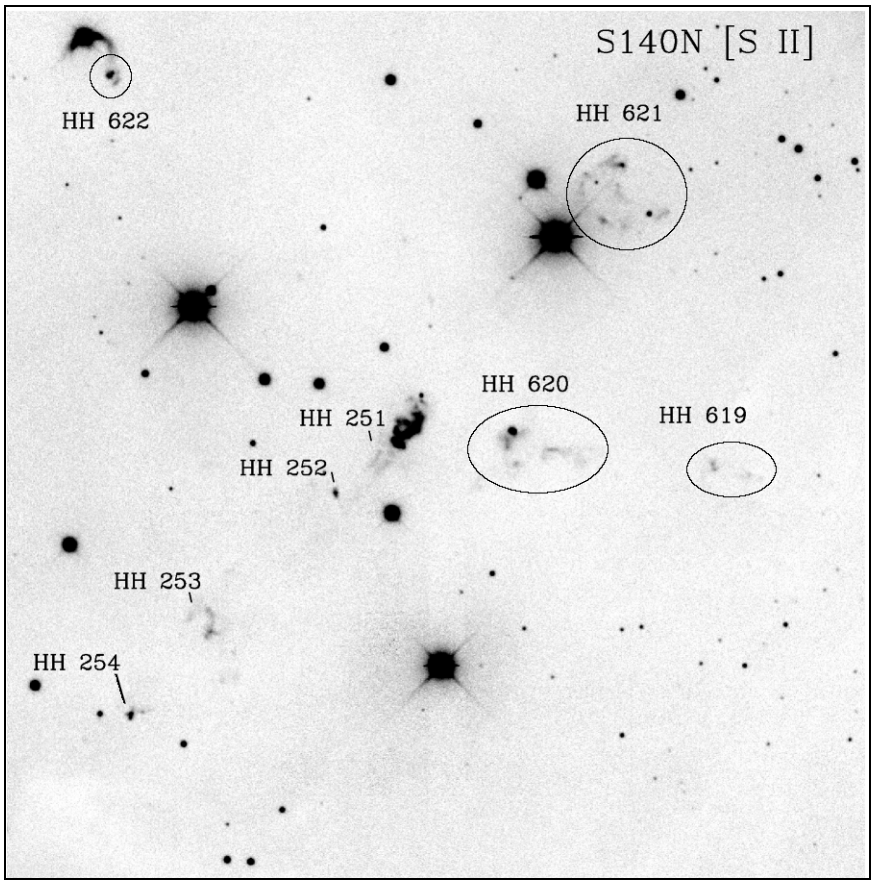


**Figure 3.5**: [SII] image showing the Herbig-Haro objects in S140 North. The field is approximately $6' \times 6'$.

lists all the Herbig-Haro objects detected in the S140 regions.

None of the outflows in the S140 region show parsec-scale dimensions. It is possible that star formation in this region has only started very recently or that the outflows have been bottled up by a combination of random flow re-orientations in the highly dynamical environment of a dense cluster or by the presence of a high-density massive cloud surrounding the site of star formation. Finally, it is possible that outflows that do burst out of the parent cloud into the HII region are rapidly dispersed by ionization and heating. The faint arch feature located about 1 pc southwest of the base of HH 616 may be a remnant of this process.

The results of this survey, as well as a spectral analysis of the Herbig-Haro objects found are presented in detail in the paper: *The Fountains of Youth: Irradiated Breakout of Outflows in S140* (Bally et al. 2002), shown in the Appendix A.1.

**Table 3.1**: Herbig-Haro objects in the S140 region.

| Object | $\alpha(2000)^a$ | $\delta(2000)^a$ | Comments |
|---|---|---|---|
| | | | S140 |
| HH 615 | 22 19 15.6 | 63 17 29 | [SII] jet aimed at HH 616A |
| HH 616A | 22 19 05.9 | 63 16 43 | Northern tip |
| HH 616B | 22 19 05.9 | 63 16 26 | Middle tip |
| HH 616C | 22 19 05.7 | 63 16 19 | Southern tip |
| HH 616D | 22 19 07.1 | 63 16 40 | Inner shock |
| HH 616E | 22 19 12.8 | 63 16 43 | [SII] edge, southern rim of HH 616 |
| HH 616F | 22 19 14.3 | 63 16 28 | [SII] edge, southeastern rim of HH 616 |
| HH 617 | 22 19 03.0 | 63 17 53 | Northern bow; tip of northern breakout |
| HH 623 | 22 19 55.0 | 63 19 30 | Faint knot east of S140IR |
| HH 618A | 22 19 53.0 | 63 19 29 | Western part of pair, east of S140IR |
| HH 618B | 22 19 54.9 | 63 19 30 | Eastern part of pair, east of S140IR |
| | | | S140 N |
| HH 251 | 22 19 34.4 | 63 32 57 | From Eiroa et al. (1993) |
| HH 252 | 22 19 37.8 | 63 32 38 | From Eiroa et al. (1993) |
| HH 253 | 22 19 45.0 | 63 31 45 | From Eiroa et al. (1993) |
| HH 254 | 22 19 49.6 | 63 31 14 | From Eiroa et al. (1993) |
| HH 619 | 22 19 16.4 | 63 32 49 | Two knots in east-west flow |
| HH 620 | 22 19 27.6 | 63 32 50 | Cluster of three knots south of nebular star |
| HH 621 | 22 19 21.5 | 63 34 44 | Cluster of knots:HH 251–254 counterflow |
| HH 622 | 22 19 50.6 | 63 35 18 | Pair of knots at P.A. = 220°from nebular star |
| | | | S140 NE |
| HH 609 | 22 21 28.8 | 63 30 02 | Southwestern [SII] knot in chain of two |
| HH 610 | 22 21 33.3 | 63 37 34 | Tiny knot west of reflection nebula |
| HH 611 | 22 21 39.5 | 63 36 53 | Compact groups of [SII] knots |
| HH 612 | 22 21 54.5 | 63 34 39 | Compact diffuse [SII] knot |
| HH 613 | 22 21 58.5 | 63 33 23 | Faint [SII] group |
| HH 614 | 22 22 01.2 | 63 27 56 | Diffuse [SII] complex |

Note $^a$ –Units of right ascension are hours, minutes, and seconds, and units of declination are degrees, arcminutes, and arcseconds.

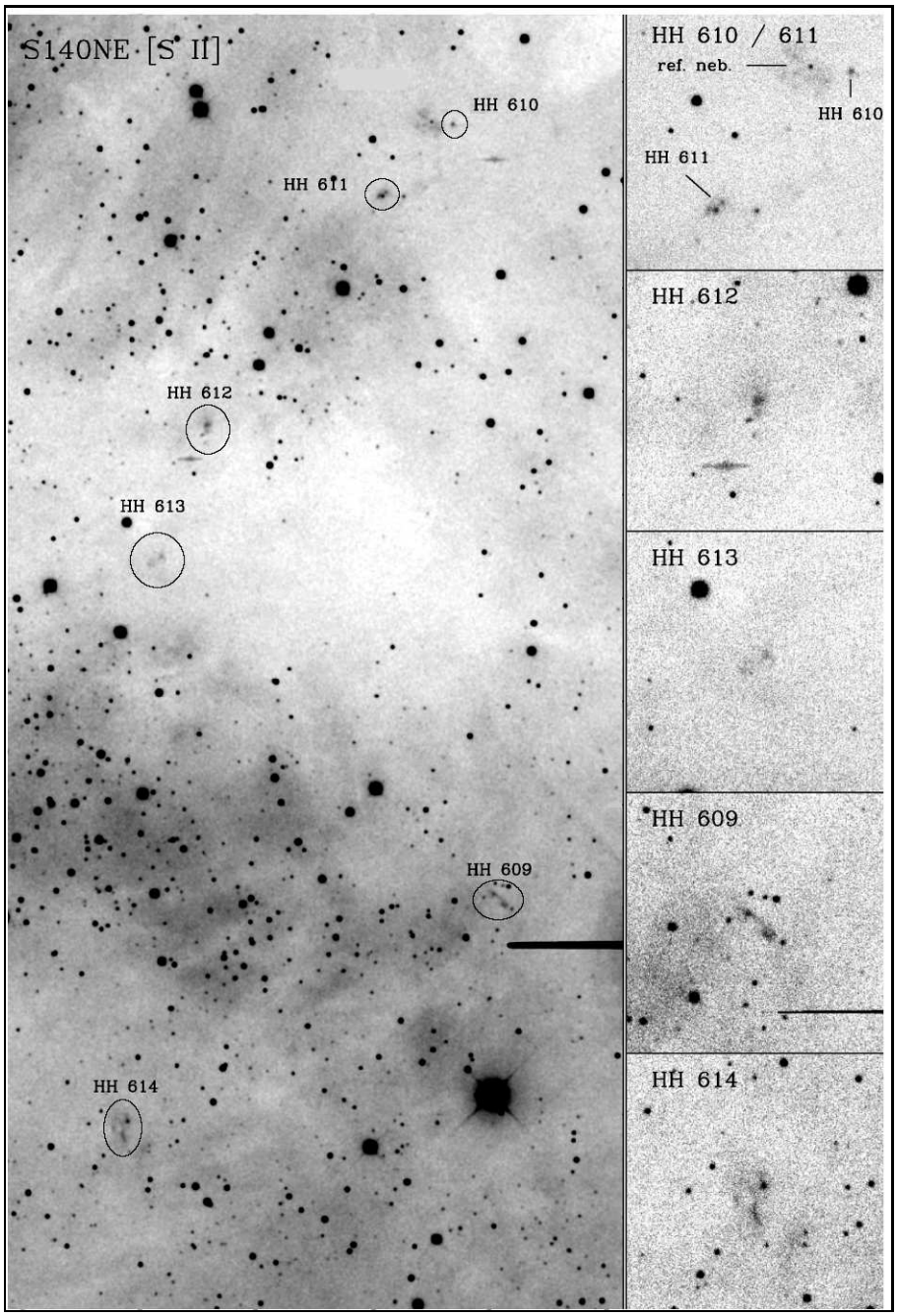


**Figure 3.6**: [SII] image image showing the Herbig-Haro objects in the S140 Northeast region, a $12\farcm5 \times 6'$ field. The small figures show the HH objects in detail.

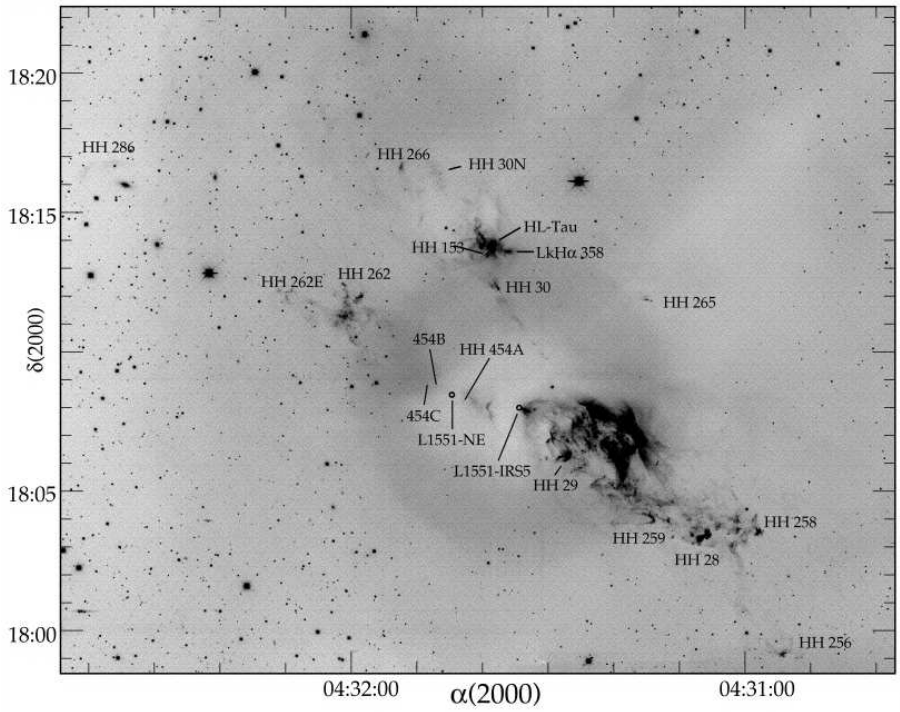


**Figure 3.7**: Wide field KPNO MOSAIC image showing the H$\alpha$ + [SII] emission in L1551. Several previously known HH objects are shown. Image from Devine et al. (1999) that shows the first epoch images used in the proper motion determination. See the instrumental reflection ring around the center, as mentioned in the text.

## 3.2 L1551

The Lynds 1551 dark cloud is a nearby (140 pc) star-forming region that has been extensively studied using various techniques (e.g., Strom et al. 1976; Stocke et al. 1988). It is part of the Taurus molecular cloud complex, where low mass star formation is occurring in a relatively quiet environment and the young stars are dispersed enough so that their evolution does not interfere with its neighbors. L1551, however, is a very active star forming region, where the several young stars drive powerful outflows that sometimes overlap, creating a very complex array of Herbig-Haro objects. The outflows play an important role for the structure of the entire region and sometimes can affect directly the evolution of a star (Yokogawa et al. 2003).

The L1551 cloud contains two main centers of outflow activity. The northern one encompasses jets and outflows from sources such as HL Tau, XZ Tau and HH 30 IRS. Proper motions of the HL Tau and HH 30 outflows have been measured by López et al. (1996).

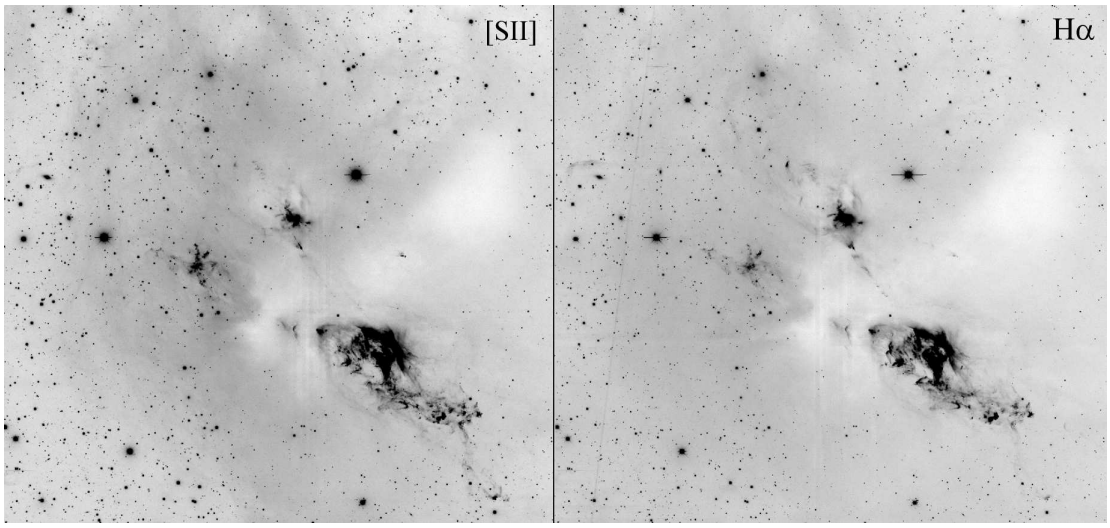


Figure 3.8: 2001 [SII] and H$\alpha$ MOSAIC images of L1551.

The larger southern complex contains numerous Herbig-Haro objects, like HH 28, HH 29, HH 258, HH 259, among others. High proper motions were noted since 1979 by Cudworth & Herbig and since then measured a number of times (e.g. Devine et al. 1999). A large bipolar molecular outflow is associated with this region (Moriarty-Schieven & Snell 1988, Pound & Bally 1991). A large blue-shifted lobe is located at the position of HH 28 and HH 29. A red-shifted lobe, extending to northeast, has a position coincident with fainter Herbig-Haro knots that are part of HH 262. Other smaller molecular flows have been identified by Pound & Bally (1991); one at the position of the HH 30 jet and another called L1551W located west of the large southern lobe.

The two main sources of this complex of flows are the very young and embedded L1551-IRS5 and L1551-NE, located mid-way between the blue and the red-shifted molecular outflows. They have been studied in detail by many authors. The brightest L1551-IRS5 (L $\sim$40 $L_\odot$) is a low mass binary system where each star is surrounded by a disk and energizes a collimated jet (Rodríguez et al. 2003a). Proper motions were detected in the components (Rodríguez et al. 2003b) and the orbital motions measured allowed an estimation of the total mass and period of the binary system as 1.2 $M_\odot$ and 260 yr, respectively. L1551-NE is a less evolved (Class 0), less luminous (L $\sim$6 $L_\odot$) deeply embedded proto-star. It is also a close binary (Reipurth et al. 2002) and likely drives the most powerful Herbig-Haro objects in the region, HH 28 and HH 29, as well as the smaller HH 454 jet. L1551-NE is located just inside the north lobe of the L1551-IRS5 outflow and it is strongly affected by it. Yokogawa et al. (2003) even suggests that the formation of NE was triggered by the impact of the swept-up shell of the outflow from IRS5.

In order to study the Herbig-Haro objects structure in more detail, at the same time having a large scale view of the whole area, proper motions for all the knots of each flow were measured in deep wide field images that cover the entire region. Additionally, we have found a few new flows.

### 3.2.1 Observations

We have used the wide field CCD imager MOSAIC at the KPNO Mayall 4m telescope to obtain images of the L1551 region in October 2001, together with the S140 images described in the previous section. An equivalent set of images taken with the same instrument in October 1997 (Fig. 3.7) was used as comparison for the proper motions.

The H$\alpha$ and [SII] narrow-band filters were used and sets of 5 dithered 600 s exposures were taken for each filter. A final $36' \times 36'$ image was obtained using the `MSCRED` package from IRAF, following the same procedure used with the S140 region (Section 3.1.1). One 60 s i' broad-band image was also taken for comparison.

A central reflection (result of a problem in the telescope optics) still persisted in the 1997 images. See Devine et al. (1999) for details in the 1997 images description and reduction (Fig. 3.7). The reflection was almost completely corrected in the 2001 images, using the procedure `RMPUPIL`, also from IRAF.

Fig. 3.8 shows the two narrow-band images obtained in 2001 of L1551. It is possible to see that the region is very obscured in some areas by the central dark cloud, especially to the northwest. Possibly the outflows have helped to clear out the northeast and southwest areas, where it is even possible to see background galaxies. Fig. 3.9 shows details of the southwestern blue-shifted lobe of L1551, with indication of the main Herbig-Haro objects. A reflection at northeast marks the edge of the cavity drawn in the cloud by the powerful outflows from IRS 5. Some Herbig-Haro objects are brighter in H$\alpha$, like HH 707, and others in [SII], like HH 256 and HH 257. The northern blue-shifted lobe (HH 262) and the HL Tau complex is shown in Fig. 3.10.

In order to measure the proper motions of the HH knots, the images of the different epochs were scaled in intensity, rotated to the same orientation and corrected for geometric distortions using standard procedures from IRAF (`LINMATCH, ROTATE, GEOMAP, GEOTRAN` respectively). The large size of MOSAIC produces really significant geometric distortions along the images. For the measurement of proper motions it is necessary to have the images very well aligned, or the precision of the proper motion determination will be affected by a large amount. Around one thousand stars in the whole field were used as reference for the registration, statistically avoiding

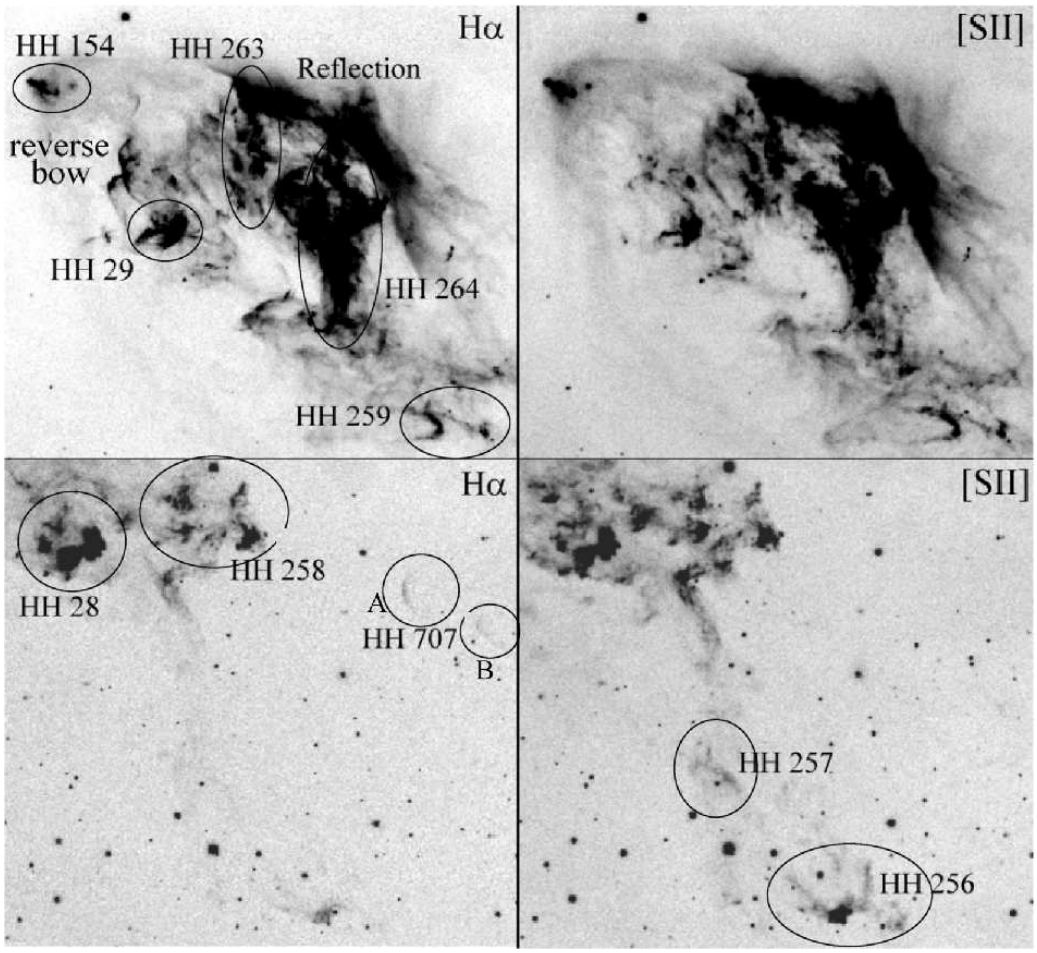


**Figure 3.9**: Details of 2001 H$\alpha$ and [SII] MOSAIC images of the southern blue-shifted lobe of L1551 showing the main HH objects. The reflection and the reverse bow shock mentioned in the text are indicated. The upper and lower images are in the same scale.

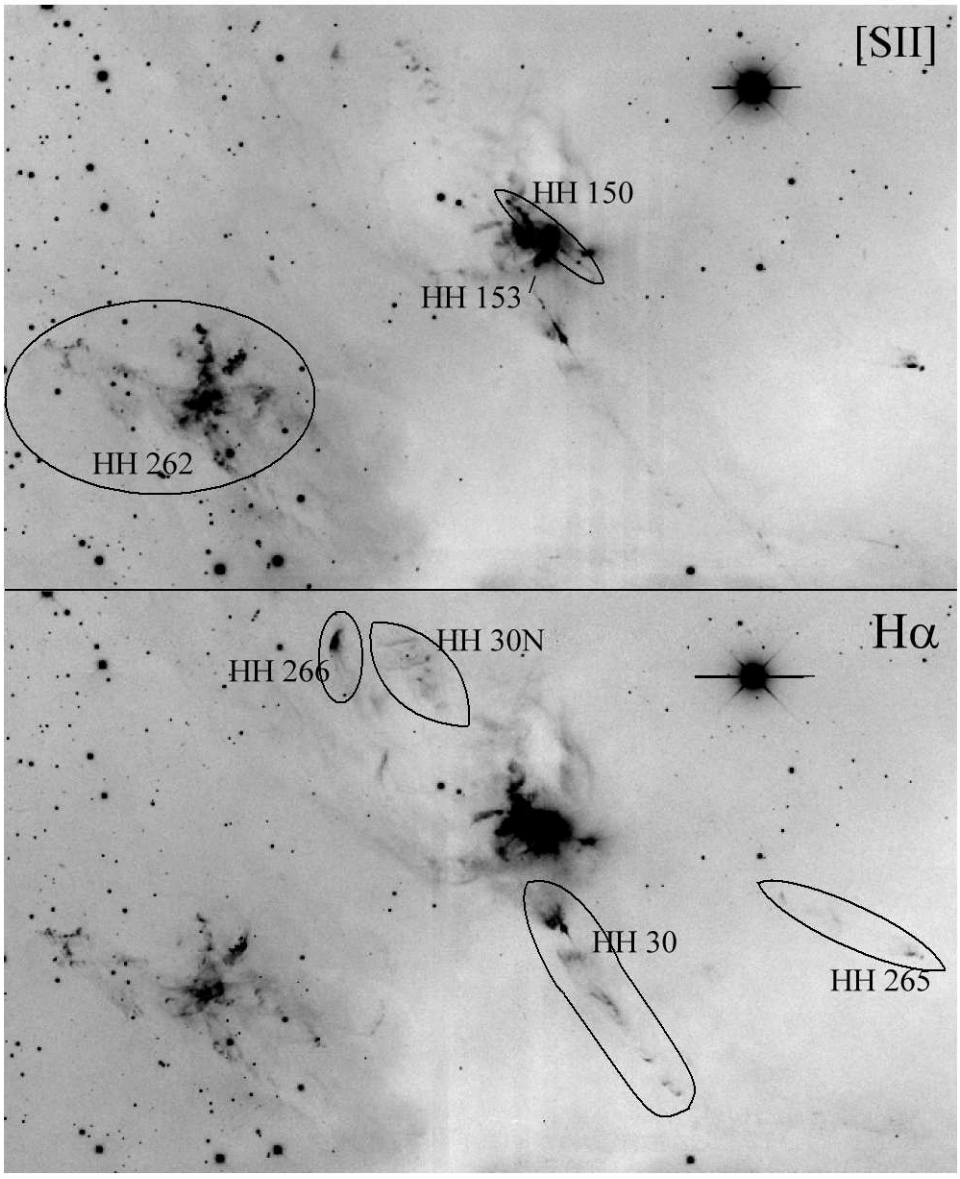


**Figure 3.10**: 2001 Hα and [SII] MOSAIC images of the northern part of L1551 showing the main HH objects.

systematic errors due to proper motion of some stars. The final images are aligned with an average precision of ∼0.2 pixel, corresponding to 0.″05, which varies with the star density in the area.

Some imperfections were found in the MOSAIC images, due to reflection of bright stars from the telescope. These artifacts look like point sources in the 1997 images and are broader and fuzzy in the 2001 images. Their nebulous appearance made us believe at first that they were Herbig-Haro objects, but further checking revealed their true nature. They were identified because of their location, that differed by around 6″in the same diagonal direction between the two epochs. Further careful investigation showed that their pattern matches the pattern of bright stars, dislocated ∼9′ to the South. We located all these artifacts and they did no interfere with the proper motion measurement.

### 3.2.2 Proper Motions

The proper motions were measured using a code written by Jon Morse (Morse et al. 2001), based on a difference squared cross correlation algorithm developed by Currie et al. (1996). It calculates the square differences between an emission feature from one epoch to another, inside a rectangular region, for a set of shifts on both axes. This generates a correlation image whose maximum is at the position of the shift that corresponds to the best alignment of the features. Using a centroid algorithm, the position of the maximum, that corresponds to the shift, is determined.

It is necessary to provide the positions for the rectangular boxes around the HH objects, as well as an initial "guess" for the shifts, in order to start running the code. The determination of the boxes is not trivial, since the cross-correlation is affected by any feature inside the box. We must, for example, prevent stars to fall inside a box together with an HH feature. The much stronger emission from the star will dominate in the cross-correlation and the proper motion determined will be negligible or smaller than the real one. Also, in some areas, the HH emission from different objects are located so close that they may fall inside the same box, or else the box should be so small that does not contain the full knot. In both cases the proper motion will be affected and the errors will be large.

Figs. 3.11 and 3.12 show [SII] and H$\alpha$ images of the whole L1551 complex, with the proper motion vectors for all the knots measured between 1997 and 2001 (more than 300 boxes in each filter). Figs. 3.13 to 3.16 are excerpts of the full images showing the proper motions in more detail. The proper motions measured in H$\alpha$ agree well with most of the [SII] knots, except in knots where the H$\alpha$ and [SII] lines obviously traces different regions, with different physical properties.

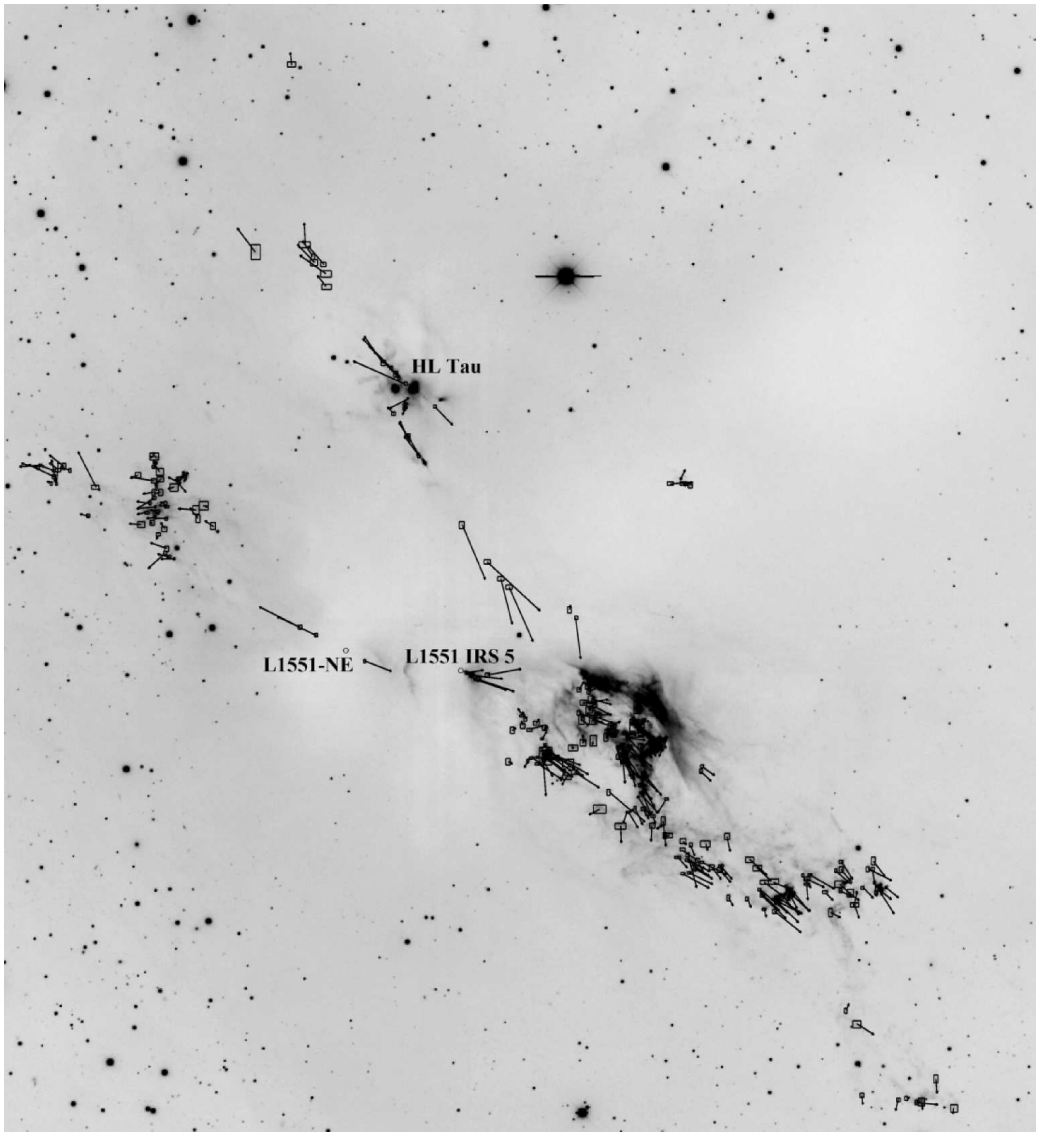


**Figure 3.11**: [SII] image of the whole L1551 complex, showing the proper motion vectors for all the knots measured. The main young sources (L1551-IRS5, L1551-NE and HL Tau) are indicated. Note the main general preferred direction for the vectors.

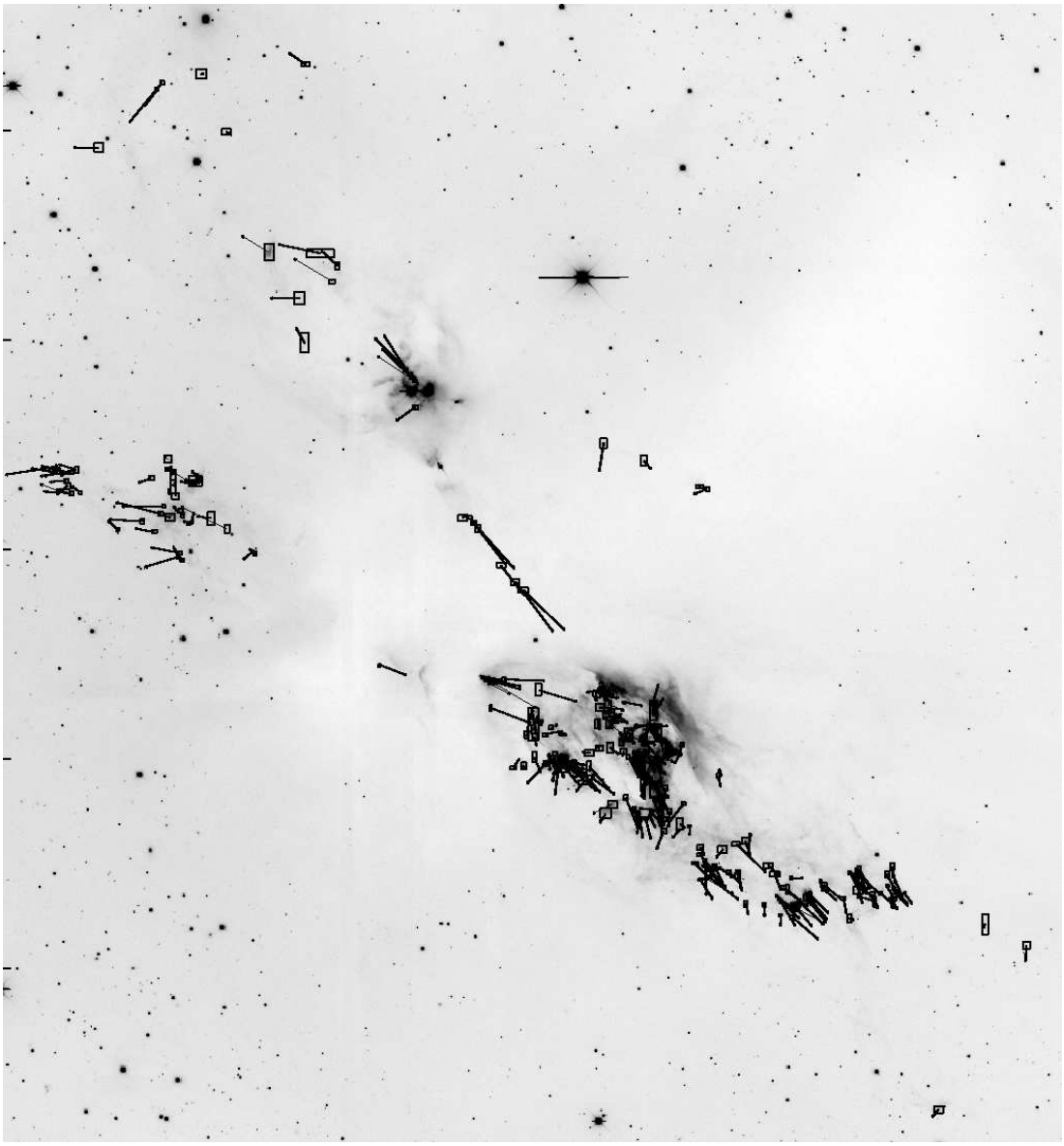

**Figure 3.12**: H$\alpha$ image of the whole L1551 complex, showing the proper motion vectors for all the knots measured.

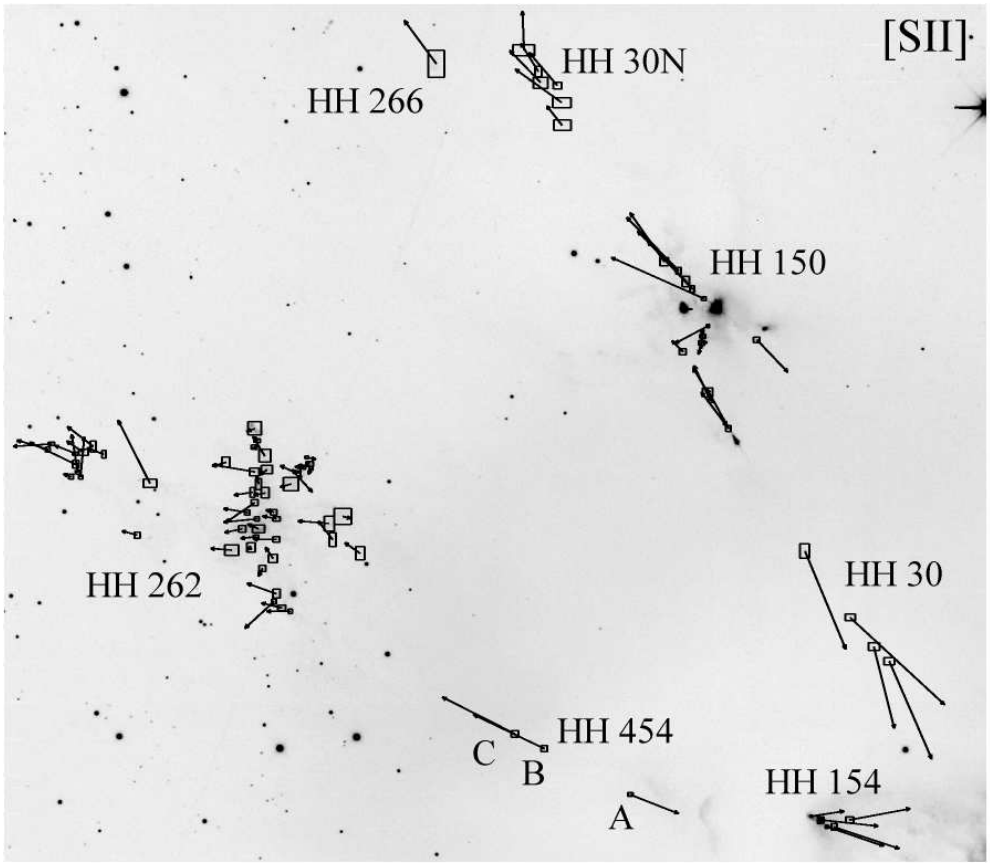


**Figure 3.13**: Proper motions of HH 262 and the HL Tau complex in the [SII] filter. The L1551-NE and IRS 5 jets, HH 454 and HH 154, are also shown. Main HH objects are indicated.

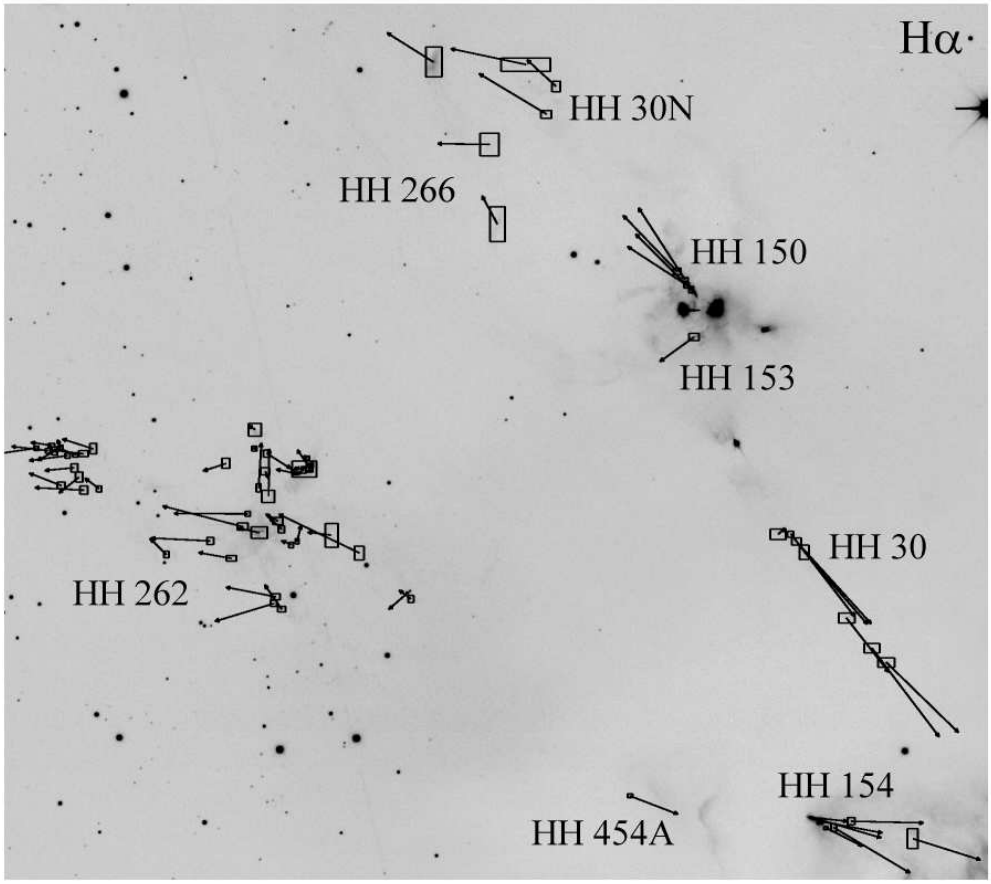


**Figure 3.14**: Proper motions for HH 262 and the HL Tau complex in H$\alpha$. The L1551-NE and IRS 5 jets, HH 454 and HH 154, are also shown. HH objects are indicated.

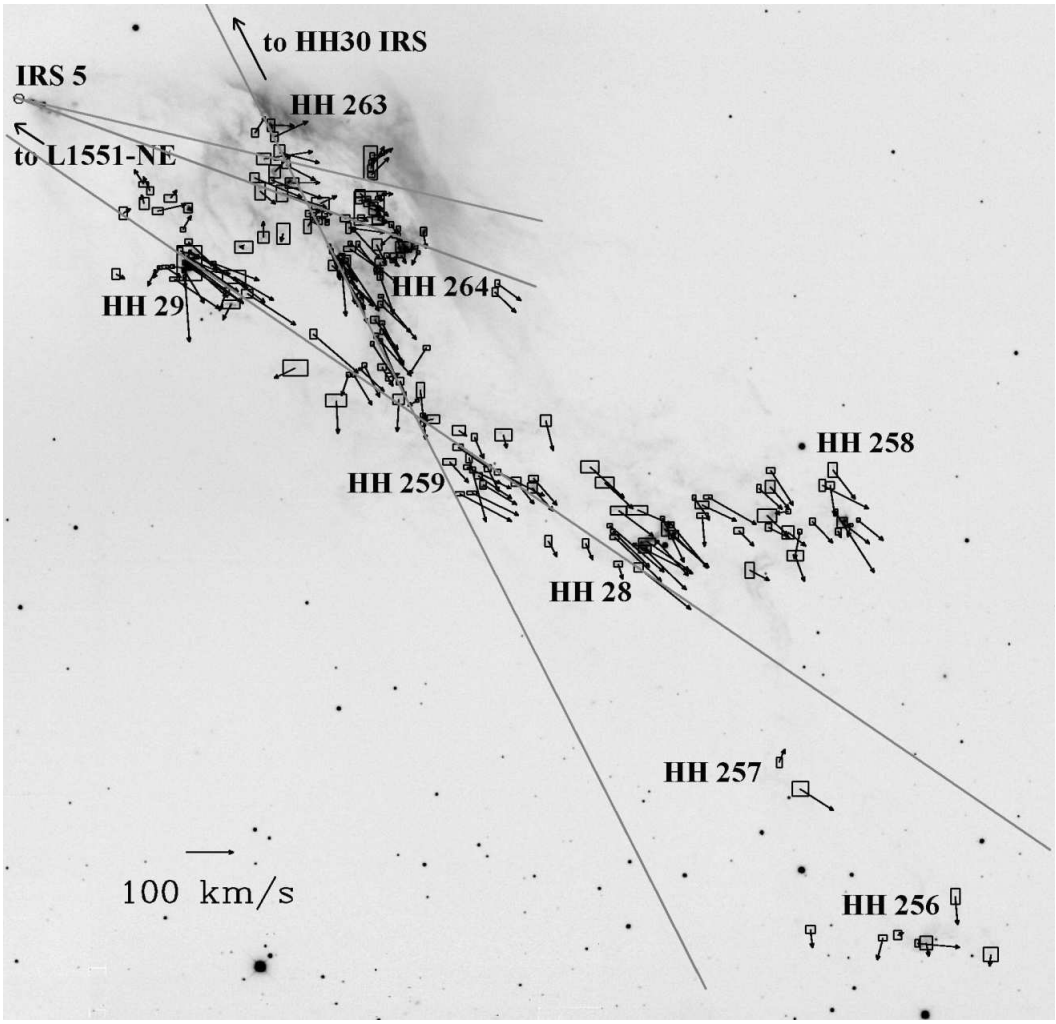


**Figure 3.15**: South-western complex in the [SII] filter. The grey lines pass through the main young sources of the complex: L1551-NE, IRS 5 and HH 30 IRS. The direction of the lines is determined by the closest jet of each source: HH 454, the two IRS 5 jets (HH 154) and HH 30. The main HH objects are indicated.

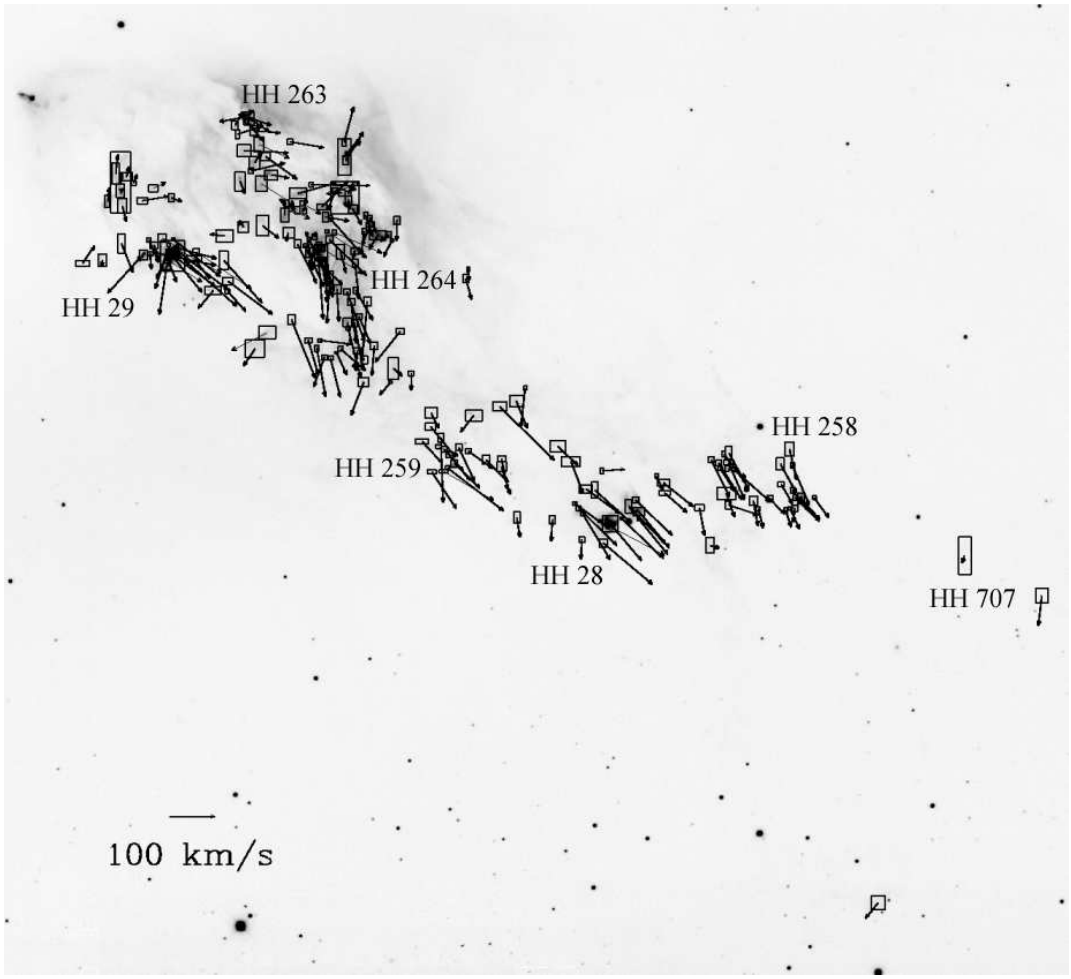


Figure 3.16: South-western complex in the H$\alpha$ filter. HH objects are indicated.

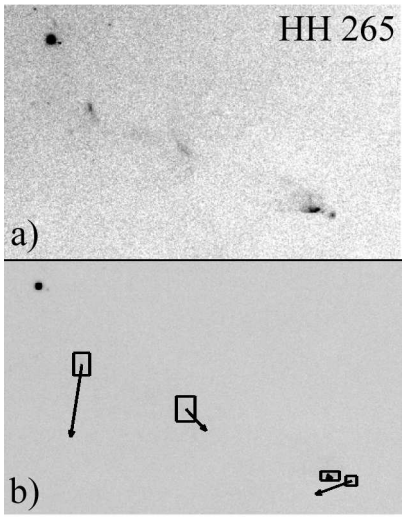


Figure 3.17: HH 265: a) H$\alpha$ image; b) proper motion vectors.

The projected velocities calculated are of the order of 100 km/s with uncertainties around 3-4%. Knots located in problematic regions (close to stars or overlapped to other HH objects) have larger errors, reaching 30%. Tables with projected velocities and position angles for all the knots measured are available electronically at `www.fisica.ufmg.br/~tina/l1551`.

*Sources of the HH objects:*

In the northern part of the L1551 cloud, the Herbig-Haro flows associated with HL Tau, HH 150 and HH 266, are well aligned (Figs. 3.13 and 3.14). The small HH 153, that could be driven by HL Tau or by a more embedded source, is seen brighter in [SII] in a direction perpendicular to HH 150. The HH 30 jet also has its northern and southern flows well aligned, the southern one likely extending to the blue-shifted lobe of L1551. There is a large bow shock bright in H$\alpha$ surrounding the region of HH 266 and HH 30N that is likely an extent of one of those. No significant proper motions where measured for this structure.

HH 265 lies west of HH 30 and its H$\alpha$ knots may indicate an origin in LkH$\alpha$ 385 (just southwest of HL Tau). But the proper motion vectors do not provide an estimate of the direction of its origin. The difference in the proper motion vectors may be caused by the lack of stars in that region, compromising the perfect alignment of the different epoch images. A detail of HH 265 structure and the proper motions determined are shown in Fig. 3.17.

The Herbig-Haro objects in the southern part of L1551 show a very complex structure, but we are able to identify some main groups of knots that move approximately

in the same direction (Figs. 3.15 and 3.16). As observed by Devine et al. (1999), the HH 29, HH 259 and HH 28 proper motion vectors are quite well aligned along a line that connects them to L1551-NE, and that line is perfectly aligned with HH 454, which is driven by L1551-NE. The region just east of HH 29 resembles a bow shock brighter in H$\alpha$, in the opposite direction of the flows. Some of its proper motion vectors in the [SII] filter points opposite to the flows. In the H$\alpha$ filter the vectors deviate bilaterally away from the main flow, what also happens with a few knots inside HH 29 itself. HH 29 is known to be over-running a denser clump of material (Devine et al. 1999 and Hartigan et al. 2000) and the "inverted" bow shock may be an effect of that fact.

A line drawn along the HH 154 (IRS 5 north jet) passes through HH 263, and most of the vectors of these HH knots agree with that direction, specially the central ones. The proper motions of HH 263 show a spread in the position angle that could be due to the dispersion of the flow in its shocks with the high density dark cloud. Alternatively, the southern HH 263 vectors align very well with the second (southern) jet from IRS5. The HH 263 knots could be in fact *two* different objects powered by the two IRS5 jets.

The same happens to part of HH 264. The northernmost knots point mainly in the direction of the reflection nebulae that traces the cavity drawn by the flows, and indicates a stronger interaction with denser material. The central knots of HH 264 could be driven by the southern IRS5 jet. The southern knots in HH 264, however, move in directions that are close to the main HH 30 axis. The source of HH 30 lies further north of IRS 5, close to the HL Tau complex. Thus it seems that we are seeing three or perhaps four major flows overlapping each other (Fig. 3.15).

HH 256 and HH 257 have proper motion vectors that are not exactly along any of the flow axes of IRS 5 or L1551-NE or HH 30 IRS. Within the errors each one could be driven by any of those sources, but with the data available it is not possible to determine. Maybe observations at future epochs will help to settle such issues.

HH 258 could also be driven either by L1551-NE or IRS5. It might be noted that its proper motion vectors and the knots structure are quite similar to HH 262, that is located in the north-eastern part of L1551. HH 262 and HH 258 maybe represent a pair of flows from the same source. They could be driven by IRS 5 (possibly the southern jet), but the mean position angle of the vectors point a few degrees displaced from the original IRS 5 jet, as if the outflow has been deflected, perhaps by the high density cloud that surrounds the central part of L1551. Both HH 262 and HH 258 could also be driven by L1551-NE, but the proper motion vectors are not well aligned to HH 454 as well.

There are faint jet-like structures northwest of IRS 5, best seen in [SII] (Fig. 3.18).

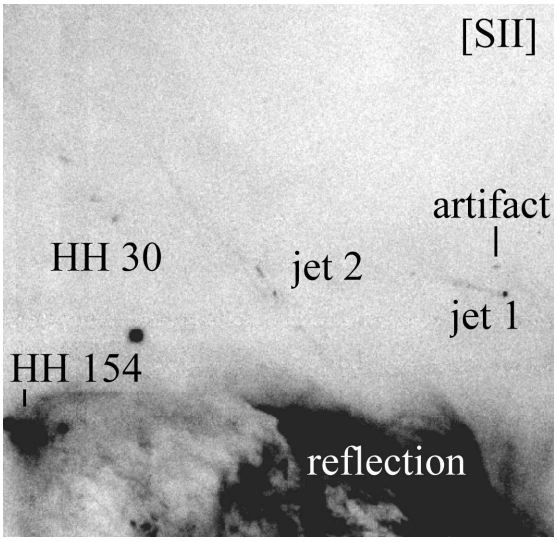


**Figure 3.18**: [SII] image of the jet-like structures of unknown nature located north of the southern lobe of L1551.

The one marked *jet 1* in Fig. 3.18 looks like a point source followed by a jet pointing northeast. The point source is coincident with a near-infrared source detected by 2MASS (04311587+1809116), that is located $\sim 23''$ southwest of an X-Ray source detected by Bally et al. (2003; source 10). Curiously the "jet" points to HH 262 and even agrees with the direction of its proper motion vectors, within the errors. No proper motion could be measured for this structure. One of the artifacts noted in the images (see Section 3.2.1) is located right to the north of this structure. There is another [SII] jet-like structure east of jet 1, parallel to HH 30S, labeled *jet 2* in Fig. 3.18. The proper motion measured for it points south, a few degrees off the line of the jet, which also may be due to a probable misalignment of the images in this region, located near the low star density area of HH 265. Jet 2 could be an extension of HH 150. More observations of this region are necessary to clarify the real nature of those structures.

In the northeastern edge of our image is HH 286, a huge H$\alpha$ bow shock shaped Herbig-Haro object pointing back to L1551-NE and IRS 5. It is very likely an extension of HH 262, but it was impossible to determine reliable proper motions for it. The large extent of the structure and the proximity to bright stars interfere in the correlation, and we could not obtain a reliable measurement. Visually inspecting the 1997 and 2001 images (Fig. 3.19) one can note a small displacement of the tip of the bow shock relative to the nearby star, implying a proper motion in the same general direction of HH 262.

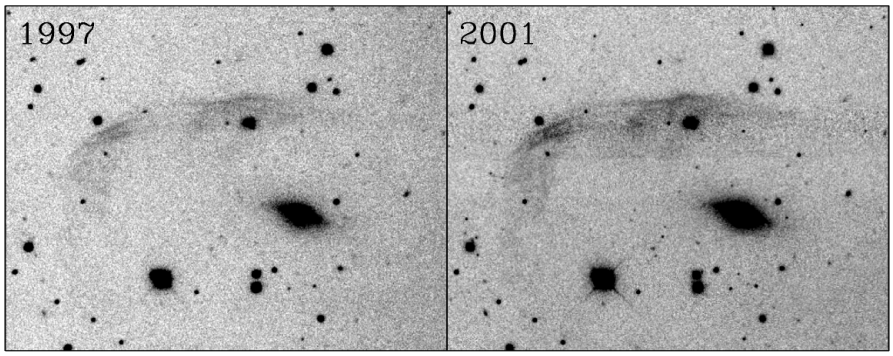


Figure 3.19: 1997 and 2001 H$\alpha$ images of the large HH 286.

Many knots all over the L1551 region have a proper motion vector pointing at completely random position angles. Sometimes that is due to non-uniform brightness changes between the epochs, that deviates the cross-correlation peak from its proper position. In some cases that indicates the strong interaction of the high velocity flow with stationary or lower velocity clumps originally in the location. Finally we note that in some vectors the error in the correlation is so large that the proper motion determined cannot be trusted.

From the figures showing the proper motion we see that, although the vectors have a very complex structure, there is a main preferential direction along a NE-SW axis. Such approximate flow alignments have been seen in other star forming regions, and is likely related to the orientation of an original magnetic field in the cloud.

Ménard & Duchêne (2004) present a detailed study of the orientation of the disks in the T Tauri stars in the Taurus-Auriga molecular cloud and conclude that the stars are randomly oriented with respect to the magnetic field. They find, though, a possible connection between the strength of the outflows and the magnetic field. The stronger outflows are oriented according to the cloud magnetic field, but weaker or shorter jets tend to be perpendicular to it. In our present work in L1551, the weaker HH 153, HH 493 and possibly HH 707 flows are not aligned with the majority of the larger flows.

In the images from 1997 and 2001, we noticed that many features show either an increase or a decrease in brightness. The time-scale for the decrease in brightness corresponds to the cooling time for shocks in the flows, which is of the order of a decade or less. Fig. 3.20 shows one example of a region with brightness increase at the different epochs. The brightness change is likely caused by a time-variable shock where an outflow interacts with a pre-existent clump. The clump that has been overrun is abruptly heated up, causing the large variation in brightness as it cools down.

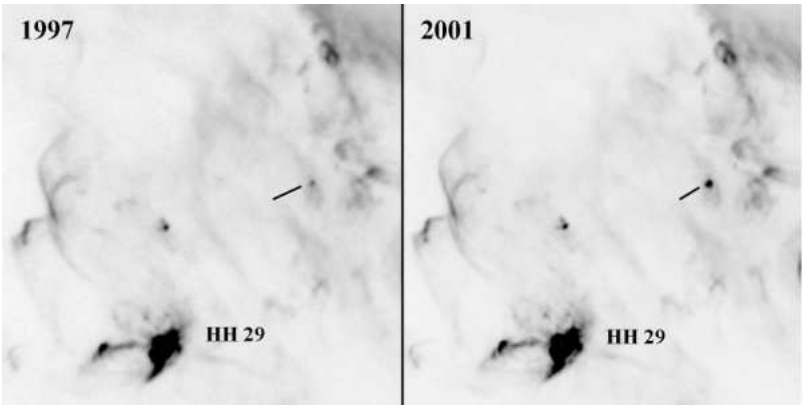


**Figure 3.20**: H$\alpha$ images taken in 1997 and 2001 showing a region close to HH 29. The knot indicated has increased its brightness between the two epochs.

### 3.2.3 New Outflow Features

Examining the H$\alpha$ and [SII] images and comparing with the broadband filter image, we found a few new Herbig-Haro objects: HH 492 and HH 493 to the northeast of the main complex, and HH 707, southwest of the larger southern complex (Fig. 3.21).

HH 707 is seen only in H$\alpha$ and it consists of two knots, of which the easternmost is bow shaped. They are located along the general flow axes of L1551-NE and IRS5, and therefore could be a result of either of these two outflows. The pronounced bow of HH 707-A faces towards the two embedded sources, so we could be seeing a small clump of dense gas that is being overtaken by the above mentioned outflows. HH 707 could be, however, associated with the L1551W molecular outflow found by Pound & Bally (1991), located north of HH 707. But the direction measured for the proper motion of the knots (Fig. 3.23) do not agree with the east/west elongation of L1551W.

The knots in HH 492 are probably an extension of HH 30N, although knots B and C show negligible proper motion (Fig. 3.22). Knot A proper motion agrees with the general direction of HH 30N and is stronger in [SII]. HH 493 moves to the Southwest, and the proper motion vectors point back to V710 Tau. This is a young binary star with spectral type K7, which shows H$\alpha$ emission and has coordinates corresponding to IRAS 04290+1815. HH 493 has the shape of a small bow shock. No HH outflows were found on the opposite side of V710 Tau.

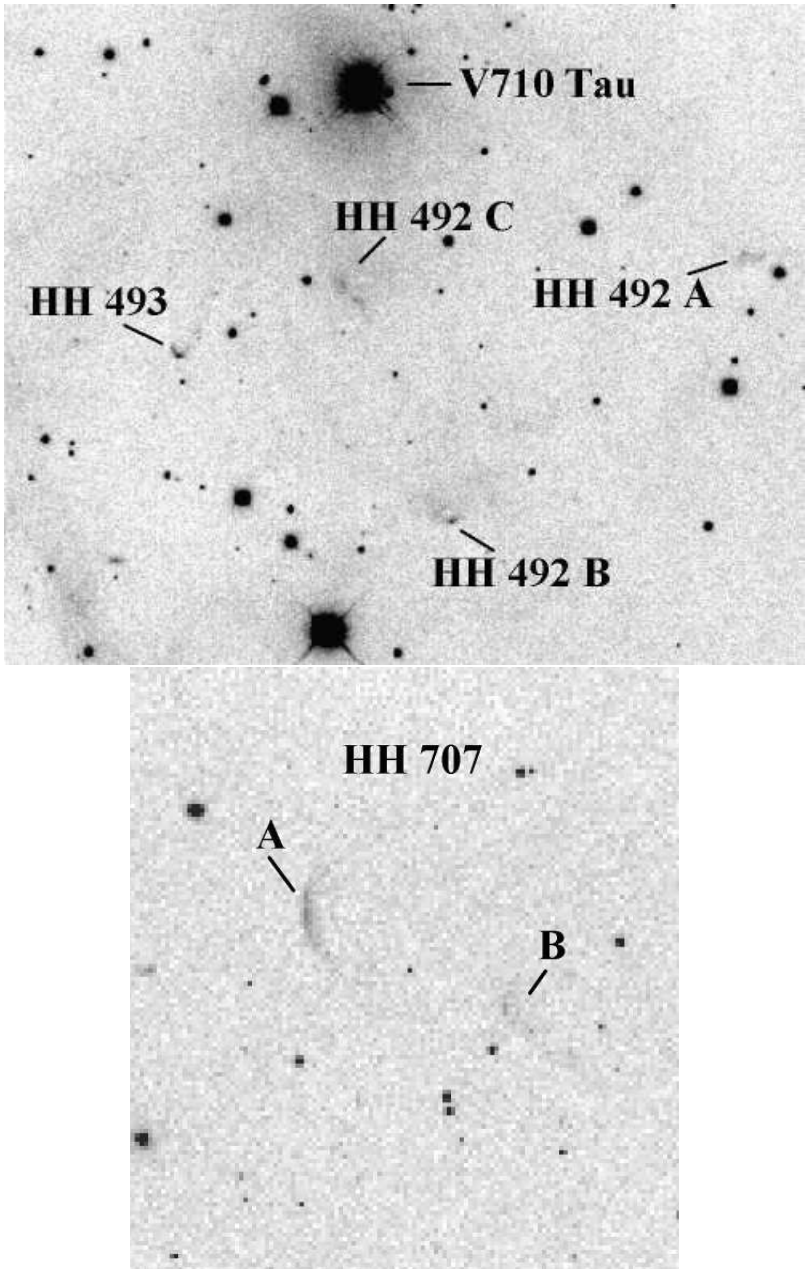


**Figure 3.21**: H$\alpha$ image of new Herbig-Haro objects in L1551: HH 492 and HH 493 in the upper image; HH 707 in the lower image.

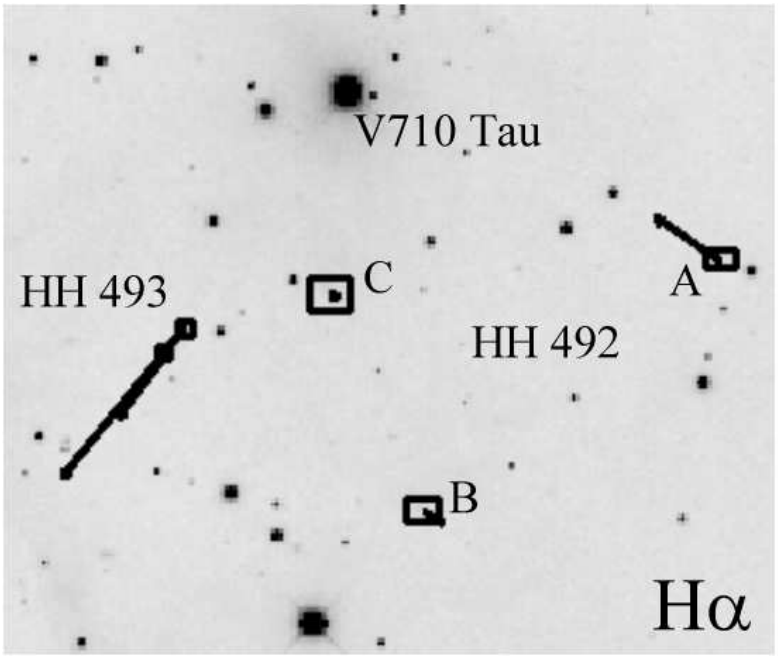


Figure 3.22: Proper motions measured in the newly found HH 492 and HH 493.

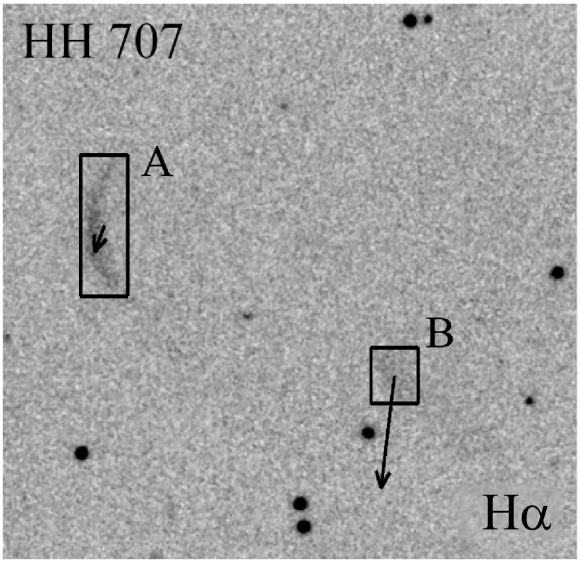


Figure 3.23: Proper motions measured in the newly found HH 707.

The wide field image obtained by MOSAIC provides a detailed, large scale view of the active star forming region of L1551. We have measured proper motions for most of the HH knots in the region and we begin to disentangle the groups of overlapping HH flows, allowing us to associate individual shocks with specific driving sources. We confirm the proposition that HH 28, 29 and 259 are driven by L1551-NE. The HH 30 complex seems to really extend far to the south, crossing the main lobes of the flows from the IRS 5 and NE sources. Parts of HH 264 and even HH 258, HH 257 and HH 256 may be part of the HH 30 flow. We have also identified new knots in the area: HH 493 is likely to be driven by V710 Tau and does not move in the general direction (NE-SW) of the majority of the HH knots in L1551, while HH 707 has an unknown origin.

**Figure 3.24**: HST color image of HH 47. The image was rotated ∼140° clockwise so that the flow axis becomes horizontal.

## 3.3 HH 47

HH 46/47 is one of the best examples and one of the best studied Herbig-Haro jets. It is located in the Gum Nebula and is driven by HH 47 IRS (IRAS 08242–5050, Reipurth & Heathcote 1991), a low mass Class I protostellar source embedded in an isolated Bok globule. The jet emerges from the globule in a bipolar outflow: an approaching lobe that comprises HH 46, HH 47A, HH 47B and HH 47D, and a receding lobe that is optically partially hidden behind the globule (HH 47C). Recently the jet has been imaged in the infrared by the *Spitzer Space Telescope* by Noriega-Crespo et al. (2004) that revealed the structure of the invisible lobe that ends at HH 47C.

The distance assumed is 450 pc, which makes the projected extent of the jet to be 0.57 pc. Stanke et al. (1999) found a pair of large bow-shock shaped Herbig-Haro objects on each side of the HH 46/47 jet, 10′ away, increasing the total length of the complex to nearly 3 pc.

Proper motions have already been measured in the optical (e.g. Eisloffel & Mundt 1994) and in the near infrared (e.g. Micono et al. 1998), implying velocities of ∼300 km/s. Heathcote et al. (1996) present high resolution Hubble Space Telescope (HST) images through H$\alpha$ and [SII] filters and a detailed study of the structure of the approaching lobe of HH 47. After a time interval of about 5 years, another set of images were obtained for proper motion measurement of the knots with unprecedent resolution. The spatial resolution was 0.″1/pix, corresponding to 45 AU at the distance of HH 46/47. The total exposure time was 11900 s for each filter.

I have used the same method described in the previous section in order to obtain proper motions with the HST set of images. Rectangular areas were selected around each knot and a cross correlation between the epochs gives the shift of the emission over the time. The boxes and arrows that indicate the amount and direction of the proper motion are shown in Fig. 3.25 for both filters.

Table 3.2 lists the distance to the source, the tangential velocities (assuming a distance of 450 pc), the position angle, and the age of each knot (i.e. the time in years for the object to move from the source to its present location at its current velocity).

For the assumed distance of 450 pc, the average tangential velocity of the knots is $\sim$200 km/s and does not change significantly with the distance to the source. A few objects show small proper motions and position angles that deviate much from the average flow axis of $\sim$50°. Those are probably oblique shocks with the ambient medium (e.g. northern HH 46 flow and southern knots in HH 47A).

A large box was selected to represent the overall motion of HH 47A at the first stage. The average velocity of this structure was then subtracted from the images and the relative proper motions were measured for each knot inside HH 47A, in order to study its internal motion (Fig. 3.26). The relative velocities average around $\sim$35 km/s and many point backwards to the source, especially at the southern edge.

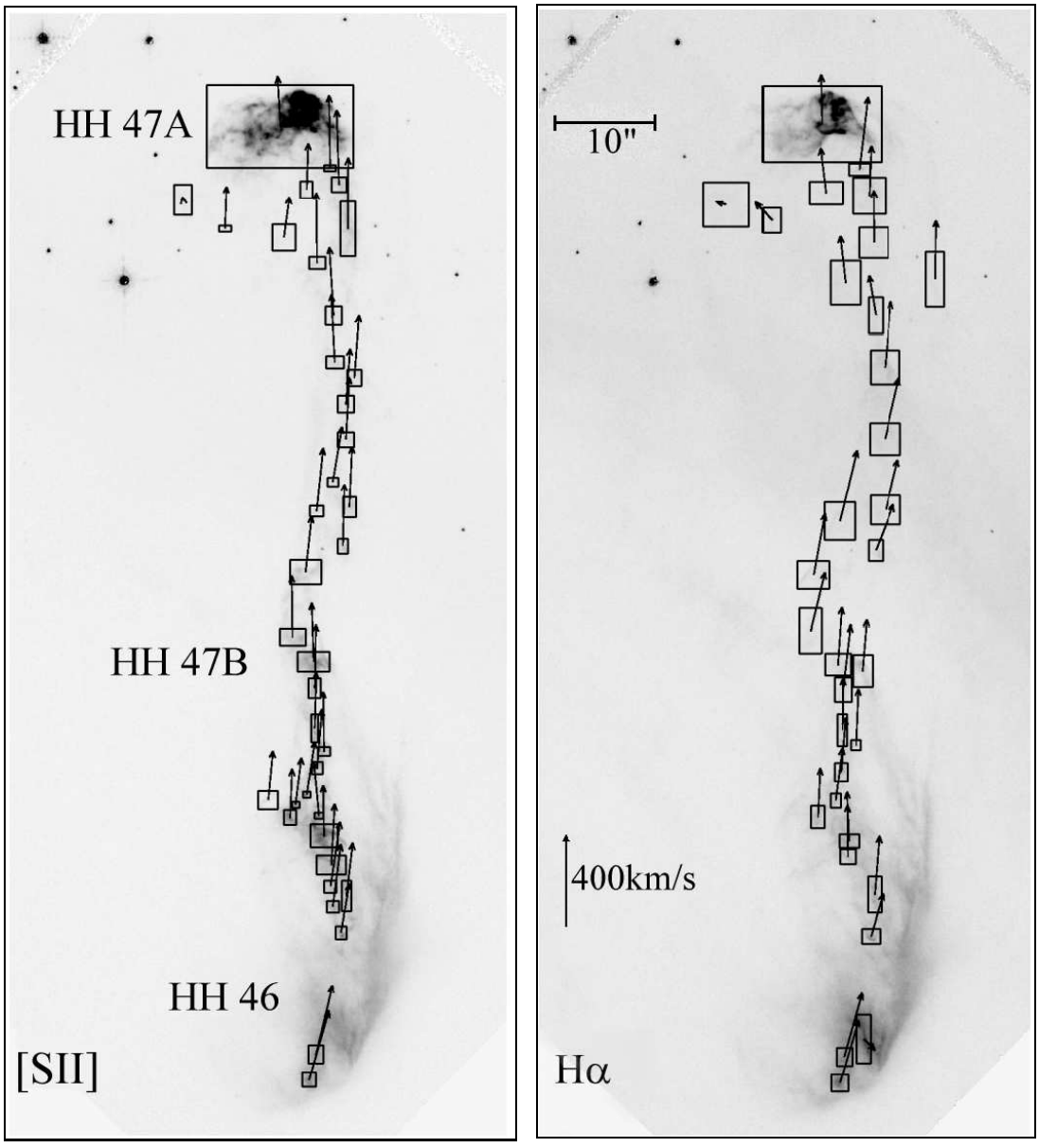


**Figure 3.25**: [SII] and H$\alpha$ images of HH 47 with the boxes used in the determination of the proper motions. The arrows indicate the direction and modulus of the proper motions. The images were rotated $\sim 50°$ clockwise so that the main flow axis becomes vertical.

**Table 3.2**: Proper motion measured for the HH knots in H$\alpha$ and [SII].

| Knot H$\alpha$ | Dist.[a] ($''$) | V [b] (km/s) | P.A.[c] (°) | Age [d] (years) | Knot [SII] | Dist.[a] ($''$) | V [b] (km/s) | P.A.[c] (°) | Age [d] (years) |
|---|---|---|---|---|---|---|---|---|---|
| 1 | 2.2 | 268.3± 1.2 | 33.7 | 17 | 1 | 2.2 | 293.5± 2.1 | 34.1 | 16 |
| 2 | 4.1 | 271.4± 9.8 | 34.5 | 32 | 2 | 4.2 | 288.2± 4.3 | 36.6 | 31 |
| 3 | 5.9 | 63.9± 2.9 | 274.6 | 196 | 3 | 13.5 | 197.6± 1.9 | 39.9 | 145 |
| 4 | 13.4 | 176.7± 3.1 | 33.9 | 161 | 4 | 15.2 | 254.3± 1.0 | 42.9 | 127 |
| 5 | 16.4 | 237.4± 1.3 | 45.5 | 147 | 5 | 16.2 | 217.3± 1.1 | 43.4 | 158 |
| 6 | 19.0 | 207.7± 2.3 | 50.8 | 195 | 6 | 16.7 | 265.3± 1.5 | 41.6 | 134 |
| 7 | 20.2 | 198.5± 1.0 | 52.7 | 217 | 7 | 18.3 | 248.9± 1.9 | 46.8 | 156 |
| 8 | 22.0 | 201.3± 1.4 | 47.4 | 232 | 8 | 20.4 | 205.6± 0.7 | 50.8 | 211 |
| 9 | 23.2 | 218.1± 1.5 | 42.8 | 226 | 9 | 21.8 | 200.2± 0.9 | 47.7 | 232 |
| 10 | 25.4 | 221.9± 1.8 | 45.4 | 243 | 10 | 21.9 | 221.1± 0.6 | 55.1 | 211 |
| 11 | 27.4 | 229.7± 0.8 | 47.7 | 254 | 11 | 22.7 | 194.8± 2.0 | 43.1 | 248 |
| 12 | 28.5 | 210.6± 1.1 | 49.2 | 288 | 12 | 23.2 | 203.0± 1.5 | 44.5 | 244 |
| 13 | 31.5 | 262.3± 2.0 | 43.2 | 256 | 13 | 23.5 | 220.6± 0.6 | 41.3 | 227 |
| 14 | 33.0 | 205.5± 1.6 | 45.2 | 342 | 14 | 25.6 | 239.5± 1.0 | 45.2 | 227 |
| 15 | 33.4 | 229.7± 2.3 | 46.3 | 309 | 15 | 26.8 | 242.6± 1.8 | 50.6 | 235 |
| 16 | 35.9 | 241.7± 7.6 | 36.0 | 317 | 16 | 28.5 | 228.0± 0.6 | 48.5 | 266 |
| 17 | 40.1 | 252.1± 2.7 | 39.6 | 338 | 17 | 31.5 | 255.0± 2.7 | 48.8 | 263 |
| 18 | 42.0 | 199.7±11.5 | 28.4 | 448 | 18 | 33.5 | 234.7± 0.9 | 51.9 | 304 |
| 19 | 44.1 | 297.3±12.3 | 36.6 | 316 | 19 | 35.3 | 245.0± 1.3 | 51.1 | 307 |
| 20 | 45.1 | 210.9±13.4 | 36.0 | 455 | 20 | 40.1 | 229.7± 1.4 | 43.7 | 372 |
| 21 | 50.4 | 252.4± 5.3 | 37.0 | 425 | 21 | 42.1 | 252.8± 1.1 | 48.7 | 355 |
| 22 | 55.7 | 265.4± 2.5 | 24.7 | 447 | 22 | 44.7 | 257.8± 1.4 | 44.0 | 369 |
| 23 | 59.5 | 164.2±14.8 | 59.9 | 772 | 23 | 45.1 | 249.3± 1.3 | 47.5 | 385 |
| 24 | 61.8 | 191.2± 8.7 | 56.6 | 689 | 24 | 46.9 | 227.9± 3.6 | 40.8 | 439 |
| 25 | 62.6 | 239.5±21.5 | 49.2 | 557 | 25 | 50.2 | 252.4± 1.9 | 46.8 | 423 |
| 26 | 64.9 | 213.8± 4.4 | 50.5 | 647 | 26 | 52.8 | 224.7± 1.9 | 45.7 | 501 |
| 27 | 66.7 | 99.0± 8.5 | 91.4 | * | 27 | 54.8 | 250.3± 2.0 | 45.9 | 467 |
| 28 | 68.2 | 42.5±14.8 | 122.1 | * | 28 | 55.9 | 269.7± 2.2 | 53.0 | 442 |
| 29 | 68.5 | 202.8± 8.6 | 47.6 | 720 | 29 | 59.3 | 276.5± 4.0 | 53.4 | 457 |
| 30 | 68.6 | 185.4±29.9 | 56.8 | 789 | 30 | 63.2 | 285.3± 7.1 | 50.6 | 472 |
| 31 | 70.4 | 296.8±22.1 | 43.4 | 505 | 31 | 65.1 | 165.7± 9.4 | 42.6 | 838 |
| 32 | 73.8 | 199.3± 0.9 | 51.3 | 789 | 32 | 65.8 | 290.1± 4.4 | 49.6 | 484 |
| | | | | | 33 | 66.0 | 174.1±13.3 | 48.2 | 808 |
| | | | | | 34 | 68.5 | 11.0±16.7 | 61.9 | * |
| | | | | | 35 | 68.7 | 189.0± 3.2 | 48.3 | 775 |
| | | | | | 36 | 69.1 | 303.6± 7.2 | 51.9 | 485 |
| | | | | | 37 | 70.3 | 296.2± 2.0 | 50.7 | 506 |
| | | | | | 38 | 73.5 | 202.1± 0.7 | 53.2 | 775 |

Notes:
[a] – Distance to the source in arc-seconds.
[b] – Tangential velocity in kilometers per second, assuming a distance of 450 pc.
[c] – Position Angle of the proper motion vector in degrees.
[d] – Time in years for the object to move from the source to its present location at its current velocity. * indicates that small proper motions and high position angles prevent reasonable age determination.

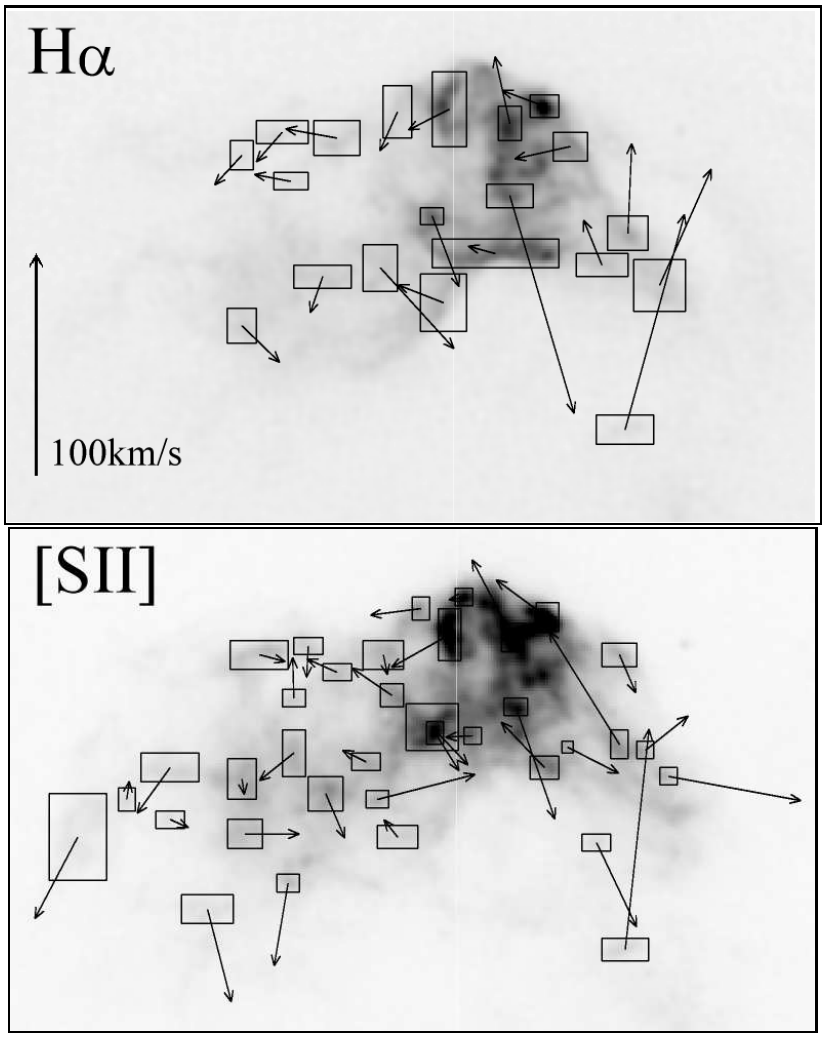


**Figure 3.26**: H$\alpha$ and [SII] image of HH 47A. The arrows indicate the internal proper motion of the knots. The orientation in the sky is the same of Fig. 3.25

# Chapter 4

# Study of Selected Star Forming Regions

In this chapter we explore some star formation regions using more than one observing technique. Optical images and spectra are obtained in addition to near- and mid-infrared data in order to study different aspects of each region. The optical data detects outflow activity and H$\alpha$ emission stars, that are already at least partially exposed to us. The infrared images see through the clouds and show us embedded sources and outflows. With the combination, we have a better overview of the processes that occur in the entire region.

## 4.1 IC 1396 North

IC 1396 is a large HII region located at a distance of 750 pc (Osterbrock 1957). The region is ionized by a group of massive stars, Trumpler 37, that contains numerous B stars and the more luminous O6.5 star HD 206267. Osterbrock (1957) identified a number of dust globules in IC 1396, some with cometary appearance and bright rims facing the central exciting star. The association of some of these globules with IRAS sources (Schwartz et al. 1991 and Sugitani et al. 1991) has given support to the hypothesis that those are sites of formation of a second generation of stars induced by the compression due to the ionization shock front.

The most luminous IRAS source detected in the region is associated with the globule IC 1396 North, located at a projected distance of 11 pc from HD 206267.

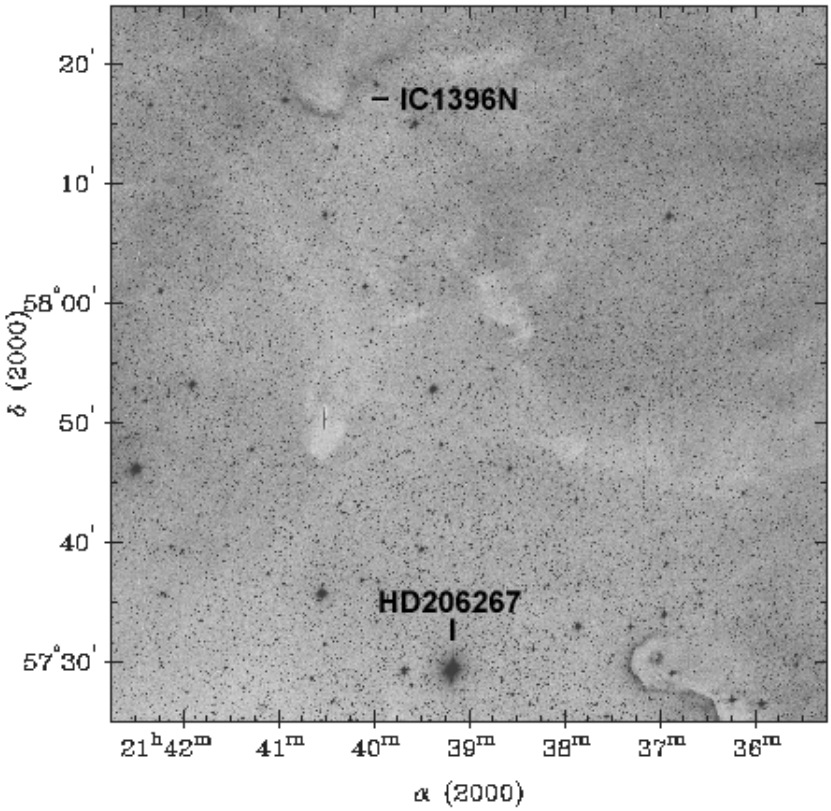


**Figure 4.1**: DSS blue image showing the IC 1396N globule and the O type star HD 206267, as well as other clumps in the region.

IRAS 21391+5802 has a luminosity of $\sim$350 $L_{\odot}$ and is known to drive a molecular outflow (Saraceno et al. 1996 and Beltrán et al. 2002).

Several other embedded sources and outflows have been found inside IC 1396N showing that it is an active site of star formation. Codella et al. (2001) identified two molecular outflows in a millimeter-wave multi-line study, where the energy sources were detected in the millimeter radio continuum. Nisini et al. (2001) imaged the cloud in the near-infrared and found a number of molecular hydrogen flows and embedded sources. Herbig-Haro flows were detected by Ogura et al. (2002) who has also found 16 H$\alpha$ emission stars near the edge of the cloud. Beltrán et al. (2002) obtained 3.6 cm Very Large Array (VLA) maps and millimeter and continuum Berkeley-Illinois-Maryland Association maps that revealed actually three sources associated with IRAS 21391+5802 and further outflow activity.

For further investigation of this globule, we have imaged it through optical, near-

and mid-infrared filters. The images obtained are deeper and with higher resolution than the observations published so far.

### 4.1.1 Observations

We have obtained CCD images of the IC 1396N cloud with the University of Hawaii 2.2 m telescope at Mauna Kea on 2002 July 14 and 15, using the Wide Field Grism Spectrograph and a 2048×2048 Tektronix CCD with a scale of 0.″34/pixel. Two narrow-band filters were used, centered on the H$\alpha$ 6563Å and the [SII] 6717Å, 6731Å lines. Three 10 minutes dithered exposures were taken for H$\alpha$ and three 15 minute duration for [SII]. Four low-dispersion (3.8Å/ pixel) long-slit spectra were taken, each of 20 minute duration, of the new Herbig-Haro object found, with a red grism using the same instrument. The reductions were made using standard `IRAF` procedures.

Near-infrared $JHK$ images were obtained of the IC 1396N core with the United Kingdom Infrared Telescope (UKIRT) at Mauna Kea on 2002 July 13, using the UKIRT Fast-Track Imager and a 1024×1024 HgCdTe Rockwell detector array providing a scale of 0.″091/ pixel. Total exposure times were 300 s in each filter. Other images were taken through narrow-band filters, centered on $H_2$ 2.122 $\mu$m and [FeII] 1.644 $\mu$m lines, with total exposures of 500 s per position. Finally, mid-infrared images were obtained at 11.6 $\mu$m, also on 2002 July 13, using Michelle, which employs a 320×240 pixel SBRC Si:As detector array providing a field of view of 67″×50″ with a scale of 0.″21/pixel. Both the near- and mid-infrared observations were done in non-photometric conditions. The images were reduced during the observing run with the standard UKIRT pipeline.

### 4.1.2 New Herbig-Haro objects

We have identified four new HH flows in that cloud, which we call HH 777, 778, 779, and 780 (Table 4.1). Other small flows have also been recently found by by Ogura et al. (2002) in the same cloud. Fig. 4.2 shows the [SII] filter image with indications of the new and previously known flows.

The most impressive flow discovered by us is HH 777, which forms a bright working surface leading a trail or tube of incandescent gas to the west. The flow abruptly emerges from the sharp rim of the cloud core, and its rather well-defined axis points back toward the center of the core. It is another example of an "irradiated" Herbig-Haro object, like the ones detected in the S140 region. A comparison of the H$\alpha$ and [SII] images shows that the bow shock, although bright in [SII], is dominated by H$\alpha$

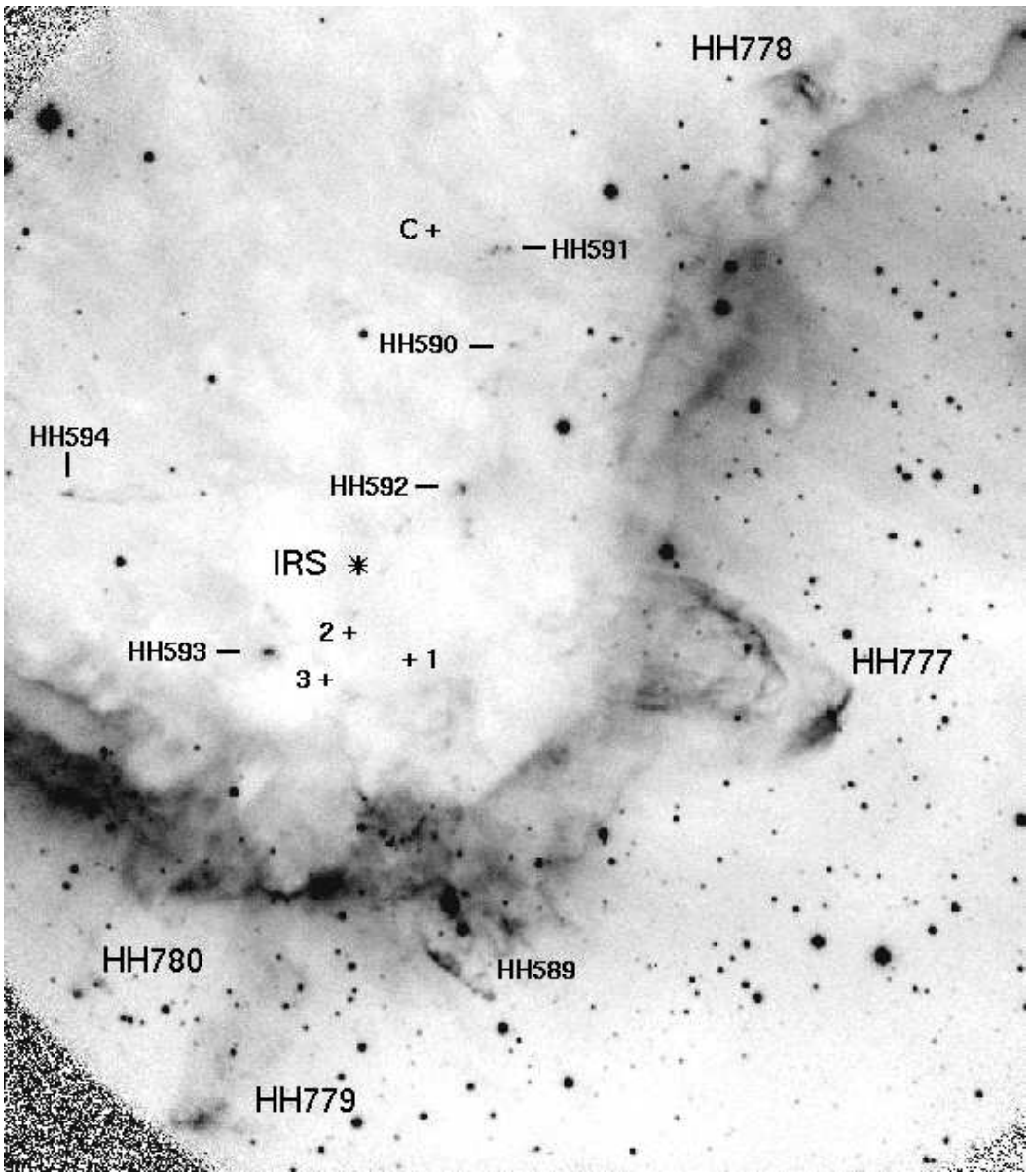


**Figure 4.2**: [SII] image of the IC 1396 North cloud. HH numbers 589 to 594 are from Ogura et al. (2002), numbers 777 to 780 were identified in our observations. The crosses labeled 1, 2 and 3 refer to the millimeter/centimeter continuum sources of Beltrán et al. (2002), and the one marked C is from Codella et al. (2001). The position of IRAS 21391+5802 is approximately between 2 and 3. The location of the embedded source HH 777 IRS is indicated by an asterisk. The field size is $5'15'' \times 6'30''$.

**Table 4.1**: Coordinates of Objects in the IC 1396N Region.

| Object | $\alpha(2000)^a$ | $\delta(2000)^a$ | comments |
|---|---|---|---|
| HH 777 IRS | 21 40 41.6 | +58 16 38 | Measured at K |
| HH 777 | 21 40 21.6 | +58 15 49 | Bright knot in western bow shock |
| HH 778 | 21 40 22.8 | +58 19 19 | Northernmost apex |
| HH 779 | 21 40 47.9 | +58 13 35 | Brightest knot |
| HH 780 | 21 40 53.1 | +58 14 16 | Brightest knot |

Note.[a] – The positions are measured at the brightest point.

emission, partly because the shock where the flow encounters the ambient medium is relatively strong and partly because of the external photo-ionization caused by the OB stars in the Trumpler 37 group.

East of the HH 777 bow shock, we see what appears to be two flow components: one consists of weak emission that trails the large bow shock, and the other is what looks like a pointed bow shock interior to the western bow shock, as if a second ejection episode is catching up with the first one. We have obtained a long-slit spectrum of the bright northern rim of this interior bow, and it shows much stronger [SII], about two-thirds the strength of H$\alpha$, indicating a substantial component of shock emission. That confirms the Herbig-Haro classification of this large structure that surprisingly had not earlier been identified as such, probably being confused with an "elephant trunk", simply ionized by the external UV radiation. The visible section of HH 777 is 80″ long (0.3 pc) and 45″ wide (0.16 pc) where it emerges from the cloud.

Three other new HH flows are seen in the image. HH 778 is located to the north and forms a double bow shock facing away from the southern front of the globule. HH 779 is a diffuse working surface followed by a trail of faint incandescent gas leading into the dense core. Finally, HH 780 consists of two almost stellar-like knots with faint wisps of emission also leading toward the core. Fig. 4.3 shows the new Herbig-Haro objects in more detail.

### 4.1.3 Embedded sources

The morphology of HH 777 strongly suggests that its energy source is located near the center of the cometary globule. The luminous young IRAS source 21391+5802 is located between two radio continuum sources named A and B by Codella et al. (2001) and marked 2 and 3, respectively, in Fig. 4.2. None of these sources appear to lie sufficiently near the flow axis of HH 777 to be a likely driving source. We have

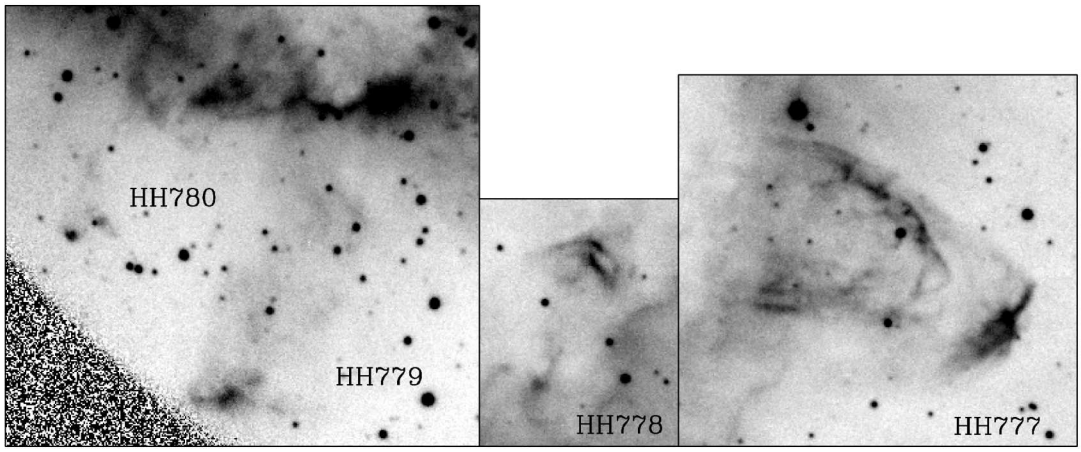


Figure 4.3: Herbig-Haro Objects seen in detail in the [SII] image.

therefore imaged the interior of the cloud core in the near-infrared at $J$, $H$ and $K$ as well as in the mid-infrared at 11.6 $\mu$m. A composite $JHK$ false color image is inserted on top of the [SII] image in Fig. 4.4 and shows a ridge with three bright infrared reflection nebulae around the location of the IRAS and radio continuum sources.

Because of non-photometric conditions during our near-infrared observations, we were not able to determine accurate magnitudes, but we used the observations of the Two Micron All Sky Survey (2MASS) to calibrate our magnitudes. 2MASS finds 21 stars in the region observed by us, 10 of which are detected in all the three bands. Our observations are much deeper and better resolved than 2MASS and we see 64 stars in our field, 36 in $J$, $H$ and $K$. The dispersion of our magnitudes relative to 2MASS is about 0.2 mag and that is what we assume as our accuracy level. Table 4.2 lists the magnitudes obtained and Fig. 4.5 shows a color-color diagram of all sources detected in $J$, $H$ and $K$, with the location of the main sequence and giant stars as well as the reddening vectors.

Many sources have colors typical for young stars with infrared excess (see also Nisini et al. 2001). One source stands out because of its high $J-H$ and $H-K$ values, its brightness at $K$, its nebulous nature, and its location along the HH 777 flow axis. The location of this particular source in the color-color diagram suggests a heavily reddened object with considerable infrared excess. At 11.6 $\mu$m, the only source detected in the field is located within $2''$ of the position of this near-infrared source, which is within the pointing errors, suggesting that the near- and mid-infrared sources are one and the same. From now on, we refer to this source as HH 777 IRS.

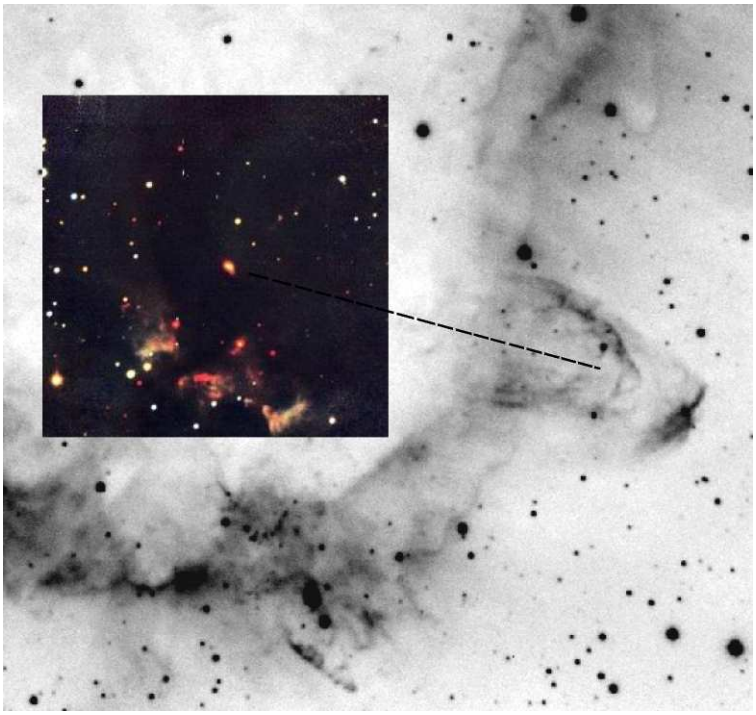

**Figure 4.4**: [SII] image in grey scale with insert of $JHK$ color image showing reflection nebulae and many embedded sources in the interior of the cloud. The near-infrared image field is $90' \times 90'$. The dashed line indicates the HH 777 flow axis pointing back to HH 777 IRS.

**Table 4.2**: Near-infrared sources detected in IC 1396N.

| $\alpha$(2000) | $\delta$(2000) | J | H | K | | $\alpha$(2000) | $\delta$(2000) | J | H | K |
|---|---|---|---|---|---|---|---|---|---|---|
| 21 40 35.4 | 58 17 24 | 17.00 | 15.89 | 15.33 | | 21 40 43.6 | 58 16 00 | – | – | 15.15 |
| 21 40 35.5 | 58 16 54 | 18.33 | 16.80 | 15.99 | | 21 40 43.7 | 58 16 19 | – | 19.29 | 13.48 |
| 21 40 35.5 | 58 17 00 | 18.55 | 16.63 | 15.72 | | 21 40 43.7 | 58 16 21 | 19.03 | 17.85 | 13.39 |
| 21 40 35.6 | 58 16 31 | – | – | 17.65 | | 21 40 43.7 | 58 16 12 | 18.73 | 17.20 | 15.59 |
| 21 40 35.7 | 58 16 50 | – | 18.60 | 18.07 | | 21 40 44.4 | 58 16 52 | – | – | 16.84 |
| 21 40 36.2 | 58 16 52 | 18.16 | 16.62 | 16.01 | | 21 40 44.7 | 58 15 52 | 16.11 | 15.27 | 14.79 |
| 21 40 36.4 | 58 17 21 | 19.75 | 19.64 | 18.37 | | 21 40 44.8 | 58 16 09 | 18.07 | 16.95 | 15.74 |
| 21 40 36.6 | 58 16 29 | – | – | 17.34 | | 21 40 44.8 | 58 17 05 | 16.75 | 15.26 | 14.18 |
| 21 40 36.7 | 58 16 47 | – | – | 17.80 | | 21 40 44.9 | 58 16 05 | 16.79 | 14.31 | 12.95 |
| 21 40 36.8 | 58 17 06 | 16.26 | 14.75 | 14.03 | | 21 40 45.3 | 58 16 00 | – | – | 15.51 |
| 21 40 37.3 | 58 15 47 | 16.67 | 15.12 | 14.19 | | 21 40 45.4 | 58 16 53 | – | – | 16.37 |
| 21 40 37.7 | 58 16 01 | – | – | 17.55 | | 21 40 45.4 | 58 16 41 | 17.48 | 16.35 | 15.57 |
| 21 40 37.8 | 58 16 40 | – | – | 18.17 | | 21 40 45.6 | 58 16 45 | – | 17.63 | 16.06 |
| 21 40 38.0 | 58 17 19 | – | – | 18.28 | | 21 40 45.6 | 58 16 03 | 15.56 | 13.66 | 12.74 |
| 21 40 38.0 | 58 17 07 | 20.65 | 18.96 | 18.34 | | 21 40 45.8 | 58 16 27 | 19.63 | 16.86 | 15.48 |
| 21 40 38.7 | 58 16 54 | 19.99 | 17.73 | 16.53 | | 21 40 45.9 | 58 15 49 | – | – | 17.56 |
| 21 40 39.5 | 58 16 40 | – | 18.88 | 17.30 | | 21 40 46.2 | 58 16 58 | – | 19.14 | 17.09 |
| 21 40 39.7 | 58 16 09 | – | – | 15.41 | –B1 | 21 40 46.2 | 58 16 06 | 18.25 | 16.63 | 15.76 |
| 21 40 40.0 | 58 17 07 | – | 18.94 | 17.81 | | 21 40 46.6 | 58 15 52 | – | – | 18.12 |
| 21 40 40.3 | 58 16 18 | – | – | 16.78 | | 21 40 47.5 | 58 16 37 | 19.12 | 16.23 | 14.61 |
| 21 40 40.5 | 58 16 45 | – | 17.88 | 16.48 | | 21 40 47.5 | 58 15 43 | 19.27 | 18.15 | 16.93 |
| 21 40 40.5 | 58 15 59 | 19.26 | 17.55 | 16.57 | | 21 40 47.5 | 58 17 01 | 19.87 | 16.71 | 15.45 |
| 21 40 40.7 | 58 17 11 | 19.43 | 17.65 | 16.65 | | 21 40 47.9 | 58 17 01 | 15.73 | 14.83 | 14.61 |
| 21 40 41.1 | 58 16 12 | – | 16.79 | 13.54 | | 21 40 48.4 | 58 16 19 | 18.44 | 17.12 | 16.48 |
| 21 40 41.1 | 58 16 52 | 18.02 | 15.41 | 14.09 | | 21 40 48.4 | 58 16 53 | – | 17.67 | 16.52 |
| 21 40 41.2 | 58 15 54 | 17.25 | 16.51 | 16.35 | | 21 40 48.7 | 58 16 01 | 15.62 | 13.23 | 11.60 |
| 21 40 41.5 | 58 16 38 | 19.04 | 15.54 | 12.59 | –IRS | 21 40 48.7 | 58 16 37 | 16.37 | 15.06 | 14.41 |
| 21 40 41.8 | 58 16 13 | – | – | 17.74 | –B2 | 21 40 48.7 | 58 16 19 | – | 18.83 | 17.87 |
| 21 40 41.9 | 58 17 08 | – | 18.93 | 17.31 | | 21 40 48.8 | 58 16 09 | – | 18.70 | 16.44 |
| 21 40 42.2 | 58 15 53 | 16.57 | 15.47 | 14.71 | | 21 40 48.8 | 58 16 26 | 17.96 | 16.70 | 16.04 |
| 21 40 42.9 | 58 15 45 | 16.37 | 15.44 | 14.77 | | 21 40 49.0 | 58 16 23 | 16.07 | 15.18 | 14.63 |
| 21 40 43.5 | 58 17 16 | – | 18.37 | 15.40 | | 21 40 49.0 | 58 16 60 | 19.44 | 17.49 | 16.82 |

Note. –B1 and B2 refer to the millimeter/centimeter continuum sources of Beltrán et al. (2002) and IRS is HH 777 IRS.

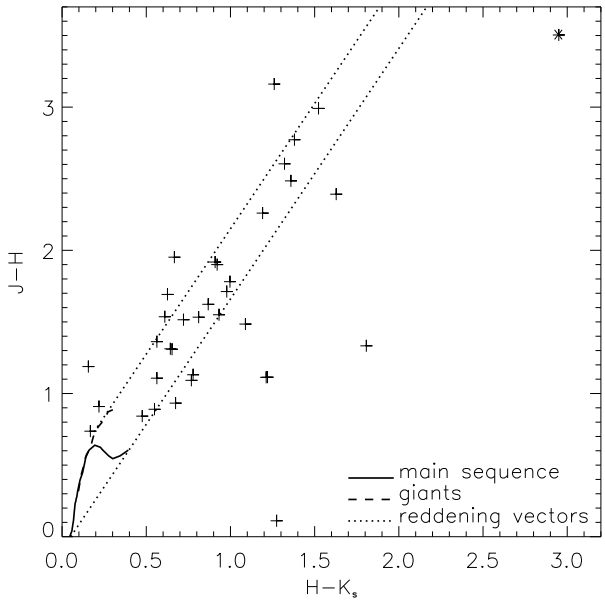


**Figure 4.5**: Color-color diagram showing the stars detected in $J$, $H$ and $K$. 10 sources show infrared excess. The asterisk marks the position of HH 777 IRS ($J - H = 3.50$ and $H - K_s = 2.95$).

HH 777 IRS also lies midway between HH 592 and HH 593 (see Fig. 4.2) and if it is their energy source, it may indicate that HH 777 IRS is a binary. In that case each star is driving an outflow in different directions.

Two of the millimeter/centimeter continuum sources of Beltrán et al. (2002) marked in Fig. 4.1 are visible in our K images (sources 1 and 2), but source 3 could not be identified, at least as a point source. There is a very nebulous extended emission in K coinciding with the source 3 coordinates.

The reddest stars in the field observed are marked in Fig. 4.6, overplotted on a K band image. The open diamonds mark the 10 stars that exhibit infrared excess according to the color-color diagram, and the stars only seen in the K band are marked with a plus. These stars are scattered within the globule center, around HH 777 IRS and the IRAS source, many seem associated with the nebulosities seen at K. That region is also the more active in molecular outflows detected in the millimeter maps. The location of the H$\alpha$ emission stars found by Ogura et al. (2002), mostly at the southern edge of the cloud, suggests that the older stars are close to the bright rim or already outside the cloud, and the younger stars are still embedded. The configuration of the cloud indeed seems to indicate that the UV radiation of the exciting star is triggering the star formation in the globule. But the position of

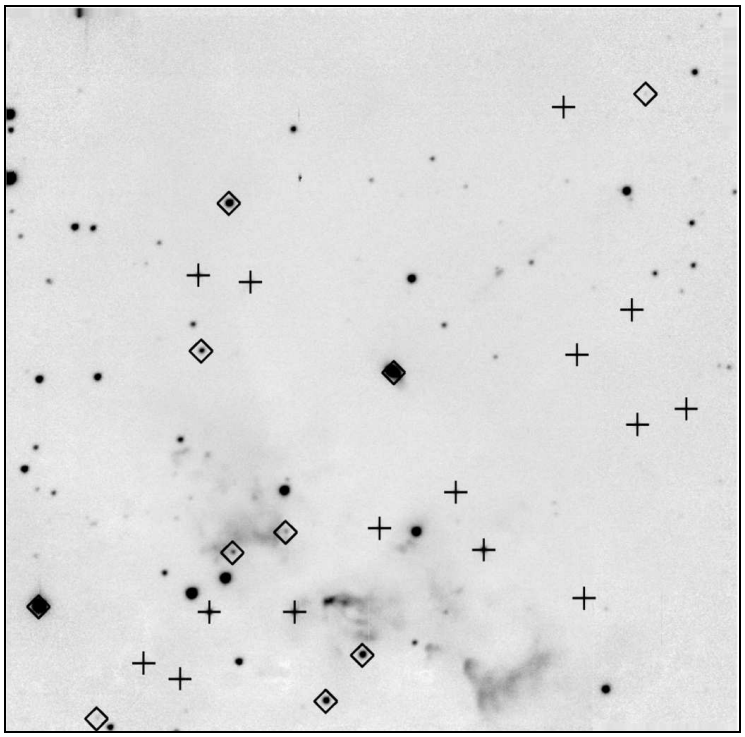

**Figure 4.6**: K band image where the stars that show infrared excess are marked with a diamond and the stars only visible at K are marked with a plus. The field size is $\sim 90' \times 90'$.

the H$\alpha$ emission stars may only be the result of the photo-evaporation of the cloud edge, revealing the stars that were being formed in that area. Our study cannot actually confirm the ages of the stars, so it is not clear whether the visible stars are actually older than the ones that are still embedded. Also we cannot say how the age distribution of the embedded stars varies from the center to the regions closer to the edge.

### 4.1.4 Embedded flows

In order to search for shock components of HH 777 within the globule, we have obtained $H_2$ and [FeII] images in the central field around HH 777 IRS as well as farther west along the HH 777 flow axis (Fig. 4.7). Somewhat to our surprise, we did not find any obvious extension of HH 777 in these transitions. In [FeII] we see essentially no emission anywhere, whereas in $H_2$ we see numerous clumps and flows of shock-excited gas (labeled in Fig. 4.7). Some of those flows (A and G) were already identified by Nisini et al. (2001) in images with less resolution ($1\farcs04$/pixel) than ours ($0\farcs21$/pixel). Here we use and extend Nisini's nomenclature (flows H to

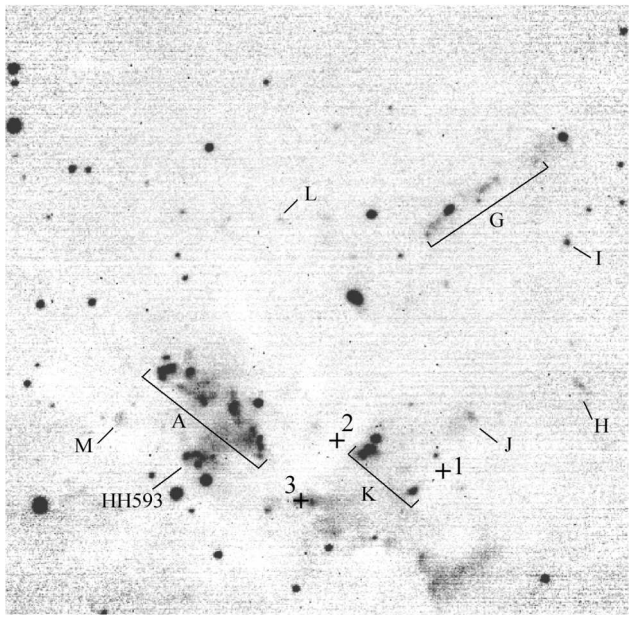


**Figure 4.7**: Infrared image taken through a narrow-band $H_2$ filter at 2.122 $\mu$m and approximately centered on the infrared source HH 777 IRS. The field size is $\sim 90' \times 90'$. The image shows a large number of molecular hydrogen flow components. The flows labeled A and G are from Nisini et al. (2001) and the flows H to M were identified in our images. The three radio continuum sources VLA 1, 2 and 3 from Beltrán et al. (2002) are indicated as well as the position of the optical HH 593 from Ogura et al. (2002).

M).

The main flow, marked A, appears to be driven by VLA 3, whereas flow G points right back toward HH 777 IRS, and if driven by this source, it is probably part of the HH 592/593 complex and a stronger indication that HH 777 IRS is a binary.

Only the western-most of the many $H_2$ knots (knot H) is close to the flow axis of HH 777 and is possibly part of this flow. Table 4.3 lists the approximate positions of the six infrared clumps identified by us.

The IRAS source seems to be associated with the more energetic millimeter molecular outflow. IRAS 21391+5802 (probably VLA 2) is an intermediate mass Class 0 source (Nisini et al. 2001) that should actually drive higher energy outflows. The molecular outflows and the stronger near-infrared flows seem to have the same general orientation, with an inclination of $\sim 80^\circ$ in relation to the North direction. But in general the Herbig-Haro flows point radially back to the core of the cloud, not suggesting any particular alignment. Although one could say that the stronger HH 777 and also HH 589 are aligned with the molecular flow and that the weaker HH 778, HH 779 and HH 780 are perpendicular to it.

**Table 4.3**: Coordinates of $H_2$ flows detected in the IC 1396N region.

| Clump | $\alpha(2000)^a$ | $\delta(2000)^a$ |
|---|---|---|
| H | 21 40 36.5 | +58 16 21 |
| I | 21 40 36.7 | +58 16 47 |
| J | 21 40 38.9 | +58 16 16 |
| K | 21 40 41.3 | +58 16 10 |
| L | 21 40 43.2 | +58 16 51 |
| M | 21 40 46.9 | +58 16 16 |

Note.[a] –The positions are measured at the brightest point.

It is unclear whether a jet (with parameters of a typical HH outflow) emerging from a dense clump into an HII region can produce a morphology similar to the one of HH 777. In order to study this question, Alex Raga and Bo Reipurth have carried out a three-dimensional numerical simulation with the adaptive grid "yguazú" code (Raga et al. 1999, Raga et al. 2000, Masciadri & Raga 2001 and Raga & Reipurth, 2004), to model optically thick flows in the presence of an ionizing radiation field. They find a satisfying match to the observations assuming realistic parameters for the flow, the globule, the HII region, and the ionizing sources. The description and discussion of the simulation can be found at *Blowout from IC 1396N: the emergence of Herbig-Haro flows from a cloud core* (Reipurth, Armond, Raga & Bally 2003) shown in Appendix A.2, where we also present the results of the work described in this chapter.

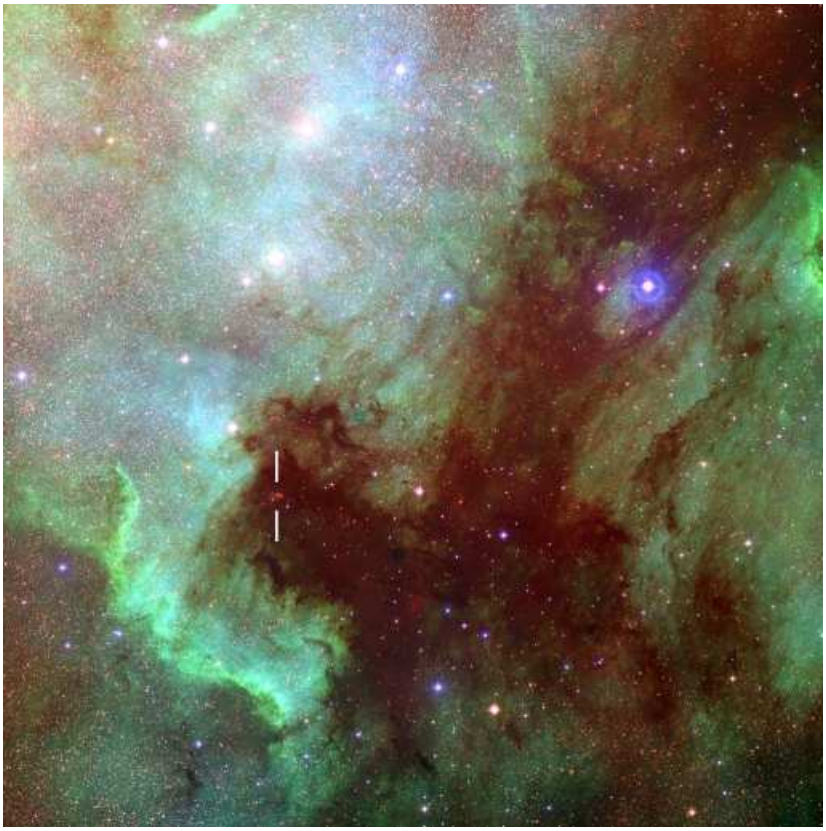

**Figure 4.8**: Optical color image of the North America and Pelican Nebulae, obtained with blue, red and far-red Digitized Sky Survey images. The reddened optical cluster discovered by Herbig is indicated between the two white marks.This image is almost 2° sided.

## 4.2 Gulf of Mexico

W80 is a large HII complex, which has a foreground dust lane optically obscuring its central region, so that this single nebula appears to us as two distinct bright emission nebulae: the North America (NGC7000) and the Pelican (IC5070) nebulae. Bally & Scoville (1980) modeled W80 as an expanding molecular shell, a cloud being disrupted by early type stars born inside. The dust lane hides the region of maximum emission of W80, as well as the energy sources of the complex. We adopt a distance to W80 of 500 ± 100 pc as estimated by Wendker et al. (1983) and supported by Straižys et al. (1993).

The presence of T Tauri and H$\alpha$ emission stars (detected by Herbig 1958 and Cohen & Kuhi 1979, among others) indicates that low mass star formation is occurring. Many of those young stars are thought to be inside the molecular shell. The formation of those stars may be triggered by the expansion of a shock wave through the

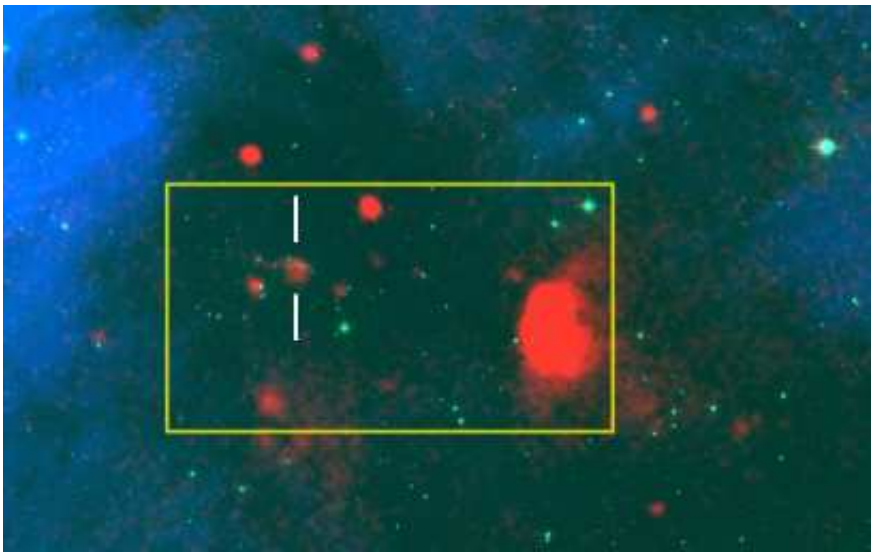

**Figure 4.9**: Color composite image from the Gulf of Mexico made with DSS (blue and green) and MSX (red). The yellow box indicates approximately the region surveyed of $\sim 7' \times 14'$. The optical cluster is indicated by the white marks.

shell. Particularly, there is a small cluster of faint red stars located in the obscured region corresponding to the "Gulf of Mexico". The cluster was discovered by Herbig (1958) and also noted by Cambrésy et al. (2002) and includes the H$\alpha$ emission stars LkH$\alpha$ 186 to 189. Looking at the Midcourse Space Experiment (MSX, Price et al. 2001) 8 $\mu$m images of that region, we can see many warm structures hidden behind the dark cloud (see Fig. 4.9). There is a small structure that coincides with the optical cluster, and a much larger one, located to the west, among other reddened sources.

In order to study this region in more detail, we have observed it in different wavelengths, looking for Herbig-Haro objects, H$\alpha$ emission stars and embedded sources. The region surveyed is marked in Fig. 4.9 by the yellow box.

### 4.2.1 Observations

We have used the University of Hawaii 2.2m telescope at Mauna Kea on June 16 and 17, 2002, with a 2048 $\times$ 2048 Tektronic CCD (scale of $0\farcs22$ /pixel) to image the region centered on the optical cluster. We used a narrow band filter centered on the [SII] 6717/6731Å lines, and a broad band $I$ filter for comparison. $V$ and $R$ images were also obtained for photometry. On July 13, 2002, we used the same telescope and CCD, except that this time we also had the Wide Field Grism Spectrograph

mounted, which gave us a scale of 0.″34 /pixel. Two narrow band filters were used for direct imaging, one centered on H$\alpha$ 6563Å and the same [SII] filter used in June. This time we also pointed at the region adjacent to the west of the cluster, so we have a final mosaic of two images covering a field of approximately $7' \times 14'$ (marked in Fig. 4.9). The seeing varied between 0.″6 and 0.″9. We also got grism images with the H$\alpha$ filter to detect H$\alpha$ emission in the stars through slitless spectroscopy. The spectra obtained through a slit for the stars have a dispersion of 141 Å/mm, with the H$\alpha$ emission line approximately at the center. The total exposure time was 45 minutes for each field. All the observations were reduced using the standard procedures from `IRAF`.

Besides the multi-wavelength images we also got optical low resolution spectra for some of the cluster stars. Due to instrumental problems we could not extract correctly the continuum of the spectra, but we may be able to identify lines that indicate the spectral types of these stars, although we cannot make an accurate spectral classification.

Near-infrared $JHK$ images were obtained with the 4m United Kingdom Infrared Telescope (UKIRT) at Mauna Kea on July 13, 2002, using UFTI with a scale of 0.″091 /pixel. Total exposure times were 300 s for each filter. A 12 point mosaic covered an area of $3.'5 \times 10.'5$. We used narrow-band $H_2$ and [FeII] filters to observe selected regions in 4 pointings, each with 500 s exposure time. Additionally, using Michelle we got a mid-infrared image at 11.6 microns, pointing to the center of the optical cluster. The images were reduced during the observing run with the standard UKIRT pipeline. In some images the reductions were repeated later using the same packages, to remove a few problems, like guide stars lost or saturated stars in a few frames.

We had access to $JHKL'$ images of the optical cluster, obtained and reduced by Colin Aspin in August 1999, using the NASA IRTF Telescope. The instrument used was the NSFCAM, a 1 to 5$\mu$m imager with a 256×256 InSb detector, giving a field of $\sim 75''$ with a plate scale of 0.″30 /pixel.

### 4.2.2 New Herbig-Haro flows

In our [SII] and H$\alpha$ images we have found 28 new Herbig-Haro flows, that are shown in Fig. 4.10. Most of them appear only in the [SII] images; the few that are detected in H$\alpha$ are stronger in [SII], showing that these are low excitation shocked jet material, and not photo-ionized nebulae. The Herbig-Haro flows and their identification are shown in Figs. 4.12 and 4.13 in the [SII] images. In Figs. 4.14 to 4.16 we see each set of flows in every narrow-band filter observed.

**Figure 4.10**: Color composite image from the region surveyed in the optical narrow-bands, with H$\alpha$ in green and [SII] in red. In the western part of the region we see the edge of the emission in the North America Nebula. The Herbig-Haro objects, brighter in [SII], are seen mostly in red.

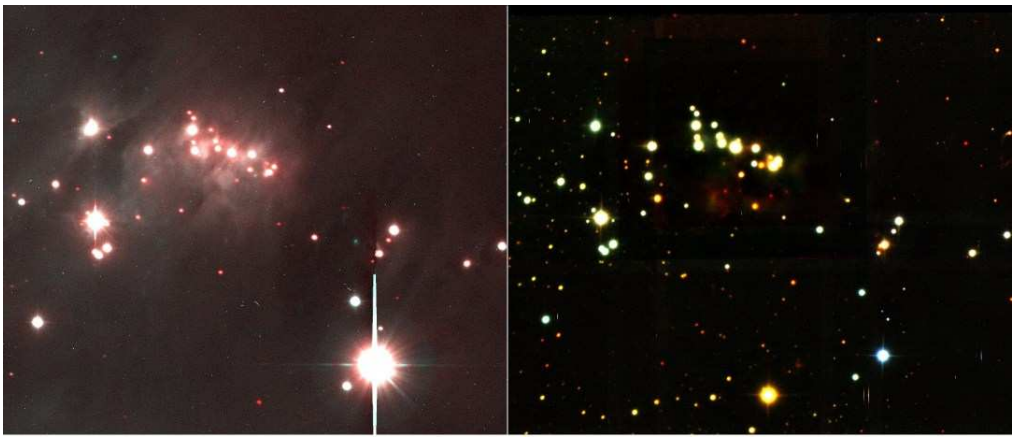

**Figure 4.11**: Color composite image from the cluster region in the optical $VRI$ (left) and in the near-infrared $JHK$ (right).

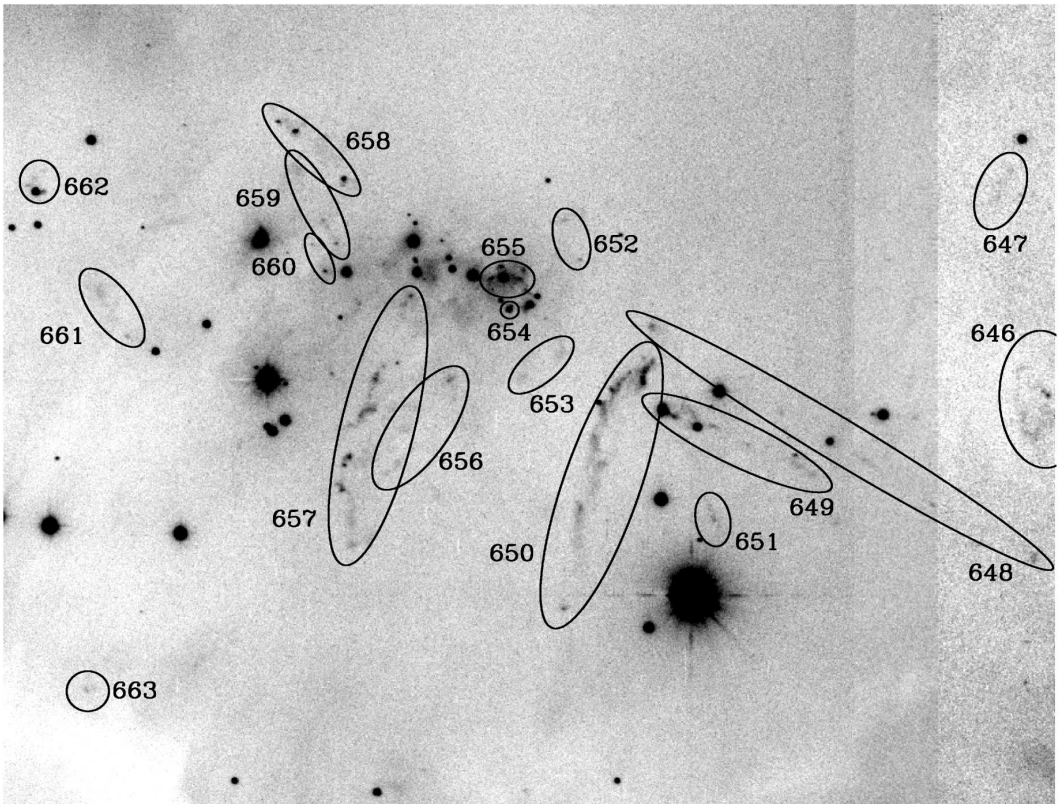


**Figure 4.12**: [SII] image of the eastern part of the region observed with identification for the Herbig-Haro flows.

Most of the flows are brighter in [SII] than in H$\alpha$ . There are some also bright in $H_2$, like HH 654, 655 and 656, which are more embedded flows, likely to be associated with more embedded sources. HH 656 lies in a position where it can be driven by an infrared source right to its north, seen in the $H_2$ image. HH 649 and 650 are very bright in [SII] and the "head" of HH 649 is so bright that it can be seen in the broadband $R$ (that includes the H$\alpha$ and [SII] lines) image.

To the west (Fig. 4.15), the curved filament near HH 644 is a reflection nebula, probably a cavity formed by a molecular outflow. HH 644 is a single knot see in H$\alpha$ , strong in [SII], and with a substantial continuum component presumably illuminated by the embedded driving source. There is a faint sign of what could be the embedded part of HH 644 in the $H_2$ image. HH 645 is probably an extension of HH 644, but we cannot be absolutely sure of that without velocity measurements. A faint emission in H$\alpha$ west of the reflection is probably an extension of HH 644 and if the east and west parts of HH 644 are actually driven by the same source, they point to different directions, and that could indicate that the source is a binary. HH 641 and 642 could be part of the same complex, but that is not clear. The western-most

**Table 4.4**: Herbig-Haro objects in the Gulf of Mexico.

| HH | $\alpha(2000)^a$ | $\delta(2000)^a$ | [SII]$^b$ | H$\alpha^b$ | $H_2^b$ | Notes$^c$ |
|---|---|---|---|---|---|---|
| 636 | 20 57 45.40 | 43 52 46.6 | y | w | n | extends 1.′1 to S |
| 637 | 20 57 45.40 | 43 53 57.5 | y | y | y | strong, knotty shape |
| 638 | 20 57 51.56 | 43 51 39.9 | y | y | - | strong, knot shape |
| 639 | 20 57 55.50 | 43 50 14.4 | y | y | - | very strong, bow-shock shape |
| 640 | 20 57 47.35 | 43 53 24.1 | y | y | y | extends to E and W, 1.′1 wide |
| 641 | 20 57 52.77 | 43 54 00.6 | y | n | n | other knot 6″ NW |
| 642 | 20 57 55.49 | 43 54 06.2 | y | y | n | ∼7″ wide |
| 643 | 20 57 56.47 | 43 52 51.0 | y | n | y | ∼7″ wide |
| 644 | 20 57 55.36 | 43 53 37.1 | y | y | w | extends 30″ to NE |
| 645 | 20 57 59.60 | 43 54 07.2 | y | y | n | extends to N and S, 40″ wide |
| 646 | 20 58 01.43 | 43 53 06.5 | y | y | n | ∼25″ wide |
| 647 | 20 58 02.78 | 43 54 11.7 | w | n | n | weak, 25″ wide |
| 648 | 20 58 01.81 | 43 52 16.2 | y | n | n | extends 2.′3 to NE |
| 649 | 20 58 12.52 | 43 53 02.4 | y | y | n | extends 53″ to SW |
| 650 | 20 58 13.15 | 43 53 13.0 | y | w | n | extends 1.′3 to S |
| 651 | 20 58 11.00 | 43 52 28.4 | w | n | - | weak, 10″ long |
| 652 | 20 58 15.29 | 43 54 00.0 | w | n | w | weak, other knot 15″ SW |
| 653 | 20 58 15.42 | 43 53 19.0 | w | w | n | weak, other diffuse knot 18″ SE |
| 654 | 20 58 16.90 | 43 53 33.1 | y | y | n | strong, stellar-like |
| 655 | 20 58 17.12 | 43 53 46.2 | y | w | y | around star, 10″ wide |
| 656 | 20 58 18.66 | 43 53 10.7 | y | n | y | extends 37″ to SE |
| 657 | 20 58 19.71 | 43 53 36.9 | y | w | n | extends 1.′3 to S |
| 658 | 20 58 21.66 | 43 54 13.4 | y | y | n | extends 30″ to NE |
| 659 | 20 58 21.89 | 43 53 53.2 | y | w | n | extends 30″ to NE |
| 660 | 20 58 22.21 | 43 53 44.6 | y | n | n | extends 10″ to NE |
| 661 | 20 58 27.89 | 43 53 24.3 | y | w | - | extends 20″ to NE |
| 662 | 20 58 30.33 | 43 54 09.2 | y | n | - | around star, 7″ wide |
| 663 | 20 58 28.00 | 43 51 34.3 | w | n | - | weak |

Notes:
[a] –The positions are measured at the brightest point.
[b] –Indicates if the flow is observed at each filter. y means yes, n means no, w means weak and - means it is out of the observed field in that filter.
[c] –Approximate description of how the HH appears in the [SII] image.

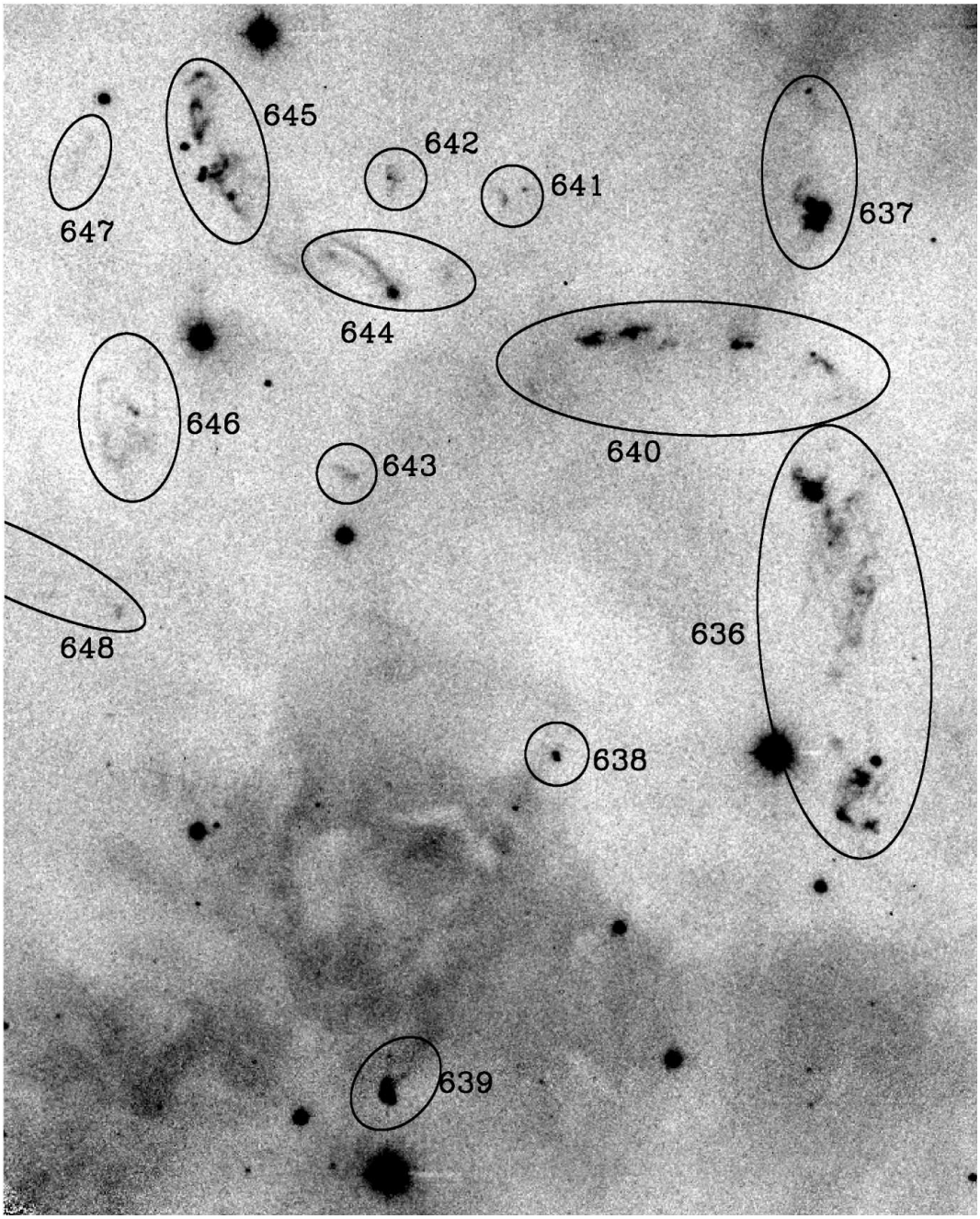


**Figure 4.13**: [SII] image of the western part of the region observed with identification for the newly discovered Herbig-Haro flows.

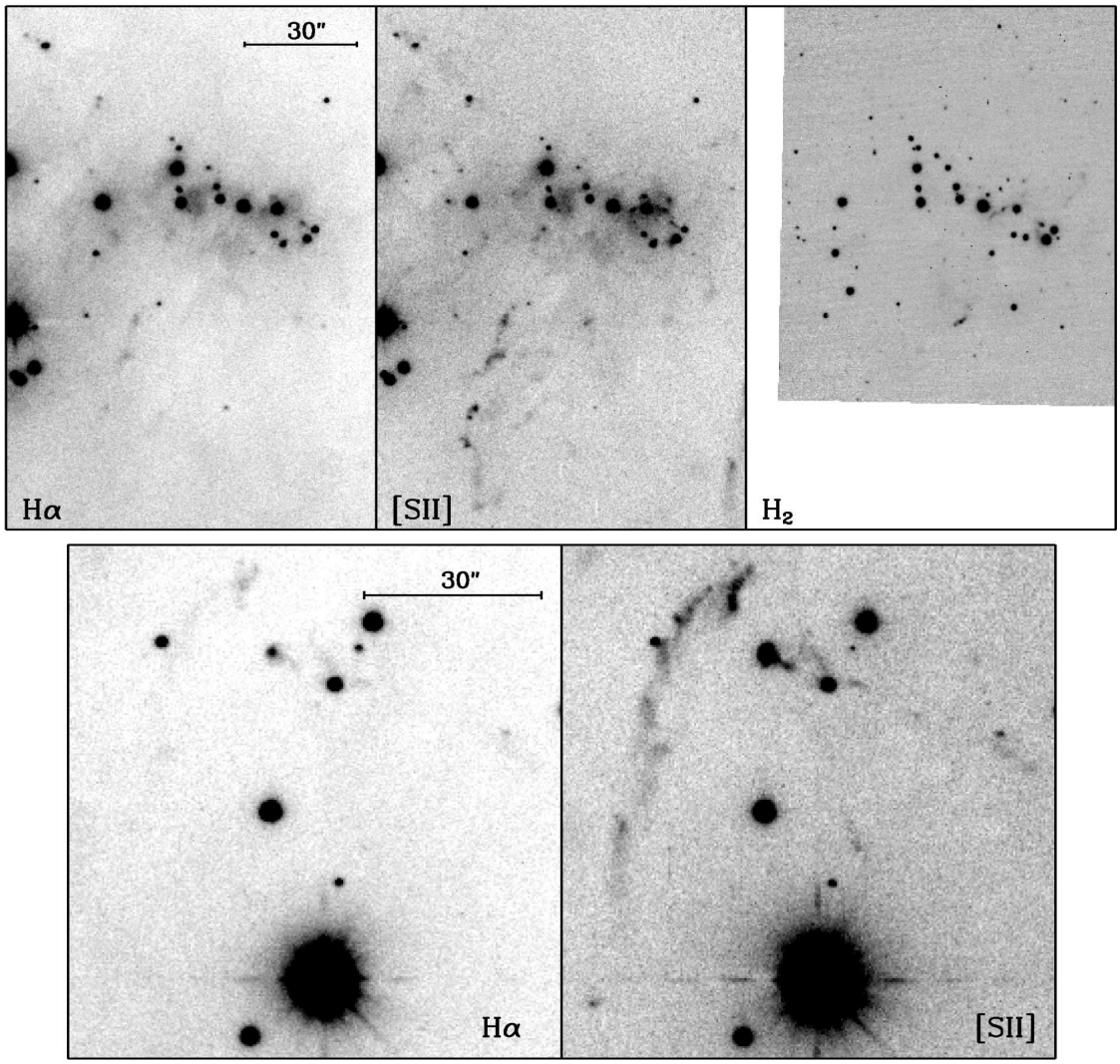


**Figure 4.14**: The upper figure shows the region of the optical cluster and the flows in H$\alpha$, [SII] and $H_2$ filters. We note that most of the flows are brighter in [SII], but there are some also bright in $H_2$, that are more embedded. The lower image shows a south-western region, with the flows seen mostly in [SII]. This area is out of the field of view surveyed in $H_2$.

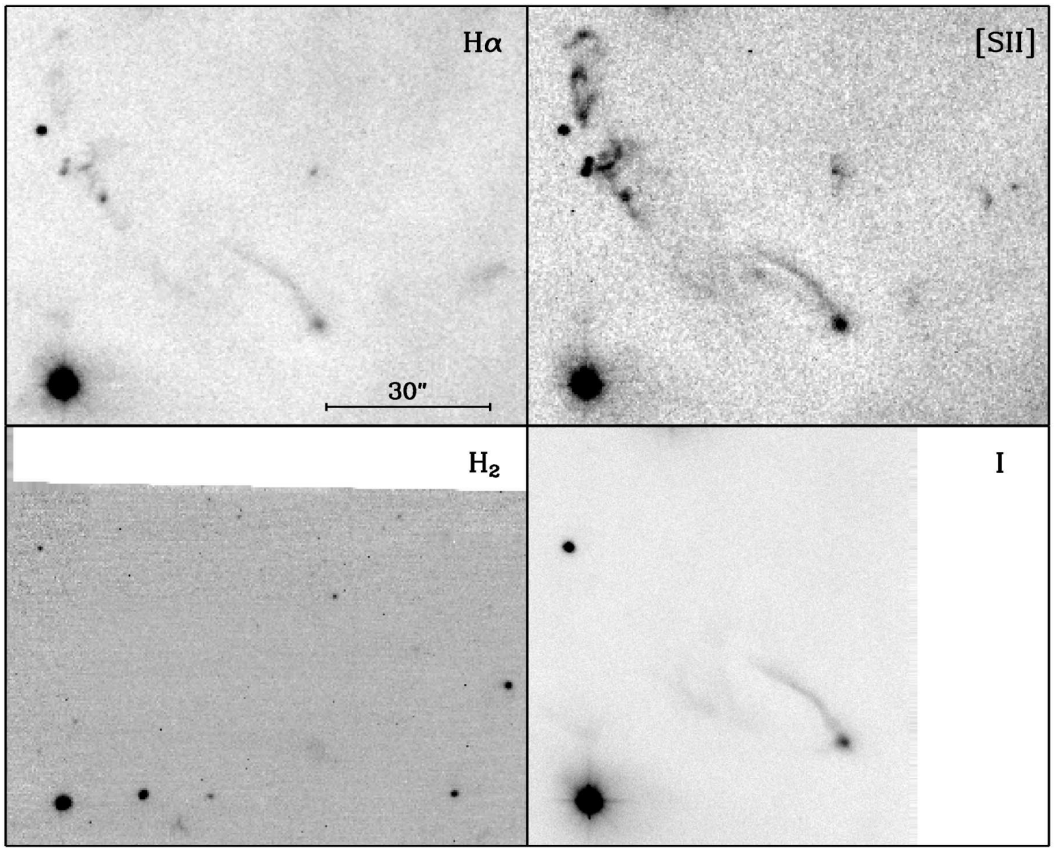


**Figure 4.15**: The region around HH 644 in H$\alpha$, [SII], $H_2$ and the broadband $I$. The curved filament in the center is a reflection nebulae, visible at $I$, an it is probably a cavity drawn by HH 644, that is only seen in [SII]. There is a faint sign of what could be the embedded part of HH 644 in the $H_2$ image, and also what could be an extension of the western part of HH 644 in H$\alpha$.

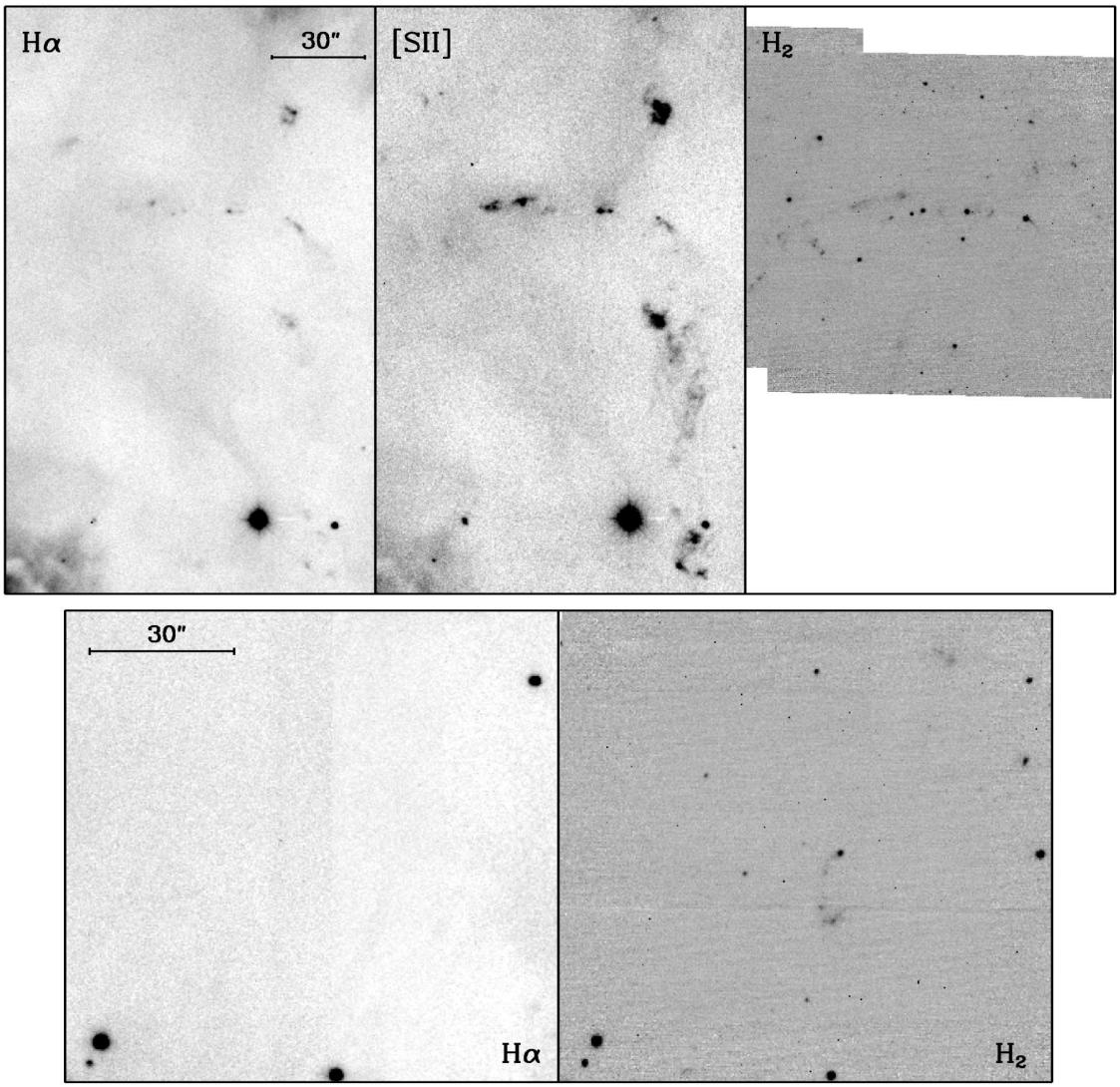


**Figure 4.16**: Upper figure: the western-most flows in Hα, [SII] and $H_2$. They are very bright in [SII], especially the "heads". The central region, more embedded, is bright in the infrared. Lower figure: a region near the center of the field surveyed, where nothing is seen in the optical, but some features are seen in the infrared.

flows HH 636, 637 and 640 are shown in the upper image of Fig. 4.16. They are very bright in [SII], especially the "heads". The central region, more embedded, is bright in the infrared.

In the center of the field surveyed nothing is seen in the optical images, but some features are seen in the infrared, shown in the lower image of Fig. 4.16.

### 4.2.3 Young sources

*Hα emission stars*

In our grism images using the Hα filter, the emission line is approximately centered in the spectra and it is rather easy to detect the point-like emission and at the same time have a panoramic view of the whole area (Fig. 4.17). The images are deep and we can detect the continuum of stars up to V = 23 mag.

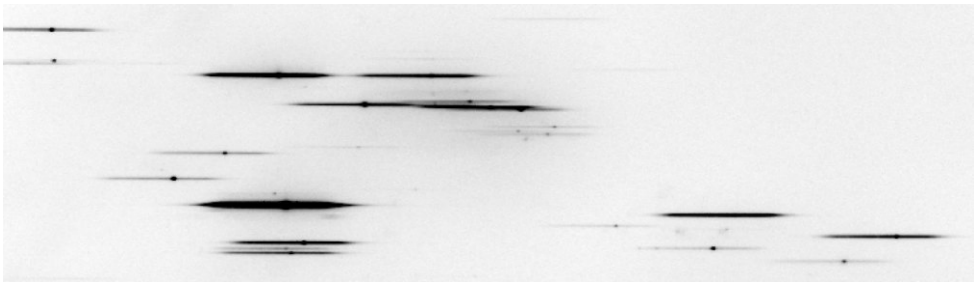

**Figure 4.17**: Excerpt of the grism image showing many Hα emission stars in the cluster region. A Herbig-Haro object (a knot of HH 649) is seen at the lower right, as two diffuse emission lines, in contrast to the point-like shape of the Hα emission on top of the continuum of the stars.

The images were examined using `imexamine` from IRAF to check for stars with emission. The equivalent widths were also measured with IRAF. 38 Hα emission stars where found in the region surveyed (see Fig. 4.18). They are located mostly around the LkHα 186 cluster, but there are also Hα emission stars to the west. Almost all the stars around the cluster seen in the optical show emission in Hα. A few of them were previously known (LkHα 185 to 189 from Herbig 1958).

In 1998, George Herbig observed the LkHα 186 cluster region with the same instrument we used. He detected almost all the Hα emission stars we do (25 out of the 30 we detected in the common field of view). Table 4.5 lists the coordinates of the emission stars, the optical $VRI$ magnitudes obtained with our broadband images, the $JHK_s$ magnitudes listed in the 2MASS All Sky Survey Catalog and the equivalent widths obtained by us and by George Herbig.

**Table 4.5**: H$\alpha$ emission line stars in the Gulf of Mexico.

| MKH$\alpha$ | LkH$\alpha$ | $\alpha$(2000) | $\delta$(2000) | V | R | I | J$^a$ | H $^a$ | K$_s^a$ | W$_{(2002)}$ | W$^b_{(1998)}$ |
|---|---|---|---|---|---|---|---|---|---|---|---|
| 1 | | 20 57 41.8 | +43 49 54 | 20.85 | 19.37 | * | 13.97 | 13.16 | 12.86 | 10 | |
| 2 | | 20 57 48.9 | +43 50 24 | 17.17 | 16.18 | * | 12.56 | 11.96 | 11.73 | 10 | |
| 3 | | 20 57 59.5 | +43 51 23 | 22.17 | 20.73 | 18.94 | 15.70 | 14.78 | 14.34 | 8 | |
| | 185 | 20 57 59.9 | +43 53 26 | 16.22 | 15.08 | 14.60 | 11.85 | 10.87 | 10.25 | 114 | |
| 4 | | 20 58 06.1 | +43 49 34 | 18.32 | 17.28 | 16.39 | 13.89 | 13.12 | 12.78 | 26 | |
| 5 | | 20 58 06.2 | +43 53 01 | 17.93 | 16.74 | 15.95 | 13.41 | 12.58 | 12.21 | 30 | |
| 6 | | 20 58 07.6 | +43 52 53 | 20.55 | 18.90 | 17.52 | 14.10 | 12.79 | 11.98 | 48 | |
| 7 | | 20 58 11.4 | +43 52 58 | 16.63 | 16.43 | 16.14 | 13.75 | 12.21 | 11.21 | 108 | 97 |
| 8 | | 20 58 14.3 | +43 53 05 | 20.89 | 19.44 | 17.53 | 14.17 | 13.39 | 12.94 | 32 | 45 |
| 9 | | 20 58 16.1 | +43 53 37 | 21.22 | 19.38 | 17.43 | 13.46 | 11.33L | 10.58L | 24 | 26 |
| 10 | | 20 58 16.3 | +43 53 35 | 20.24 | 18.53 | 16.94 | 13.03 | 11.21L | 10.42L | 14 | 22 |
| 11 | 188/G4 | 20 58 17.0 | +43 53 43 | 19.09 | 17.67 | 16.55 | 13.25 | 12.21 | 11.46 | 70 | 68 |
| 12 | | 20 58 17.1 | +43 53 36 | 21.77 | 20.15 | 18.00 | 14.09L | 13.00L | 12.96 | 12 | 22 |
| 13 | 188/G3 | 20 58 17.9 | +43 53 44 | 18.58 | 16.84 | 15.48 | 11.77 | 10.42 | 9.70 | 14 | 11 |
| 14 | 188/G2 | 20 58 18.5 | +43 53 47 | 20.53 | 18.75 | 17.08 | 13.21L | 12.18 | 11.39 | 28 | 30 |
| 15 | | 20 58 18.6 | +43 53 49 | 21.83 | 19.90 | 18.30 | 13.39L | 12.76 | 11.96 | 6 | 9 |
| 16 | | 20 58 19.5 | +43 53 45 | 19.34 | 17.65 | 16.18 | 12.62 | 11.35 | 10.84 | 7 | – |
| 17 | | 20 58 19.6 | +43 53 48 | 22.71 | 20.58 | 18.90 | – | – | – | 5 | 15 |
| 18 | | 20 58 19.6 | +43 54 00 | 21.70 | 20.13 | 18.08 | 13.79L | 13.69 | 13.29 | 4 | – |
| | 186 | 20 58 19.6 | +43 53 55 | 18.12 | 16.68 | 15.85 | 12.69 | 11.49 | 10.92 | 31 | 33 |
| | 187 | 20 58 21.6 | +43 53 45 | 18.56 | 17.05 | 16.00 | 12.80 | 11.49 | 10.71 | 72 | 40 |
| 19 | | 20 58 21.7 | +43 53 31 | 22.40 | 20.62 | 18.17 | 13.77 | 12.36 | 11.80 | 8 | – |
| 20 | | 20 58 23.3 | +43 53 51 | – | 22.27 | 18.10 | 15.82 | 14.88 | 14.41 | 6 | nc |
| 21 | | 20 58 23.3 | +43 52 59 | 17.81 | 16.62 | 15.65 | 12.77 | 11.81 | 11.34 | 41 | 25 |
| 22 | | 20 58 23.7 | +43 52 56 | 18.30 | 16.98 | 15.87 | 12.87 | 12.07 | 11.74 | 23 | 12 |
| 23 | | 20 58 23.9 | +43 52 57 | 18.62 | 17.29 | 16.06 | – | – | – | 5 | 4 |
| | 188 | 20 58 23.8 | +43 53 12 | 14.65 | 13.69 | 13.37 | 10.56 | 9.62 | 8.84 | 48 | 28 |
| 24 | | 20 58 24.4 | +43 53 15 | 20.79 | 19.56 | 18.31 | – | – | – | 16 | – |
| | 189 | 20 58 24.0 | +43 53 55 | 17.10 | 15.80 | 15.03 | 12.23 | 11.16 | 10.69 | 47 | 29 |
| 25 | | 20 58 25.6 | +43 53 29 | 19.58 | 18.11 | 16.81 | 13.60 | 12.40 | 11.73 | 44 | 37 |
| 26 | | 20 58 27.1 | +43 53 20 | 19.54 | 18.20 | 17.26 | 14.02 | 12.92 | 12.25 | 71 | 45 |
| 27 | | 20 58 27.4 | +43 53 24 | 23.60 | 21.78 | 19.86 | 16.08 | 15.03 | 14.34 | 12 | – |
| 28 | | 20 58 27.5 | +43 53 58 | 22.80 | 21.51 | 19.41 | 15.28 | 14.32 | 13.79 | 4 | 15 |
| 29 | | 20 58 27.3 | +43 54 55 | 23.65 | 21.81 | 19.98 | 15.87 | 15.03 | 14.40 | 18 | nc |
| 30 | | 20 58 30.4 | +43 53 59 | 19.87 | 18.61 | 17.41 | 14.82 | 13.67 | 12.89 | 34 | 42 |
| 31 | | 20 58 30.5 | +43 54 10 | 20.68 | 19.20 | 17.63 | 13.79 | 12.84 | 12.41 | 33 | 17 |
| 32 | | 20 58 31.2 | +43 53 58 | 19.10 | 17.78 | 16.63 | 15.33 | 14.04 | 13.29 | 4 | 5 |

Notes:
* – means stars not within I-image.
$^a$ – $JHK_s$ magnitudes extracted from the 2MASS All-Sky Catalog. All magnitudes marked L are upper limits.
$^b$ – H$\alpha$ equivalent widths measured by George Herbig in 1998. *nc* means H$\alpha$ emission with no or very faint continuum.

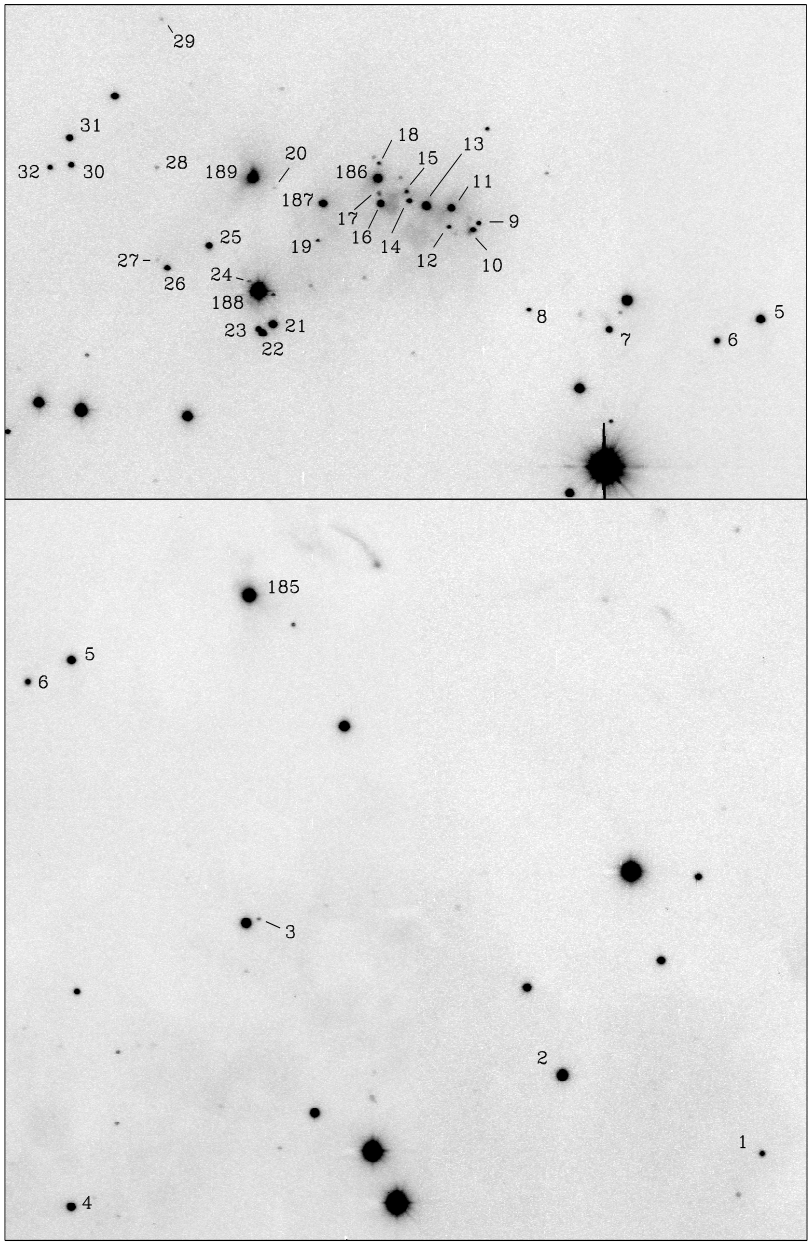


**Figure 4.18**: $R$ band image showing the H$\alpha$ emission stars found. The upper image is the eastern field and at the bottom is the western field. Stars 5 and 6 appear in both images, so it is easy to locate the two fields, that are shown in the same scale. Stars numbered 185 to 189 are LkH$\alpha$ emission stars, as in Table 4.5

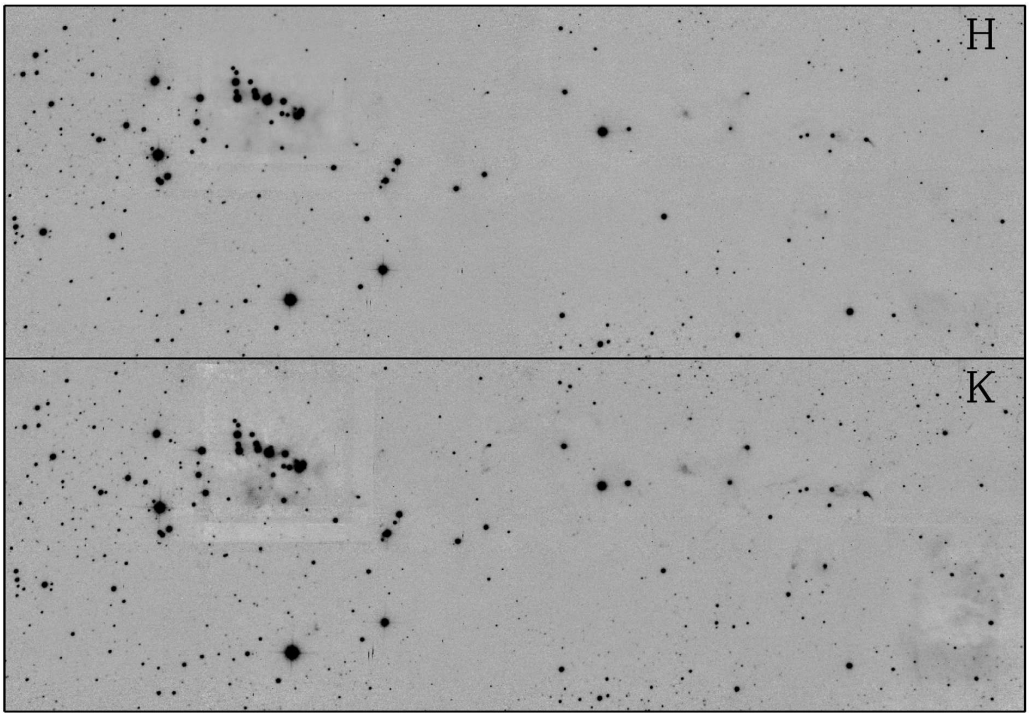


**Figure 4.19**: $H$ and $K$ mosaics. The number of stars increases as we move to larger wavelengths. The exposures of the optical cluster region were about twice as large as the others, so the final mosaic image is not perfect in the overlapped region around the cluster.

*Embedded sources*

The $JHK$ images from UKIRT (Mauna Kea) were obtained in non-photometric conditions. There were thin clouds in the sky and the variability of the conditions from one pointing to another makes it impossible to obtain good photometry. An attempt was made to calibrate the near-infrared images with 2MASS, as was done for IC 1396N, but the dispersion of magnitudes reached 0.5 mag, due to the difference between the 13 fields observed to form a mosaic covering almost all the field surveyed in the optical. Therefore we use these infrared images only to visually try to locate the regions where the stars look more embedded, and to try to locate probable sources for the flows found.

Mosaics made with the $H$ and $K$ images are shown in Fig. 4.19, where we see an increase of the number of sources as we move from $H$ to $K$ band, as expected, particularly south of the optical cluster. There is a faint sign of a nebulosity at the lower right corner of the image, the same location of the MSX large extended structure shown in Fig. 4.9. The nebulosity right south of the optical cluster may also be related to the MSX source detected approximately at the position of the cluster.

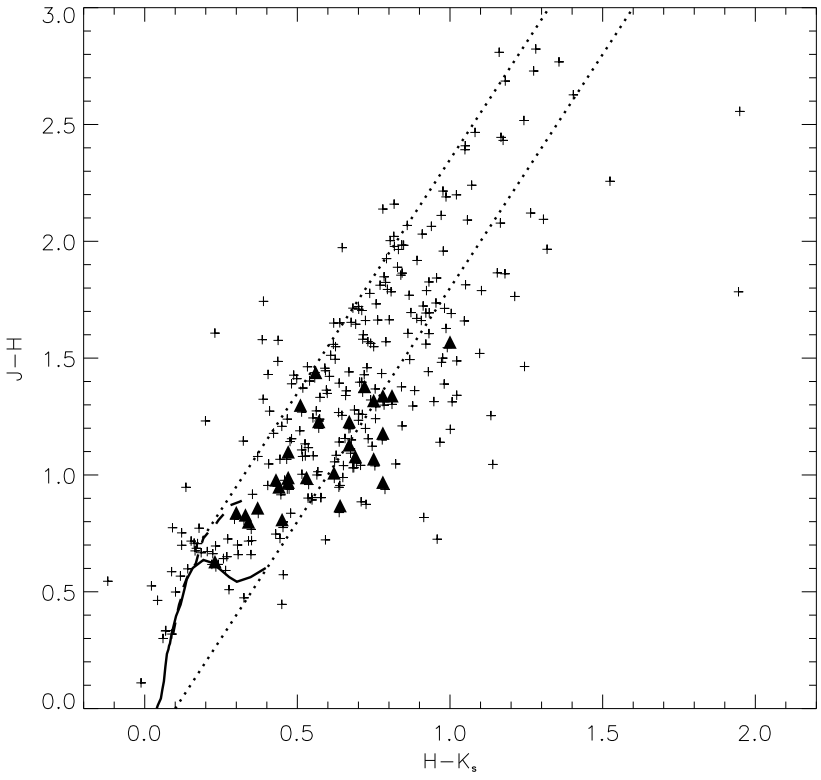


**Figure 4.20**: $JHK_s$ diagram of the stars detected in all the 3 bands with 2MASS. Solid triangles are the H$\alpha$ emission stars in Table 4.3. The solid and dashed lines are respectively the location of main sequence and giant stars from Bessell & Brett (1988) corrected to the 2MASS photometric system (Carpenter 2001). The dotted lines are interstellar reddening vectors from Rieke & Lebofsky (1985).

We use the $JHK_s$ 2MASS magnitudes of the stars in the field surveyed to make a color-color diagram (Fig. 4.20) to identify stars with infrared excess, presumably the result of circumstellar material, and currently used as an indication of a disk. About 25% of the stars show infrared excess, almost the same fraction of the NGC 2264 region (Section 2.1). So according to Lada et al. (1996) we can have an age estimate of $\sim 5 - 6 \times 10^6$ years for that region. Mostly all the stars to the left of the reddening vectors have larger photometric errors in the $J$ band than the average 2MASS uncertainties. That is because most of the stars just begin to be detected at $J$ and are more visible at larger wavelengths. The spatial distribution of the infrared excess stars does not show any indication of a larger concentration of more embedded stars in any region, close to the optical cluster or to the west, where there are many flows, but few optically visible stars (Fig. 4.21).

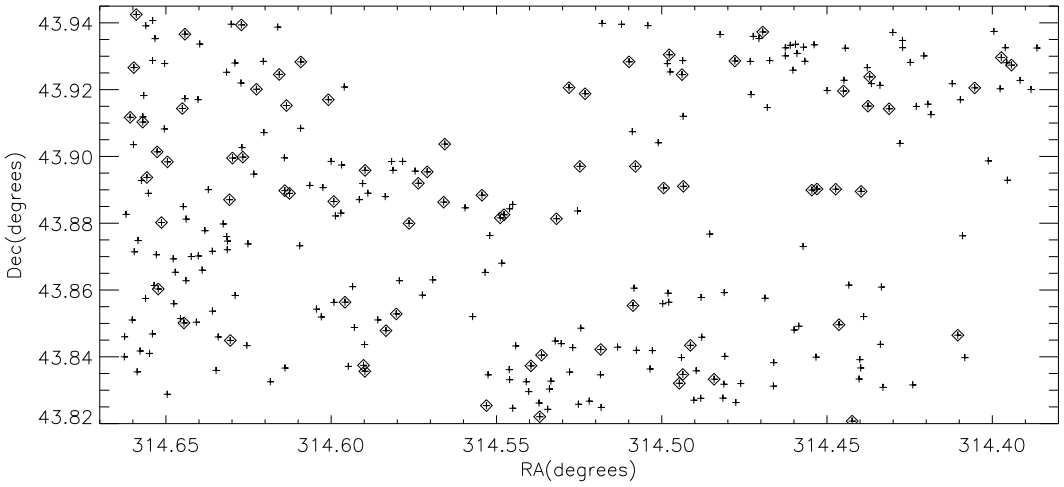


**Figure 4.21**: The distribution of stars detected in all the three 2MASS bands. The diamonds indicate the stars with infrared excess.

The H$\alpha$ emission stars are marked as solid triangles in the $JHK_s$ diagram and about 10 of them show some infrared excess, following the same fraction of all the stars in the area. The rest of them show colors typical of non-embedded sources, as we could expect for more evolved young stars that are already revealed at optical wavelengths.

The $JHKL'$ IRTF images cover only the central cluster area, but they were obtained in perfect conditions, so photometry was performed only for those stars. The average uncertainties were of the order of 0.05 mag. Fig. 4.22 shows the images of the four bands and Fig. 4.23 is a sum of all the four images, with the identification numbers of the stars detected, as used in Table 4.6.

A color-color diagram was plotted in a similar way to the one built with 2MASS magnitudes (Fig 4.24). This time the tracks were not corrected for the 2MASS photometric system, as we use the standard IRTF $JHK$ filters. Among the 22 stars detected in all the three bands, $7 \pm 2$ have infrared excess (36%), a larger fraction than the previous, using 2MASS $JHK_s$ magnitudes. Our observations are more sensitive and are concentrated in an area where certainly all the stars are young, so it is not a surprise that we have a larger amount of stars with signs of circumstellar disks. Two stars lie in the forbidden region, to the left of the reddening vectors, the stars labeled 2 and 12 in Fig. 4.23. Star 12 is located close to the bright star 14, so the photometric accuracy may be compromised. Star 2 do not have larger photometric errors, and is isolated from the main cluster. Its particular location in the diagram may indicate that this is a binary star.

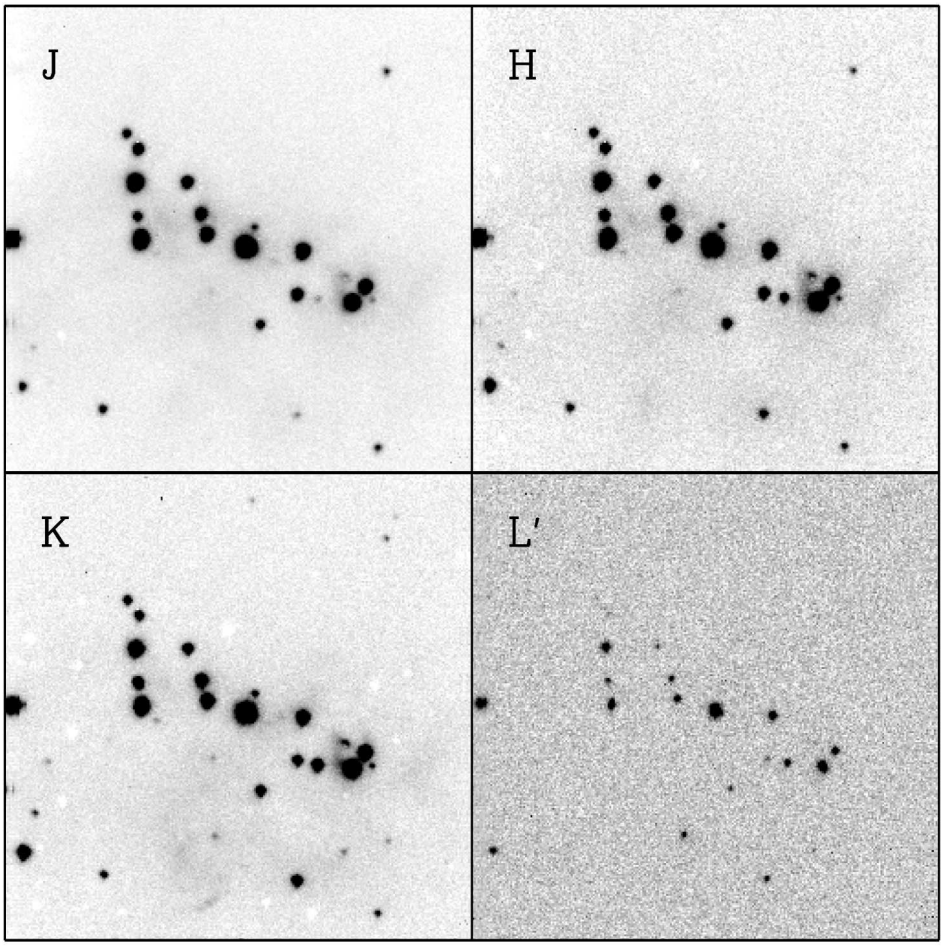


Figure 4.22: The LkH$\alpha$ 186 cluster $JHKL'$ images observed at IRTF.

At 11.6$\mu$m (UKIRT Michelle observations) we detect three sources, that are therefore, quite embedded. Their positions coincide, within the errors, with the stars labeled 7, 15 and midway between stars 12 and 14 in Table 4.6 and Fig. 4.23. Star 7 is located at the upper right corner of the $JHK$ color-color diagram and it is one of the stars with higher infrared excess. It is barely seen at $J$ and very bright at $K$ and $L'$. Star 15 is only seen at $K$ and $L'$ and it is close to a nebulosity seen at $K$ and an $H_2$ flow associated with HH 656. Its position indicates that it could be the source of this flow, that also show signs of being embedded in the cloud. Star 12 shows regular near infrared colors and it is not seen in $L'$, while star 14 has an H$\alpha$ emission (MKH$\alpha$ 13) and is also bright at $L'$. Thus it is more likely that the 11.6$\mu$m source is associated with star 14.

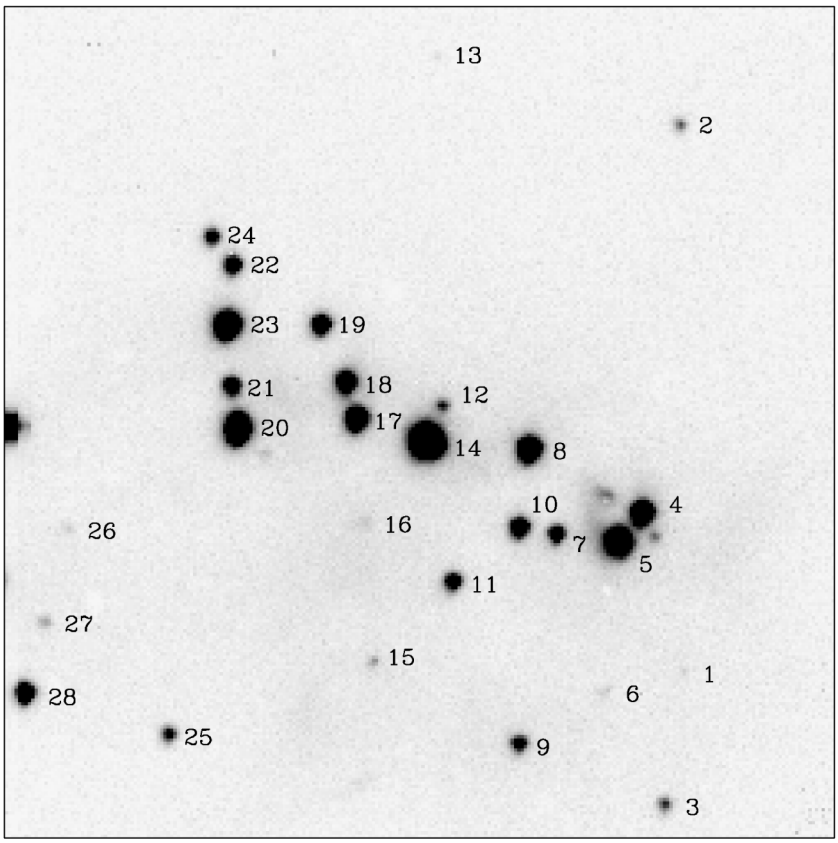


**Figure 4.23**: Sum of $J$, $H$, $K$ and $L'$ images with identification numbers for the LkH$\alpha$ 186 cluster used in Table 4.6.

**Table 4.6**: $JHKL'$ observations of LkH$\alpha$ 186 cluster.

| Id | H$\alpha$ Number | $\alpha$(2000) | $\delta$(2000) | J | H | K | L$'$ | IRX |
|---|---|---|---|---|---|---|---|---|
| 1 | | 20 58 15.7 | +43 53 23 | - | - | 15.97 | - | |
| 2 | | 20 58 15.7 | +43 54 12 | 16.39 | 15.62 | 15.65 | - | |
| 3 | | 20 58 15.8 | +43 53 12 | 16.15 | 15.33 | 14.72 | - | * |
| 4 | MKH$\alpha$ 9 | 20 58 16.1 | +43 53 37 | 13.49 | 12.04 | 11.38 | 8.21 | |
| 5 | MKH$\alpha$ 10 | 20 58 16.3 | +43 53 35 | 13.36 | 11.70 | 10.79 | 7.30 | |
| 6 | | 20 58 16.4 | +43 53 22 | - | - | 15.70 | - | |
| 7 | | 20 58 16.8 | +43 53 36 | 17.49 | 14.22 | 12.27 | 8.44 | * |
| 8 | MKH$\alpha$ 11 | 20 58 17.0 | +43 53 43 | 13.18 | 12.00 | 11.41 | 7.69 | |
| 9 | | 20 58 17.1 | +43 53 17 | 17.17 | 14.42 | 12.72 | 9.06 | * |
| 10 | MKH$\alpha$ 12 | 20 58 17.1 | +43 53 36 | 14.24 | 13.30 | 12.94 | - | |
| 11 | | 20 58 17.7 | +43 53 31 | 15.37 | 13.77 | 12.89 | 9.61 | |
| 12 | | 20 58 17.8 | +43 53 47 | 15.85 | 14.39 | 14.07 | - | |
| 13 | | 20 58 17.8 | +43 54 18 | - | - | 16.28 | - | |
| 14 | MKH$\alpha$ 13 | 20 58 17.9 | +43 53 44 | 11.72 | 10.33 | 9.65 | 6.24 | |
| 15 | | 20 58 18.4 | +43 53 24 | - | - | 15.68 | 8.89 | |
| 16 | | 20 58 18.4 | +43 53 37 | - | 16.80 | 16.54 | - | |
| 17 | MKH$\alpha$ 14 | 20 58 18.5 | +43 53 47 | 13.62 | 12.13 | 11.46 | 8.20 | |
| 18 | MKH$\alpha$ 15 | 20 58 18.6 | +43 53 49 | 14.38 | 12.74 | 11.97 | 8.95 | |
| 19 | | 20 58 18.8 | +43 53 54 | 14.29 | 13.19 | 12.69 | 9.75 | |
| 20 | MKH$\alpha$ 16 | 20 58 19.5 | +43 53 45 | 12.66 | 11.32 | 10.82 | 7.86 | |
| 21 | MKH$\alpha$ 17 | 20 58 19.6 | +43 53 48 | 15.27 | 13.56 | 12.54 | 9.16 | * |
| 22 | MKH$\alpha$ 18 | 20 58 19.6 | +43 54 00 | 14.55 | 13.76 | 13.49 | - | |
| 23 | LkH$\alpha$ 186 | 20 58 19.6 | +43 53 55 | 12.63 | 11.39 | 10.84 | 7.52 | |
| 24 | | 20 58 19.8 | +43 54 02 | 15.34 | 14.19 | 13.63 | - | |
| 25 | | 20 58 20.1 | +43 53 17 | 15.68 | 14.74 | 14.25 | - | |
| 26 | | 20 58 21.0 | +43 53 35 | - | - | 16.06 | - | |
| 27 | | 20 58 21.2 | +43 53 27 | 18.09 | 16.35 | 15.20 | - | * |
| 28 | | 20 58 21.3 | +43 53 21 | 15.69 | 13.05 | 11.60 | 8.50 | * |

Note. –* marks the stars with infrared excess according to the $JHK$ color-color diagram (Fig. 4.23)

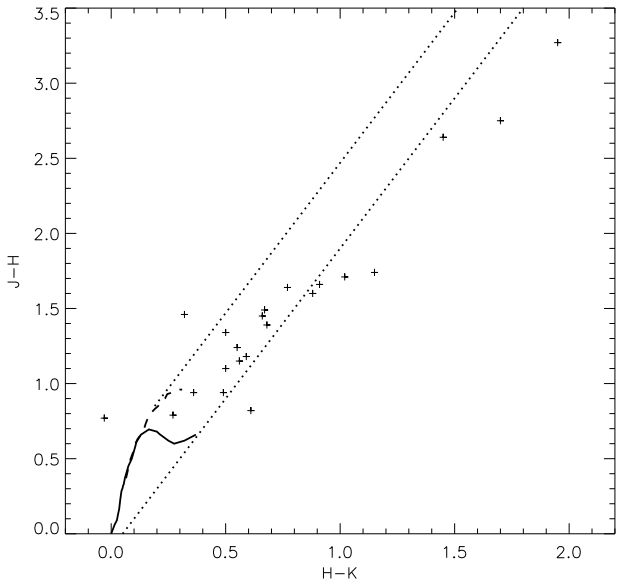


**Figure 4.24**: $JHK$ diagram of LkH$\alpha$ 186 cluster showing the stars detected in the IRTF $J$, $H$ and $K$ images. The solid and dashed lines are respectively the location of main sequence and giant stars from Bessell & Brett (1988) and the dotted lines are interstellar reddening vectors from Rieke & Lebofsky (1985). The stars with infrared excess are marked in Table 4.6.

*Flows and sources*

It is not easy to relate the flows described in Section 4.2.2 with the young sources found in Section 4.2.3. Some of the new Herbig-Haro objects have a curved overall shape (eg. HH 636, 640, 645), a few appear more as a straight line (HH 648, 658, 659) and many show a very knotty structure (HH 650, 657). This is a complex region, very dense in gas, with many sources highly embedded, but the stars of the optical cluster are certainly young and drive some of the HH objects.

As mentioned earlier, HH 656 is likely driven by the near infrared source labeled star 15 in Fig. 4.23. HH 654 could be associated with the near infrared (and also 11.6$\mu$m source) star 7, while HH 655 is certainly associated with the central stars in the LkH$\alpha$ 186 cluster and MKH$\alpha$ 16 could be the source of HH 657. Both MKH$\alpha$ 26 or 27 could be the source of HH 661. The other flows in that eastern region could be associated with the stars in the cluster, with the surrounding H$\alpha$ emission stars or to other more embedded sources.

MKH$\alpha$ 6 (Table 4.5) is at the projected center of HH 648 and could be its source. In the near infrared mosaic we can identify a source that is likely driving HH 650, as it is located at the point where the flow seems to begin. The near infrared star 9 (Table 4.6) may drive HH 653.

At the western region, it is even more difficult to find the flow sources, as the region has less optical or near infrared candidates. Some near-infrared sources are associated with HH 640 and possibly to HH 637. If those two have the same origin, we have another indication of binarity.

Without proper motions or radial velocities it is rather difficult to locate precisely the source for each flow. The large distance of the cloud makes proper motion measurements difficult, because the time necessary for detecting them is larger than the time scale for changes in brightness of the small structures of the flows. However, images taken with several years of interval may reveal the overall motion of the HH objects, maybe indicating their sources.

In general the flows do not have a particular orientation, opposite to what happened in the L1551 region. The average projected extent of the larger flows is approximately $1'$, which, at a distance of 500pc, gives $\sim$0.15 pc. Thus, the flows have not reached larger distances yet, indicating that this region has begun to form stars rather recently. The presence of the larger density of H$\alpha$ emission line stars near the optical cluster at east shows that this is the site where the star formation began. The region right south of it, where there are the more embedded sources, including the ones detected at 11.6$\mu$m, is in a less evolved stage. The western region, where there are outflows in the optical and near-infrared, an extended structure bright at 8$\mu$m (MSX), but only a few H$\alpha$ emitters, is probably in an even less evolved stage of star formation.

We have surveyed the region of the Gulf of Mexico around the optical cluster that contains LkH$\alpha$ 186 to 188 using H$\alpha$ and [SII] filters and we found 28 new Herbig-Haro objects. The search for H$\alpha$ emission stars resulted in many more emission stars than previously known; 38 in the region surveyed. Also, the infrared images confirm that there are many embedded young sources in the region.

It would be nice to have all the region surveyed again with this resolution and depth in the near-infrared, using $J$, $H$, $K$ **and** $L$ filters, under photometric conditions. A finer analysis of the spectra we obtained could tell us about spectral types, but high quality higher resolution spectra could give us mass and age distribution of the young stars. Images taken in a few years could indicate the direction of the flows and radial velocities would give us a three-dimensional view of the area.

We conclude that star formation is much more active in that area than previously suspected. The optical cluster of H$\alpha$ emission stars is only a small portion of the total number of stars being formed there. The presence of Herbig-Haro flows, the reddened sources and the big structure shown in 8$\mu$m (from MSX) suggest that this is a large site of widespread star formation, still partially hidden behind the dark cloud, suggesting the need for further studies in the Gulf of Mexico.

# Chapter 5

# Conclusions and Perspectives

The main results of the work presented here are:

1. The detection of a large number of new H$\alpha$ emission stars in the very well known star forming regions NGC 2264 and M 42. We used the classical photographic technique instead of digital CCD detectors, but using the most sensitive and fine-grained films currently available on one of the worlds largest Schmidt telescopes located at an excellent observing site, we have pushed this classical technique to its present-day limits, surveying an area of 25 square degrees in the sky and detecting many previously unknown H$\alpha$ emission stars. In NGC 2264 we have also searched for double stars, obtaining a binary frequency consistent with similar studies. A correlation with the molecular gas distribution suggests that star formation is an ongoing process in the region, at least for several million years. A table with estimates for H$\alpha$ emission strength and other characteristics for the stars was produced, as well as finding charts for each star. The results of this work were published in 2004 by the *Astronomical Journal* (Reipurth et al. 2004). In M 42 we have detected almost 2000 H$\alpha$ emission stars, most were unknown. A table similar to NGC 2264 were produced and the study of the spatial distribution, of the correlation of the emission with infrared excess and with variability will be performed for publication.

2. The measurement of proper motions of Herbig-Haro objects in deep wide field images of L1551, simultaneously calculating the projected velocities of the

outflows in the entire region, yielding an overall view of the outflows and their relationship with unprecedented detail. We confirm the association of Herbig-Haro objects with some sources and propose some others. The deep images are detailed enough to study the structure of the shocks, comparing H$\alpha$ and [SII] emission, tracers of different shock regions, and also comparing the change of structure over the time. And that can be done simultaneously all over the L1551 cloud, while the previous studies were restricted to selected areas.

3. The detection of new Herbig-Haro objects in different star forming regions: S140, L1551, IC 1396N and the Gulf of Mexico. Some of them were very small and not related to the main centers of star formation, and would probably not be detected without the large field of view of our images. Others were surprisingly strong and probably were not detected before for being confused with the bright rims of the clouds near which they were located (S140 and IC 1396N). The region of the Gulf of Mexico is probably one of the last regions of such an active star formation being discovered nowadays. Around 30 Herbig-Haro objects are concentrated in a relatively small region of the sky, associated with traces of embedded flows in the near-infrared, with H$\alpha$ emission stars and many embedded near-infrared sources.

4. Comparing the Herbig-Haro objects studied, we observe that the largest outflows are relatively well aligned with the assumed overall magnetic field in the region, as can be seen in the large L1551 flows and in the largest and deeply embedded outflows in the globular clouds S140 and IC 1396N. The smaller flows are apparently aligned perpendicularly to the larger outflow axis (e.g. HH 153, HH 493 and maybe HH 707 in L1551) or do not show a particular alignment at all (like in the Gulf of Mexico).

5. Using modern CCD detectors with a grism spectrograph, we have searched for H$\alpha$ emission stars in the Gulf of Mexico. The region surveyed was much smaller than what is normally obtained with the photographic surveys, but it covered our region of interest, and we detected more than 30 new H$\alpha$ emission stars. Their distribution indicates a region where the star formation is going on for a longer time, associated with a previously known cluster of H$\alpha$ emission stars (the LkH$\alpha$ 186 cluster), and also an adjacent region where this process is in its initial phases, that coincides with structures detected in the near and mid-infrared. As mentioned before, this region is much more active than previously thought.

6. The observations of some of the regions, both in the optical and in the near-infrared, allowed a view of the relationship between sources and outflows. We have identified some of the sources of the newly found Herbig-Haro objects,

but many others remain unknown. We have also noted a lack of relationship between stars with infrared excess and H$\alpha$ emission, that requires a more detailed study to be confirmed and understood.

We have observed different types of star forming regions: small globules (S140 and IC 1396N), regions located in giant molecular clouds (M 42 and NGC 2264 and Gulf of Mexico) and in intermediate sized dark clouds (L1551).

The globules are very small in extent and are often being affected by the strong UV radiation of a nearby massive star, that interferes in the formation process, maybe even being the triggering mechanism. We usually observe one or a few IRAS sources inside, driving strong molecular outflows, some less embedded and probably more evolved young stars (some still driving outflows) and some H$\alpha$ emission stars at the edge or already outside the cloud. It is not clear, however, if the radiation of the massive star triggered the star formation towards the interior of the cloud, or if it is simply removing the material away from stars that were already in the process of formation. In that case, the age distribution would not follow the direction outside→inside the cloud. The stars could have approximately the same age, but some were deprived earlier of the material that would form them. The outer stars would form less massive stars and the inner stars would have more time to accumulate material, thus forming more massive stars.

Dark clouds such as the L1551 region in Taurus harbors low mass stars and lack both massive stars and brown dwarfs (according to the observational data so far). The outflows driven by these low mass stars are very powerful, though, and may act as a controller of the mass that could be accreted into the stars. With no massive stars around, there is no radiation to illuminate the cloud, evaporate the thinner material, irradiate outflows. The flows detected optically are Herbig-Haro objects, only visible because of the shocks with the surrounding medium. Infrared and molecular flows can also be observed. It would be interesting to compare the magnetic field of other dark clouds and the orientation of their outflows, to check if they (at least the most powerful ones) also have a similar behavior of L1551.

Giant molecular clouds are much more complex. The presence of massive stars affects the formation process adding many more variables to the problem. The result is a richer environment, forming clusters on many scales. The Gulf of Mexico is an example of low mass star formation inside a shell of an extended cloud that is being blown out by the massive stars born in its interior. It is likely a second generation of stars, triggered by the radiation pressure.

Besides some obserational problems we had (e.g. non-photometric conditions when obtaining the near-infrared images; the continuum extraction problem in the spectra in the Gulf of Mexico) there is still much to be done with the data used in the

present study. The H$\alpha$ and [SII] narrow-band images of the Herbig-Haro objects will be studied in detail, comparing H$\alpha$/[SII] intensity ratios to check the nature of the shocks, as well as the changes in brightness of some knots, when multi-epoch images are available. The broad-band optical images of the Gulf of Mexico were obtained in photometric conditions with great seeing, and the $VRI$ magnitudes for all the stars in the region will be analyzed. A less accurate analysis can be done with the $JHK$ set of observations (since the photometric errors are larger for those). We also had access to 450$\mu$m and 850$\mu$m maps of the Gulf of Mexico made at the JCMT telescope by Hervé Aussel. They show a cluster of warm dust just south of the visible cluster, extending to its southwest. That is another indication that there is an even deeper and more recent group of stars being formed there.

Besides the attempt to improve the results already obtained for the regions presented in this work, other regions were also observed and should be analyzed. For example the Barnard 62 globule has basically the same set of observations as for IC 1396N and we have already found a couple of new Herbig-Haro objects in it, associated with embedded sources. The region W40 was also observed and we initially found no Herbig-Haro object, but there are many embedded sources inside the cloud that deserve further investigation. Other regions were also surveyed for H$\alpha$ emission line with the Schmidt telescope, like the Lynds 1616 region in Orion.

The final goal is to have all the star forming regions studied in all their aspects, providing sufficient information that would allow an improvement of the current theories of star formation.

*Acknowledgments:*

We would like to express our thanks to CNPq, who provided the financial support that made this work possible.

This work makes use of data products from the Two Micron All Sky Survey (2MASS), which is a joint project of the University of Massachusetts and the Infrared Processing and Analysis Center/California Institute of Technology, funded by the National Aeronautics and Space Administration and the National Science Foundation. 2MASS science data and information services were provided by the Infrared Science Archive (IRSA) at IPAC. This work also has made use of the SIMBAD database and the VizieR database of astronomical catalogues operated at CDS, Strasbourg, France. We have also made use of the USNO-B catalog, from the US Naval Observatory, the GSC2.2 (Guide Star Catalogue-II), a joint project of the Space Telescope Science Institute and the Osservatorio Astronomico di Torino, and the MSX catalog (Midcourse Space Experiment), from the Ballistic Missile Defense Organization and NASA Office of Space Science.

# Appendix A

# Published Papers

## A.1 The fountains of youth: irradiated break-out of outflows in S140

*John Bally, Bo Reipurth, Josh Walawender and Tina Armond*
*The Astronomical Journal, 124: 2152–2163, 2002 October*

My specific contributions to this paper:

1. I was part of the observing team in October 2001 at the 4m telescope on Kitt Peak (Tucson), to obtain the MOSAIC narrow-band H$\alpha$ and [SII] images;

2. I participated in the process of reduction of the images (I have also reduced images of other regions);

3. I participated in the process of visually scanning the images, comparing different filters, in order to identify new Herbig-Haro objects.

A secondary objective was to be trained in the observing, reducing and handling of the MOSAIC images, that were obtained for several different star forming regions at that time. So, I would be able to work on those images, for instance, to measure the proper motions, as done with the L1551 images (Section 3.2).

## A.2 Blow-out from IC 1396N: the emergence of Herbig-Haro flows from a cloud core

*Bo Reipurth, Tina Armond, Alex Raga and John Bally*
*The Astrophysical Journal, 593: L47–L50, 2003 August*

My specific contributions to this paper:

1. I was part of the observing team at Mauna Kea (Hawaii) on July 13 (near- and mid-infrared images at UKIRT) and July 14 and 15 (optical images and spectra at the UH 2.2m).

2. I have reduced the optical images and spectra and corrected the automatic pipeline for the reduction of the near-infrared images taken with UKIRT, when necessary, removing some of the bad exposures (that were saturated or had lost guidimg) or simply removing bad sections of some images.

3. I got an estimate of the $JHK$ magnitudes for the near-infrared sources. Since our images were obtained in non-photometric conditions, I had to calibrate the magnitudes using the 2MASS observations, that were less deep and resolved, but provided accurate photometry at least for the brighter stars. This way we could determine the fraction of stars with infrared excess inside the field observed, that included the proposed source of HH 777.

4. I have helped to identify and locate the Herbig-Haro objects in the optical images. I registered the near-infrared (broad- and narrow-band), mid-infrared and optical images and helped in the attempt to relate embedded sources, embedded flows and optical flows.

## A.3 H$\alpha$ emission–line stars in molecular clouds. I. The NGC 2264 region

*Bo Reipurth, Bertil Petterson, Tina Armond, John Bally and Luiz Paulo R. Vaz*
*The Astronomical Journal, 127: 1117–1130, 2004 February*

My specific contributions to this paper:

1. I have basically worked on the compilation of the table of H$\alpha$ emission line stars. With the coordinates and emission strengths of the H$\alpha$ emission stars determined by Bertil Pettersson and Bo Reipurth and cross-correlated with Herbig (1954), Ogura (1984) and Walker (1984) lists, I cross-correlated these coordinates with the list of Rebull et al. (2002) and gave final ESOH$\alpha$ numbers to the newly found stars. I also obtained magnitudes in the public catalogs (USNO-B, GSC2.2 and 2MASS), thus determining the limiting magnitude of our survey, deeper than the previous ones. Using the 2MASS coordinates, after visually inspecting if the match was real, I have updated the coordinates list to the 2MASS coordinates, more accurate than the ones obtained initially.

2. Using the 2MASS magnitudes, I estimated the number of stars with infrared excess ($\sim 25\%$) and observed their spatial distribution.

3. I helped in the process of finding the close binaries among the H$\alpha$ emitters, in the deep MOSAIC H$\alpha$ image, and I estimated distances and position angles, to obtain the fraction of binaries.

# References


Adams, F.C. & Fatuzzo, M., 1996, ApJ, 464, 256

Adams, F.C., Lada, C.J. & Shu, F.H., 1987, ApJ, 312, 788

Adams, M.T., Strom, K.M. & Strom, S.E., 1979, ApJ, 230, L183

Adams, M.T., Strom, K.M. & Strom, S.E., 1983, ApJS, 53, 893

Alencar, S.H.P. & Batalha, C., 2002, ApJ, 571, 378

André, P., Ward-Thompson, D. & Barsony, M., 1993, AJ, 405, 122

Bally, J., Feigelson, E. & Reipurth, B., 2003, ApJ, 584, 843

Bally, J. & Reipurth, B., 2002, RMxAA, 13, 1

Bally, J., Reipurth, B., Walawender, J. & Armond, T., 2002, AJ, 124, 2152

Bally, J. & Scoville, N.Z., 1980, ApJ, 239, 121

Beltrán, M.T., Girart, J.M., Estalella, R., Ho, P.T.P. & Palau, A., 2002, ApJ, 573, 246

Bessell, M.S. & Brett, J.M., 1988, PASP, 100, 1134

Cambrésy, L., Beichman, C.A., Jarrett, T.H. & Cutri, R.M., 2002, AJ, 123, 2559

Comerón, F. & Pasquali, A., 2005, A&A, 430, 541

Carpenter, J.M., 2001, AJ, 121, 2851

Codella, C., Bachiller, R., Nisini, B., Saraceno, P. & Testi, L., 2001, A&A, 376, 271

Cohen, M. & Kuhi, L.V., 1979, ApJS, 41, 743

Crampton, D. & Fisher, W.A., 1974, Pub. Dom. Ap. Obs., 14, 283

Crutcher, R.M., Hartkopf, W.I. & Giguere, P.T., 1978, ApJ, 226, 839

Cudworth, K.M. & Herbig, G.H., 1979, AJ, 84, 548

Currie, D.G., Dowling, M., Shaya, E.J., 1996, AJ, 112, 1115

Cutri, R.M & 24 co-authors, 2003, Explanatory Supplement to the 2MASS All Sky Data Release:
`http://www.ipac.caltech.edu/2mass/releases/allsky/doc/explsup.html`

Davis, C.J., Moriarty-Schieven, G., Eislöffel, J., Hoare, M.G. & Ray, T.P., 1998, ApJ, 115, 1118

Devine, D., Reipurth, B. & Bally, J., 1999, AJ, 118, 972

Dubath, P., Reipurth, B., & Mayor, M., 1996, A&A, 308, 107

Eiroa, C., Lenzen, R., Miranda, L.F., Torrelles, J.M., Anglada, G. & Estalella, R., 1993, AJ, 106, 613

Eislöffel, J. & Mundt, R., 1994, A&A, 284, 530

Fukui, Y., Sugitani, K., Takaba, H., Iwata, T., Mizuno, A., Ogawa, H. & Kawabata, T., 1986, ApJ, 311, L85

Genzel, R., Reid, M.J., Moran, J.M. & Downes, D., 1981, ApJ, 244, 884

Hartigan, P., Morse, J., Palunas, P., Bally, J. & Devine, D., 2000, AJ, 119, 1872

Heathcote, S., Morse, J.A., Hartigan, P., Reipurth, B., Schwartz, R.D., Bally, J. & Stone, J.M., 1996, AJ, 112, 1141

Herbig, G.H., 1954, ApJ, 119, 483

Herbig, G.H., 1958, ApJ, 128, 259

Herbig, G.H. & Bell K.R., 1988, Lick Observatory Bull. No. 1111

Hodapp, K-W., 1987, ApJ, 319, 842

Joy, A.H., 1946, PASP, 58, 244

Kroupa, P., 2001, MNRAS, 322, 231

Kroupa, P., 2002, Science, 295, 82

Lada, C.J., 1998, *The formation of low mass stars*, in The Origins of Stars and Planetary Systems (Eds. C.J. Lada & N.D. Kylafis, Kluwer Academic Press)

Lada, C.J. & Wilking, B.A., 1984, ApJ, 287, 610

Lada, C.J., Young, E.T., & Greene, T.P., 1993, ApJ, 408, 471

Larson, R.B., 2001, *Modes of Star Formation and the Origin of Field Populations*, ASP Conference Proceedings, 285, 442 (Ed. Eva K. Grebel and Walfgang Brandner)

Larson, R.B., 2005, MNRAS, submitted (astro-ph/0412357)

Lima, G.H.R.A., 2003, MsC Dissertation, UFMG

López, R., Riera, A., Raga, A.C., Anglada, G., López, J.A. & Noriega-Crespo, A., 1996, MNRAS, 282, 470

Marcy, G.W., 1980, AJ, 85, 230

Margulis, M., Lada, C.J. & Snell, R.L., 1988, ApJ, 333, 316

Margulis, M., Lada, C.J. & Young, E.T., 1989, ApJ, 345, 906

Masciadri, E. & Raga, A.C., 2001, A&A, 376, 1073

Ménard, F. & Duchêne, G., 2004, A&A, 425, 973

Micono, M., Davis, C.J., Ray, T.P., Eislöffel, J. & Shetrone, M.D., 1998, ApJ, 494, L227

Miller, G.E. & Scalo, J.M., 1979, ApJS, 41, 513

Monet, D.G. & 28 co-authors, 2003, AJ, 125, 984

Moriarty-Schieven, G.H. & Snell, R.L., 1988, ApJ, 332, 364

Morse, J.A., Kellogg, J.R., Bally, J., Davidson, K., Balick, B. & Ebbets, D., 2001, ApJ, 548, L207

Neckel, T., Harris, A.W., Eiroa, C. 1980, A&A, 92, 9

Nisini, B., Massi, F., Vitali, F., Giannini, T., Lorenzetti, D., Di Paola, A., Codella, C., D'Alessio, F. & Speziali, R., 2001, A&A, 376, 553

Noriega-Crespo, A., Morris, P., Marleau, F.R., Carey, S., Boogert, A., van Dishoeck, E., Evans II, N.J., Keene, J., Muzerolle, J., Stapelfeldt, K., Pontoppidan, K., Lowrance, P., Allen, L. & Bourke, T.L., 2004, ApJSS, 154, 352

Ogura, K., 1984, PASJ, 36, 139

Ogura, K., Sugitani, K. & Pickles, A., 2002, AJ, 123, 2597

Oliver, R.J., Masheder, M.R.W. & Thaddeus, P., 1996, A&A, 315, 578

Osterbrock, D.E., 1957, ApJ, 125, 622

Park, B., Sung, H., Bessell, M. & Kang, Y., 2000, AJ, 120, 894

Parsamian, E.S. & Chavira, E., 1982, Bol. Tonantzintla 3, 69

Pound, M.W. & Bally, J., 1991, ApJ, 383,705

Preibisch, T., Balega, Y.Y., Schertl, D., Smith, M.D. & Weigelt, G., 2001, A&A, 378, 539

Preibisch, T. & Smith, M.D., 2002, A&A, 383, 540

Preibisch, T., Balega, Y., Schertl, D., Hofmann, K. & Weigelt, G., 2003, *Interferometry for Optical Astronomy II*, Proceedings of the SPIE, 4838, 1047 (Ed. Wesley A. Traub)

Price, S.D., Egan, M.P., Carey, S.J., Mizuno, D.R. & Kuchar, T.A., 2001, AJ, 121, 2819

Raga, A.C., Mellema, G., Arthur, S.J., Binette, L., Ferruit, P. & Steffen, W., 1999, Rev. Mex. Astron. Astrofis., 35, 123

Raga, A.C., Navarro-González, R. & Villagrán-Muniz, M., 2000, Rev. Mex. Astron. Astrofis., 36, 67

Raga, A.C. & Reipurth, B., 2004, Rev. Mex. Astron. Astrofis., 40, 15

Rebull, L.M., Hillenbrand, L.A., Strom, S.E., Duncan, D.K., Patten, B.M., Pavlovsky, C.M., Makidon, R. & Adams, M.T., 2000, AJ, 119, 3026

Rebull, L.M., Makidon, R.B., Strom, S.E., Hillenbrand, L.A., Birmingham, A., Patten, B.M., Jones, B.F., Yagi, H. & Adams, M.T., 2002, AJ, 123, 1528

Reipurth, B., 1999, *A General Catalogue of Herbig-Haro Objects* (2d ed; Boulder: Cent. Astrophys. Space Astron., Univ. Colorado)

Reipurth, B., 2000, AJ, 120, 317

Reipurth, B., Armond, T., Raga, A.C. & Bally, J., 2003, ApJ, 593, L47

Reipurth, B. & Bally, J., 2001, Annu. Rev. Astron. Astrophys., 39, 403

Reipurth, B., Corporon, P., Olberg, M. & Tenorio-Tagle, G., 1997, A&A, 327, 1185

Reipurth, B. & Eiroa, C., 1992, A&A, 256, L1

Reipurth, B. & Heathcote, S., 1991, A&A, 246, 511

Reipurth, B., Pettersson, B., Armond, T., Bally, J. & Vaz, L.P., 2004a, AJ, 127, 1117

Reipurth, B., Rodríguez, L.F., Anglada, G. & Bally, J., 2002, AJ, 124, 1045

Reipurth, B., Yu, K.C., Moriarty-Schieven, G., Bally, J., Aspin, C. & Heathcote, S., 2004b, AJ, 127, 1069

Rieke, G. H. & Lebofsky, M. J., 1985, ApJ, 288, 618

Rodríguez, L.F., Curiel, S., Cantó, J., Loinard, L., Raga, A.C. & Torreles, J.M., 2003, ApJ, 583, 330

Rodríguez, L.F., Porras, A., Claussen, M.J., Curiel, S., Wilner, J.D. & Ho, P.T.P., 2003, ApJ, 586, 137

Salpeter, E.E., 1955, ApJ, 121,161

Saraceno, P. & 38 co-authors, 1996, A&A, 315, L293

Schwartz, R.D., Gyulbudaghian, A.L. & Wilking, B.A., 1991, ApJ, 370, 263

Stanke, T., McCaughrean, M.J. & Zinnecker, H., 1999, A&A, 350, 43L

Stocke, J.T., Hartigan, P.M., Strom, S.E., Strom, K.M., Andersson, E.R., Hartmann, L.W. & Kenyon, S.J., 1988, ApJS, 68, 229

Straižys, V., Kazlauskas, A., Vansevičius, V. & Černis, K., 1993, Baltic Astronomy, 2, 171

Strom, K.M., Strom, S.E. & Vrba, F.J., 1976, AJ, 81, 320

Sugitani, K., Fukui, Y. & Ogura, K., 1991, ApJS, 77, 59

Sung, H., Bessell, M.S. & Lee, S.-W., 1997, AJ, 114, 2644

Valdes, F.G., 2001, *The Reduction of CCD Mosaic Data*, in Automated Data Analysis in Astronomy (ed. H. P. Singh and R. A. Gupta): `http://iraf.noao.edu/projects/ccdmosaic/reductions/adaa/valdes2.ps`

Walker, M.F., 1956, ApJS, 2, 365

Walsh, J.R., Ogura, K. & Reipurth, B., 1992, MNRAS, 257, 110

Ward-Thompson, D., Zylka, R., Mezger, P.G. & Sievers, A.W., 2000, A&A, 355, 1122

Wendker, H.J., Baars, J.W.M & Benz, D., 1983, A&A, 124, 116

Wiramihardja, S.D., Kogure, T., Yoshida, S., Ogura, K. & Nakano, M., 1989, PASJ, 41, 155

Wiramihardja, S.D., Kogure, T., Yoshida, S., Nakano, M., Ogura, K. & Iwata, T., 1991, PASJ, 43, 27

Wiramihardja, S.D., Kogure, T., Yoshida, S., Ogura, K. & Nakano, M., 1993, PASJ, 45, 643

Yokogawa, S., Kitamura, Y., Munetake, M. & Kawabe, R., 2003, ApJ, 595, 266